

# Sodahuskommittén

Sodahuskommitténs Rapport 2006-2  
Examensarbete Anna Lundborg - KTH

Sodahuskommittén pris till bästa examensarbete inom  
sulfatmassafabrikens kemikalieåtervinning 2006

## **Simulation of the flue gas flow through the superheater in a recovery boiler**

Anna Lundborg  
KTH

Rapport 2006-2

©Sodahuskommittén 2006



# **Simulation of the flue gas flow through the superheater in a recovery boiler**

Anna Lundborg

Master of Science Thesis  
School of Chemical Science and Engineering  
KTH-Royal Institute of Technology  
Stockholm, Sweden  
2005

Supervisors:

Jürgen Jacoby, AF-Process AB

Lars J. Pettersson, Department of Chemical Engineering and  
Technology, KTH-Royal Institute of Technology

## Abstract

The purpose of the recovery boiler is to recover the inorganic cooking chemicals used in the Kraft pulping process and to generate superheated steam from combustion of the organics in the black liquor, which is a by-product of chemical pulping. Since the recovery boiler is often a limiting factor for the pulp production, it is economically very attractive to increase its capacity. Because of the hostile environment inside the boiler detailed measurements in an operating boiler are difficult to obtain. CFD (Computational Fluid Dynamics) computer modelling is an attractive alternative tool for studying recovery boilers.

In the superheater section of the boiler saturated steam is superheated with the desire to attain a high steam temperature to maximize the generation of electricity in the steam turbine. The heating media is the hot flue gas formed during combustion of the black liquor. The effectiveness of the heat exchange between the flue gas and the steam is strongly dependent on how the flue gas flows through the superheater. Observations of the superheater section in a couple of existing recovery boilers indicate that the flow pattern is not optimal from a heat exchange point of view. A zone of recirculation flow is likely to occur at the lower portions of the superheater, which reduces the heat transfer between the flue gas and the steam. The objective of this study is to determine the flow pattern of the flue gas through the superheater section in a recovery boiler by CFD modelling using the commercial code FLUENT.

2D calculations were performed which concluded that the superheater tubes could be simplified as rectangular packages since the mass flow through the small passages in between the tubes is small.

In the 3D models the superheaters were modelled as rectangular packages of porous zones, which mean that the pressure loss due to the superheaters is simulated by introducing empirical coefficients of flow resistance as source terms in the momentum equations. The coefficients of flow resistance depend on the geometry, the tube diameter, the tube spacing and the flue gas velocity.

When studying the flow profiles of the 3D models a channelled flow is observed along the higher portions of the superheater, where the velocities are high, and a recirculation flow is obtained along the lower portions of the superheater, where the velocities are very low. In an ideal case the flue gas would flow through the superheater at the same velocity in a uniform flow. The recirculation flow causes reduced heat transfer between the flue gas and the steam, which means that the resulting steam temperature is reduced.

Two cases with different inlet profiles have been studied to evaluate the influence of the inlet conditions to the geometry on the predicted results. The inlet flow profiles represent different bull nose shapes. Since the zone of recirculation flow is considerably smaller and the flow through the superheater is more uniform when using the inlet profile corresponding to an abrupt and angular shaped nose, a conclusion is that an abrupt bull nose is better than a round and sloping nose from a heat exchange point of view.

To improve the flue gas flow pattern through the superheater, metal strips could be placed in front of the bull nose. Other possible methods could be to place screen tubes in front of the superheater or soot blowers at the location of the bull nose. The bull nose design has great impact on the flue gas flow through the superheater.

## Sammanfattning

Sodapannans syfte är att återvinna de förbrukade kokkemikalierna från massaprocessen och att generera överhettad ånga genom förbränning av de organiska föreningarna i svartluten, som är en restprodukt från den kemiska massaprocessen. Eftersom sodapannan ofta är den enhet som begränsar massaproduktionen är det ekonomiskt mycket attraktivt att öka dess kapacitet. På grund av den ogästvänliga miljön inuti pannorna är det svårt att utföra omfattande mätningar på en panna i drift. CFD (Computational Fluid Dynamics) är ett attraktivt alternativt verktyg för att studera sodapannor med hjälp av datorsimuleringar.

I överhettardelen av pannan överhettas mättad ånga för att uppnå en hög ångtemperatur och därmed maximera elgenereringen i ångturbinen. Det värmande mediet är den heta rökgasen som bildades vid förbränningen av svartluten i pannan. Effektiviteten i värmeutbytet mellan rökgasen och ångan beror i hög grad på hur rökgasen strömmar genom överhettaren. Observationer för de olika stegen i överhettaren i ett antal sodapannor indikerar att strömningsmönstret är långt ifrån optimalt ur värmeöverföringssynpunkt. Sannolikt förekommer recirkulationsströmmar i rökgasen, vilket försämrar värmeöverföringen mellan rökgasen och ångan. Målet med denna studie är att bestämma rökgasens strömningsmönster genom överhettaren i en sodapanna genom CFD-beräkningar med hjälp av det kommersiella programmet FLUENT.

2D-beräkningar genomfördes för att undersöka om överhettartuberna kunde approximeras som rektangulära paket, vilket skulle förenkla beräkningarna och minska beräkningstiden avsevärt. Denna förenkling bedömdes som acceptabel eftersom massflödet som passerar mellan tuberna är mycket litet.

I 3D-beräkningarna modellerades överhettartuberna som rektangulära paket av porösa zoner, vilket innebär att tryckfallet på grund av överhettartuberna simuleras genom att introducera empiriska tryckfallskoefficienter i en extra term i transportekvationen. Tryckfallskoefficienterna baseras på geometrin, tubdiametern, tubdelningen och rökgasens hastighet.

Strömningsprofilerna från 3D-beräkningarna visar ett kanaliserat flöde längs den övre delen av överhettaren, där hastigheterna är höga, och ett recirkulerande flöde längs den nedre delen av överhettaren, där hastigheterna är mycket låga. Under ideala förhållanden skulle rökgasen strömma genom överhettaren med konstant hastighet i ett uniformt flöde. Recirkulationen orsakar försämrade värmeöverföring mellan rökgasen och ångan, vilket leder till en lägre ångtemperatur efter överhettaren.

Två modeller med olika strömningsprofiler vid inloppet till geometrin studerades för att utvärdera randvillkorens inverkan på resultaten. Strömningsprofilerna vid inloppet representerar olika näsgeometrier. Eftersom recirkulationen är betydligt mindre utbredd och flödet genom överhettaren mer uniformt när en strömningsprofil som motsvarar en abrupt och kantig näsa används är en slutsats att en abrupt formad näsa är bättre än en rund och lutande näsa ur värmeöverföringssynpunkt.

För att förbättra rökgasens strömningsmönster genom överhettaren skulle ledskenor kunna placeras vid näsan. Andra tänkbara metoder är att placera screentuber framför överhettartuberna eller sotblåsare vid näsan. Näsans utformning har stor inverkan på strömningsmönstret.

# Table of Contents

|   |    |
|---|----|
| 1. Introduction .....   | 6  |
| 2. Literature Review .....  | 7  |
| 2.1. Flow Field .....   | 7  |
| 2.2. Model Validation.....  | 9  |
| 3. Background on CFD.....   | 11 |
| 3.1. Basic Principles of CFD .....  | 12 |
| 3.1.1. Pre-processor .....  | 12 |
| 3.1.2. Solver .....   | 13 |
| 3.1.3. Post-processor .....   | 14 |
| 4. Chemical Pulping .....   | 15 |
| 4.1. The Kraft Pulping Process.....   | 15 |
| 4.1.1. Chemical Recovery .....  | 16 |
| 4.1.2. Black Liquor.....  | 18 |
| 5. Recovery Boilers .....   | 20 |
| 5.1. The Lower Furnace .....  | 21 |
| 5.2. The Convective Heat Transfer Section .....   | 22 |
| 5.2.1. The Nose Arch .....  | 26 |
| 5.2.2. The Boiler Drum .....  | 27 |
| 5.2.3. The Screen Tubes .....   | 28 |
| 5.2.4. The Superheaters .....   | 28 |
| 5.2.5. The Boiler/Generating Bank .....   | 30 |
| 5.2.6. The Economizer .....   | 31 |
| 6. Modelling of Recovery Boilers .....  | 32 |
| 6.1. Modelling Fluid Flow in a Porous Medium .....  | 33 |
| 7. Modelling of the Superheater .....   | 35 |
| 7.1. The Purpose of the Modelling.....  | 35 |
| 7.2. Modelling in Fluent .....  | 35 |
| 7.2.1. Geometry and Materials .....   | 36 |
| 7.2.2. Boundary Conditions.....   | 39 |
| 7.2.3. Turbulence and Radiation Models .....  | 40 |
| 7.2.4. Mesh .....   | 41 |
| 8. Results .....  | 42 |
| 8.1. 2D Modelling .....   | 42 |
| 8.1.1. Case 1: The Superheaters as Cylindrical Tubes .....                                | 42 |
| 8.1.2. Case 2: The Superheaters as Rectangular Packages.....                              | 46 |
| 8.1.3. Conclusions from the 2D Modelling.....   | 48 |
| 8.2. 3D Modelling .....   | 49 |
| 8.2.1. Case 3: Modelling the Entire Domain, Inlet Flow Profile 1 .....                    | 50 |
| 8.2.2. Case 4: Modelling the Entire Domain, Inlet Flow Profile 2 .....                    | 56 |
| 8.2.3. Case 5: Modelling a Sub-Domain, Inlet Flow Profile 1 .....                         | 59 |
| 8.2.4. Case 6: Modelling a Sub-Domain, Inlet Flow Profile 2.....                          | 62 |
| 8.2.5. Influence of Inlet Flow Profile .....  | 63 |
| 8.2.6. Modelling the Entire Domain vs. a Sub-Domain .....                                 | 64 |
| 9. Discussion .....   | 65 |
| 9.1. Economical consequence of a recirculation flow in the superheater .....              | 65 |
| 9.2. Methods to improve the flue gas flow and heat transfer through the superheater ..... | 66 |
| 10. Conclusions .....   | 67 |
| Acknowledgements .....  | 68 |

|   |    |
|---|----|
| References .....  | 69 |
| List of Figures .....   | 71 |
| List of Tables .....  | 72 |
| Nomenclature .....  | 73 |
| APPENDIX A .....  | 74 |
| APPENDIX B .....  | 75 |
| APPENDIX C Recovery Boiler Chemistry .....  | 76 |
| C1. Sodium and Sulphur Chemistry .....  | 76 |
| C2. Potassium and Chlorine Chemistry .....  | 83 |
| APPENDIX D Modelling Fluid Flow in a Porous Medium .....                          | 85 |
| APPENDIX E Calculation of the Flow Resistance Coefficients .....                  | 89 |
| APPENDIX F Example of the effect of a recirculation flow in the superheater ..... | 90 |

# 1. Introduction

The recovery boiler is one of the most important units in the Kraft pulping process. It is the largest and most expensive unit used in pulp mills. The purpose of the recovery boiler is to recover the inorganic cooking chemicals used in the pulping process and to generate superheated steam from the combustion of the organics in the black liquor. The recovery boiler also plays a major role in the sulphate process as a chemical reactor. The black liquor, which is a by-product of chemical pulping, contains the inorganic cooking chemicals and the organics separated from the wood. The recovery boiler is often a limiting factor for the pulp production. It is economically very attractive to increase the capacity since it allows a greater pulp production.

In chemical pulping the raw material wood is treated mechanically and chemically in a series of different processes, for example wood preparation, cooking, washing, screening and bleaching (see *Figure 51* in Appendix A). The purpose is to remove the non-fibrous components and produce pure fibres, pulp. Wood consists of three main components; cellulose, hemicellulose and lignin. During the cooking as much lignin and hemicellulose as possible should be dissolved. The main chemical reactant in the Kraft pulping process is an aqueous solution of NaOH and Na<sub>2</sub>S. After the cooking, the fibres are washed to separate them from the by-product, weak black liquor. The solid content in the weak liquor has to be increased to more than 65% by multistage evaporation before it is burned in the recovery furnace.

The gas flow and combustion processes in a Kraft recovery furnace are very complex. Because of the harsh environment inside the furnace, the design and operation of Kraft recovery furnaces are mostly based on practical experience of the industry, rather than detailed measurements. An alternative tool for studying recovery boilers is CFD (Computational Fluid Dynamics) computer modelling. This method has great potential to improve the understanding of the phenomena which occur in a recovery furnace and to optimize the production efficiency. The gas flow field and the combustion can for example be studied, and the effects of liquor properties and operating parameters investigated.

In a recovery boiler, the saturated steam from the boiler drum is superheated in the heat exchanger section of the boiler, which is located after the furnace. The heating media is the hot flue gas formed during combustion of the black liquor in the recovery boiler. The desire is to attain a high steam temperature to maximize the generation of electricity in a steam turbine. The effectiveness of the heat exchange between the flue gas and the steam is strongly dependent on how the flue gas flows through the superheater. Observations of the superheater section in a couple of existing recovery boilers indicate that the flow pattern is not optimal from a heat exchange point of view. A zone of recirculation flow is likely to occur, which reduces the heat transfer between the flue gas and the steam. This means that the resulting steam temperature is reduced.

The object of this study is to determine the flow pattern of the flue gas through the superheater section in a recovery boiler by CFD modelling using the commercial code FLUENT. The flow is studied in the volume of the boiler from the furnace outlet to the inlet of the generating bank.

## 2. Literature Review

Recovery boilers have been studied for more than 40 years, and during the 1980s intensive research was performed in the USA, Canada, Finland and Sweden. The rapid development of numerical simulation methods has made it possible to simulate recovery boilers and predict its performance, which has increased the understanding of the processes occurring in a recovery boiler.

### 2.1. Flow Field

Among the early achievements using recovery furnace models in literature is the isothermal simulation of the flow field and mixing pattern in a recovery furnace. The gas flow patterns are determined primarily by the furnace geometry and the air inlet geometry. Considerable efforts have been devoted to determine the flow pattern in the recovery furnace.

Saviharju et al. [2004], described measurements in several modern recovery boilers as well as numerical simulations. The measured results were compared to calculations using the CFD code Fluent. Velocity and temperature fields were measured above the bull nose. The velocities above the bull nose were measured using a cooled Pitot tube, which allows dusty conditions, and a suction pyrometer was used to measure the flue gas temperatures. The flow field measurements revealed clearly a large recirculating area above the bull nose in one of the boilers. Two different approaches, a 2D and a 3D model, were used for modelling of the bull nose and the superheater region. Both models predicted flow patterns that agreed reasonably well with the field measurements. In this research modelling was shown to be an effective tool in comparison studies.

Vakkilainen et al. [1992], studied the upper furnace flow patterns using a 1:15 scale water model and numerical modelling to obtain the optimal size and shape of the bull nose. A variety of different inlet velocity profiles and temperature profiles were used to determine the sensitivity of the results to chosen inlet conditions. Two turbulence models were used, the traditional  $k-\epsilon$  model and an algebraic stress model. General features of the simulated results agree well with field measurements. The recirculating flow over the bull nose was identified, as others have observed in earlier studies for power and other type of boilers. The effect of bull nose size was investigated for three sizes and the influence of bull nose shape was studied in three different cases. A larger, abrupt bull nose results in a larger recirculation zone.

This study concluded that different turbulence models ( $k-\epsilon$  and algebraic stress turbulence models) and different inlet velocity and temperature profiles do not significantly alter the velocity field and temperature distributions. It was found, however, that the velocity and temperature distributions are sensitive to the shape and size of the bull nose.

Vakkilainen et al. [1991], performed a combination of isothermal flow experiments and computational flow calculations in order to predict the effect of changing the free flow area. Free flow area ratios were varied from 0.4 to 0.6 (distance nose-to-front wall divided by distance front-to-back wall). A ratio of 0.5 and a bull nose were determined to be acceptable. Flue gas flow and temperature fields for a real boiler could be simulated with reasonable agreement. A conclusion from the study was that if the superheaters are squeezed very close

to the front wall, a recirculation flow above the bull nose will severely lower the superheater heat transfer.

Kawaji et al. [1995], combined flue gas flow and steam side flow calculations to predict the heat transfer rates in the superheater region of recovery boilers. An iterative calculation scheme was created in which the flow field was calculated using a CFD code, and the heat transfer to the superheater tubes was evaluated in a separate code that took into account the flow field. Both the flue gas recirculation and heat loss to the bull nose were considered in the model. Good agreement between thermocouple measurements and model predictions was achieved both considering the steam and flue gas temperatures. The analysis concludes that cold flue gas in the recirculation zone can result in negative heat transfer from the flue gas to the steam.

Shen et al. [1995], investigated the flue gas flow through the upper furnace of a recovery boiler by numerical simulations. The aim was to examine the sensitivity of the velocity and the temperature distributions to common modelling assumptions. In this study the effect of the density variation and different treatments of the boiler bank on the upper furnace flow field and temperature distribution was studied. The temperature was measured at several locations in the upper furnace.

In the first model, where the flow is assumed to have constant gas temperature, the flow is severely channelled and a large recirculation zone is formed above the bull nose. The temperature in the recirculating zone is significantly lower than that in the channelled flow region. As a result, there is little, no or even negative heat transfer between the superheater platens and the flue gas in the recirculation zone. The assumption of constant gas density may introduce some error due to the large temperature variation (about 300 °C) in the flow. The temperatures in the recirculation zone are moderately lower at constant density.

The second model studied the effect of temperature-dependent gas density variation on the flow pattern and temperature distribution. The flow pattern is very similar to that in the first model, but the temperature distribution shows differences up to 150 °C in the recirculation zone. The higher temperatures in this case are caused by the higher density and leads to higher thermal conductivity. The assumption of constant density is very accurate for calculating flow patterns, but not for predicting temperature distribution.

The third model also included the effects of the boiler bank. The flow pattern and the temperature distribution in the recirculation zone change moderately from the second model as result of the boiler bank. The channelled flow narrows at the exit of the superheater and the temperature in the recirculation zone are moderately higher if the boiler bank is not included in the model. Only moderate computational savings are achieved by assuming constant flue gas density and not including the boiler bank in the model.

The simulated results agree well with measured temperature results, and show a severely channelled flow with a large recirculation zone above the bull nose. The temperatures predicted by the third model agree most closely with the measurements.

Tse et al. [1996], studied the gas flow and heat transfer in the upper furnace of a recovery boiler by applying the concepts of porosity and distributed flow resistance to simulate the hydrodynamics of gas flows past the superheater tubes. A porosity factor based on the amount of flow blockage is introduced to allow for flow acceleration through obstructed passages.

Distributed resistances are introduced as source terms in the momentum equations to simulate the pressure loss due to the tube bank obstructions. Some advantages of the porosity model are that the grid can be much coarser than the dimensions of the individual tubes and the same CFD solution algorithm can be used in the entire domain since only the terms in the governing equations are modified.

## **2.2. Model Validation**

The reliability of the results of CFD based recovery furnace models can be validated by comparisons of model predictions against experimental measurements. It is, however, extremely difficult to obtain sufficient amount of reliable data from an operating recovery boiler. CFD based recovery furnace models are capable of predicting the temperature, gas velocity, and concentration fields to a degree far beyond the capability to measure these quantities. Measurement capabilities are severely limited by the lack of access to the furnace and the hostile environment that exists within the furnace.

According to Grace et al. [1998], validation using real furnace measurements is a fallacy, because real systems are always time dependent, whereas CFD solutions only represent a steady-state situation.

In this study, validation of isothermal flow predictions against water models of furnaces at UBC (University of British Columbia), validation of flow predictions for cold flow (isothermal flow) in an actual recovery furnace, and validation of the full recovery boiler model (hot flow model) using data obtained from field measurements on two different recovery boilers, were performed.

A CFD-based recovery boiler model has been developed at the UBC – the UBC model. This model is based on a new CFD code specifically aimed at solving flows typical of recovery boilers and incorporates black liquor combustion and radiant heat transfer as terms in the energy equations. The model is capable of dealing with swirling flows and includes a partial treatment of processes occurring in the convective heat transfer section. The UBC model provides better convergence characteristics and incorporates more realistic submodels than earlier CFD models.

### **Validation of flow predictions**

There was reasonable agreement between flow predictions and measured flows in all of the UBC studies. In the air cold flow experiments carried out in an actual recovery boiler, the measured and computed flow fields were quite similar. The locations of upward flow, downward flow, zero velocity regions and the peak values of the upward and downward velocities were well predicted. Similarly, the flow predictions made by the UBC code agree generally with the scaled-down water models. The measurements show that the real flows are often only quasi-stable and that there can be significant amounts of time-dependent changes that cannot be predicted by a steady-state CFD model. For a few, simplified cases, unsteady-state CFD solutions were obtained that were in good agreement with the measured data. However, unsteady-state simulations are extremely computationally intensive. The flow predictions in operating recovery boilers have a reasonably good probability of being valid.

### **Validation of a complete recovery boiler model**

Only limited success was obtained in the validation of the complete recovery boiler model. The biggest problem was that the amount of quantitative data on furnace outputs, needed for comparison with the model predictions, was extremely limited. Also the unsteadiness of the flows contributed to the lack of success.

Isothermal flow predictions obtained with the UBC code agree generally with the flow data obtained with the water models and the cold flow data obtained from an actual recovery boiler.

Although the recovery boiler model cannot be considered completely validated, the validation work done supports the idea that model predictions can be a significant input in decision making. The models are a very useful tool and help improve recovery boiler operation. In none of the studies was there a clear contradiction between model predictions and actual performance. The most effective way to use the models appears to be to make relative comparison between simulated results for several different cases.

It must be remembered that CFD-based recovery boiler models actually consists of different parts and the different parts can have different levels of validity. When this study was performed in 1998, flow prediction capability was ahead of black liquor burning prediction capability. The black liquor burning models were at the time the weakest parts of the recovery boiler models, particularly if the objective is to predict levels of air emissions and particulate loadings.

### 3. Background on CFD

Computational Fluid Dynamics (CFD) is an engineering tool for modelling fluid flow, heat and mass transfer, chemical reactions and related phenomena in complex geometries by solving the set of governing mathematical equations. CFD analyses are a very powerful tool, which can be applied in a wide range of different areas, both industrial and non-industrial. Some examples are:

- Aerodynamics - aircraft and automobiles
- Hydrodynamics of ships
- Power plant – combustion in internal combustion engines and gas turbines
- Turbomachinery – pumps and turbines
- Heat transfer – heating and cooling systems
- Combustion
- Chemical process engineering – mixing and reacting chemicals
- External and internal environment of buildings – heating/ventilation
- Environmental engineering – transport of pollutants and effluent
- Hydrology and oceanography – flows in rivers and oceans
- Meteorology – weather prediction
- Biomedical engineering – blood flows through arteries and veins

CFD analyses can for example be used in studies of new designs, detailed product development, troubleshooting and redesign. The technique complements testing and experimentation.

CFD plays an increasing role not only as a research tool but in the simulation and optimization of industrial processes and products. Progress has been made in replacing a large number of experiments and in increasing our physical understanding and predictive capabilities. Researchers are still working hard on improving computational methods, and engineers and scientists are working on improving the models of complex processes.

Some benefits of computational modelling:

- Improve process analysis and design methods: detailed understanding, scale-up experimental results
- Reduce time and cost: optimization on computer (furnace/reactor size, shape, operating conditions), graphically and interactively visualize performance
- High degree of confidence
- Eliminates the costly process of trial and error with operation and hardware modifications
- Ability to study systems under hazardous conditions at and beyond their normal performance limits (e.g. safety studies and accident scenarios)

Some shortcomings of computational modelling:

- Only steady-state modelling is possible in practice since unsteady-state modelling is extremely computational intensive
- The people performing the modelling must have great skills to be able to properly set up the conditions for the simulation and guide the solution
- A bottleneck in modelling is the limited computer resources

From the 1960s the aircraft industry has used CFD techniques in design, R&D and manufacture of aircraft and jet engines. More recently the methods have been applied to the design of internal combustion engines, combustion chambers of gas turbines and furnaces. Automobile manufacturers nowadays routinely use CFD to predict drag forces, air flows and the in-car environment.

The main reason why CFD has lagged behind other computer-aided engineering tools is the complexity of describing fluid flows. Because of a required increase in computer power and the introduction of more user-friendly interfaces CFD has become widely used since the 1990s.

Because of its enormous potential, the use of CFD will probably increase rapidly in the future. However, there are still some difficulties in CFD modelling. A fundamental task in modelling is to establish a model, i.e. to analyze the physics and chemistry of the process and determine the governing equations. In order to establish the governing equations, it is necessary to have a good understanding of the physical and chemical processes taking place.

### **3.1. Basic Principles of CFD**

The main stages in a CFD study are:

*Pre-processing*: formulate the problem, governing equations and boundary conditions; construct computational mesh.

*Solving*: numerical solution of the governing equations

*Post-processing*: plot and analyse results

#### **3.1.1. Pre-processor**

Some of the stages in pre-processing are:

- Definition of the geometry of the region: the computational domain.
- Grid generation (the division of the domain into a number of smaller non-overlapping sub-domains): a grid (or mesh) of cells (or control volumes).
- Selection of the physical and chemical phenomena that need to be modelled.
- Definition of fluid properties.
- Specification of boundary conditions.

The solution to a flow problem (velocity, pressure, temperature etc.) is defined at nodes inside each cell. Both the accuracy of a solution and its cost in terms of necessary computer hardware and calculation time are dependent on the fineness of the grid. In general, the larger the number of cells in the grid the better the solution accuracy. Optimal meshes are often non-uniform: finer in areas where large variations occur from point to point and rougher in regions with relatively little change.

### 3.1.2. Solver

There are three different numerical solution techniques: finite difference, finite element and spectral methods. The numerical methods that form the basis of the solver perform an approximation of the unknown flow variables by simple functions, discretisation by substitution of the approximations into the governing flow equations, and solution of the algebraic equations.

The commercial CFD code FLUENT is based on the finite volume method, which is developed from the finite difference method [Versteeg et al., 1995]. The numerical algorithm consists of the following steps:

- Approximation of the flow variables by simple functions.
- Discretisation involves the substitution of a variety of finite-difference-type approximations for the terms in the integrated equations representing flow processes, such as convection and diffusion, i.e. the integral equations are approximated in terms of the values at the nodes. This converts the integral equations into a system of algebraic equations.
- Solution of the algebraic equations numerically by an iterative method.

The control volume integration distinguishes the finite volume method from all other CFD techniques. The resulting statements express the conservation of relevant properties for each cell. This clear relationship between the numerical algorithm and the underlying physical conservation principle is one of the main attractions of the finite volume method and makes its concepts much simpler to understand by engineers than the finite element and spectral methods. The conservation of a general flow variable  $\Phi$ , for example a velocity component or enthalpy, within a finite control volume can be expressed as a balance between the various processes tending to increase or decrease it. In words:

[Rate of change of  $\Phi$  in the control volume with respect to time] =  
[Net flux of  $\Phi$  due to convection into the control volume] +  
[Net flux of  $\Phi$  due to diffusion into the control volume] +  
[Net rate of creation of  $\Phi$  inside the control volume]

CFD codes contain discretisation techniques suitable for the treatment of the key transport phenomena, convection (transport due to fluid flow) and diffusion (transport due to variations of  $\Phi$  from point to point) as well as for the source terms (associated with the creation or destruction of  $\Phi$ ) and the rate of change with respect to time. The underlying physical phenomena are complex and non-linear and therefore an iterative solution approach is required.

### **3.1.3. Post-processor**

Some examples of data visualisation tools available are:

- Domain geometry and grid display
- Vector plots
- Line and shaded contour plots
- 2D and 3D surface plots
- Particle tracking
- View manipulation (translation, rotation, scaling etc.)
- Animation for dynamic result display

The graphics output capabilities for flow visualization of CFD codes have proven to be very helpful in understanding the flow and have resulted in much better communication of ideas to the non-specialist. [Versteeg et al., 1995; Salcudean, 1998]

## 4. Chemical Pulping

Various pulping methods exist, classified as mechanical, chemical or semi chemical. In this work focus is on chemical pulping, and especially the Kraft process.

In chemical pulping, the wood chips are cooked with chemicals in an aqueous solution at elevated temperature and pressure. The objective is to dissolve the lignin and leave most of the cellulose and hemicelluloses behind as intact fibres. Chemical pulping results in long and strong fibres, but the process has a low yield (about 40-55%). The two principle chemical pulping methods are the (alkaline) Kraft process and the (acidic) sulphite process. The Kraft process is dominating because of advantages in chemical recovery and pulp strength.

In the Kraft process, the wood chips are cooked in a solution of sodium hydroxide (NaOH) and sodium sulphide (Na<sub>2</sub>S). The alkaline attack causes fragmentation of the lignin molecules into smaller segments whose sodium salts is soluble in the cooking liquor. “Kraft” is the German word for force, and Kraft pulps produce strong paper. The unbleached pulp is characterized by a dark brown colour. An environmental concern is the malodorous gases, mainly organic sulphides, which is produced during the process.

The conversion of sulphate to sulphide in the cooking liquor resulted in a huge improvement in reaction kinetics and pulp properties. Because sodium sulphate has been the traditional makeup chemical, the Kraft process is sometimes referred to as the “sulphate process”.

It could be mentioned that the other principle chemical pulping method, the sulphite process, uses a mixture of sulphurous acid (H<sub>2</sub>SO<sub>3</sub>) and bisulphite ion (HSO<sub>3</sub><sup>-</sup>) to attack and solubilize the lignin.

Some of the advantages of the Kraft process compared to the sulphite process are that it produces the highest strength pulp, handles a wide variety of wood species, tolerates bark in the pulping process and utilizes proven technology for efficient chemical recovery. However, the process also has some shortcomings, principally the low yield from wood, the relatively high lignin content of bleachable grades, and the malodorous gases caused by the reduced sulphur compounds. A lot of pulping modifications have been proposed to overcome these shortcomings, for example cooking additives, chip pre-treatments and two-stage cooks.

### 4.1. The Kraft Pulping Process

A simplified figure of the Kraft liquor cycle is shown in *Figure 1*. White liquor containing the active cooking chemicals, sodium hydroxide (NaOH) and sodium sulphide (Na<sub>2</sub>S), is used for cooking the chips. After the cooking the black liquor (see chapter 4.1.2) is washed from the pulp and treated in a series of steps to recover the cooking chemicals and regenerate the cooking liquor. The black liquor, containing the reaction products of lignin solubilization, is concentrated and burned in the recovery furnace to yield an inorganic smelt of sodium carbonate (Na<sub>2</sub>CO<sub>3</sub>) and sodium sulphide. The smelt is dissolved to form green liquor, which is reacted with quick lime (CaO) to convert Na<sub>2</sub>CO<sub>3</sub> into NaOH and regenerate the original white liquor.

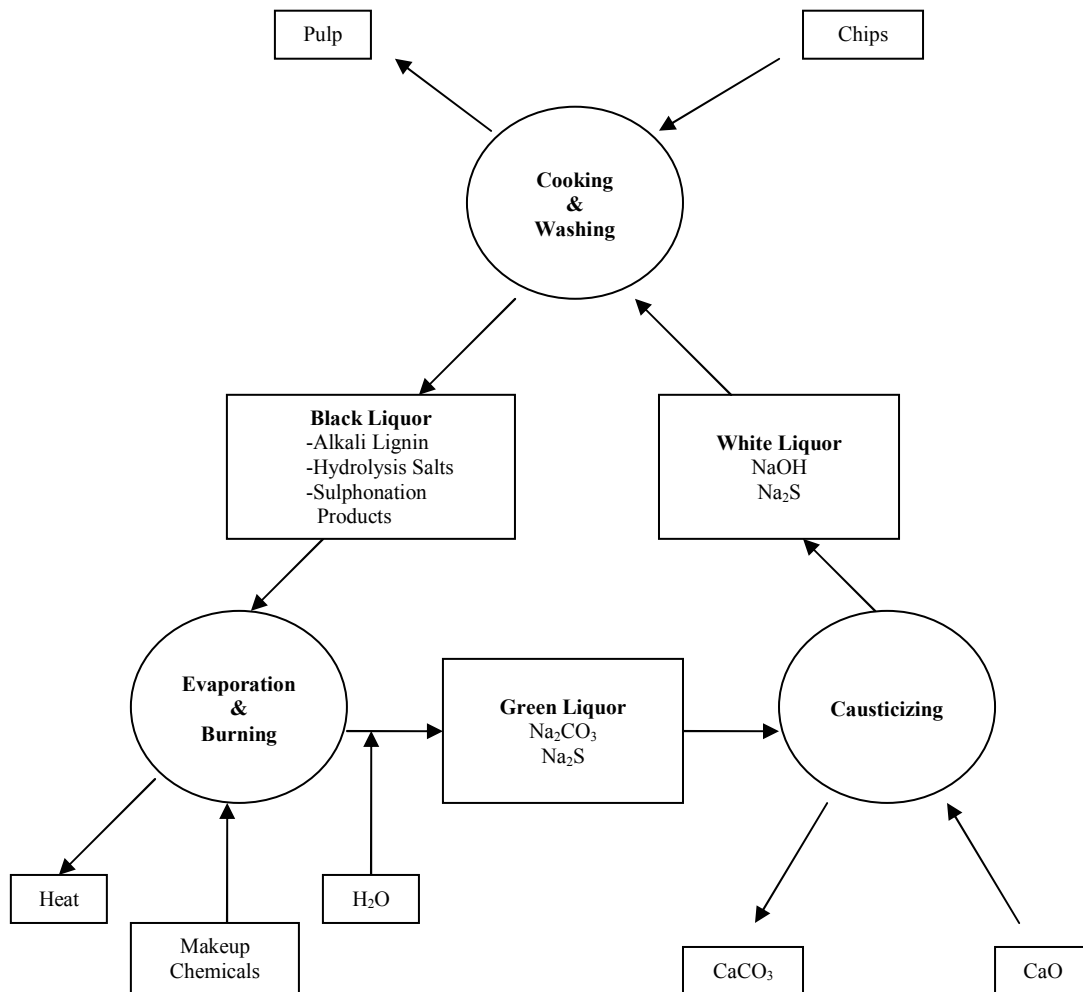


**Figure 1:** The Kraft liquor cycle.

#### 4.1.1. Chemical Recovery

The recovery of chemicals from the spent cooking liquor, the reconstitution of these chemicals to form fresh cooking liquor, the realization of energy from the combustion of organic residuals, and minimization of air and water pollution are essential parts of the chemical recovery process. The recovery of chemicals and energy from the black liquor and reconstitution of the recovered chemicals to form white liquor are integrated with the pulp mill operation.

A flow sheet of the Kraft mill liquor cycle is shown in *Figure 52* in Appendix B. The cooked pulp from the digesters must be washed in the brown stock washers, which usually consist of a series of countercurrent vacuum drum washers, in order to remove residual black liquor that would contaminate the pulp during following processing steps, and to recover the maximum

amount of spent chemicals with minimum dilution. Starting with weak black liquor (about 15% solids) from the brown stock washers, the steps in chemical recovery are:

1. Concentration through a series of evaporation and chemical addition steps to form heavy black liquor at 70-75% solids.
2. Combustion of heavy black liquor in the recovery furnace to form inorganic smelt.
3. Dissolving the smelt from the furnace in water to form green liquor.
4. Causticizing of green liquor with lime to form white liquor for the next cooking cycle.
5. Burning of lime mud to recover lime.

The recovery boiler is at the heart of the Kraft recovery process and has the following functions:

1. Evaporates residual moisture from the liquor solids.
2. Burns the organic constituents.
3. Steam generation.
4. Reduces oxidized sulphur compounds to sulphide.
5. Recovers inorganic chemicals in molten form.
6. Conditions the products of combustion to minimize chemical carryover.

The heavy black liquor from the evaporator or the concentrator is sprayed into the furnace. The liquor droplets dry and partially pyrolyse before they fall onto the char bed. Incomplete combustion in the porous char bed causes carbon and carbon monoxide to act as reducing agents, thus converting sulphate and thiosulphate to sulphide. The heat is enough to melt the sodium salts, which filter through the char bed to the floor of the furnace. The smelt then flows by gravity through water-cooled spouts to the dissolving tanks.

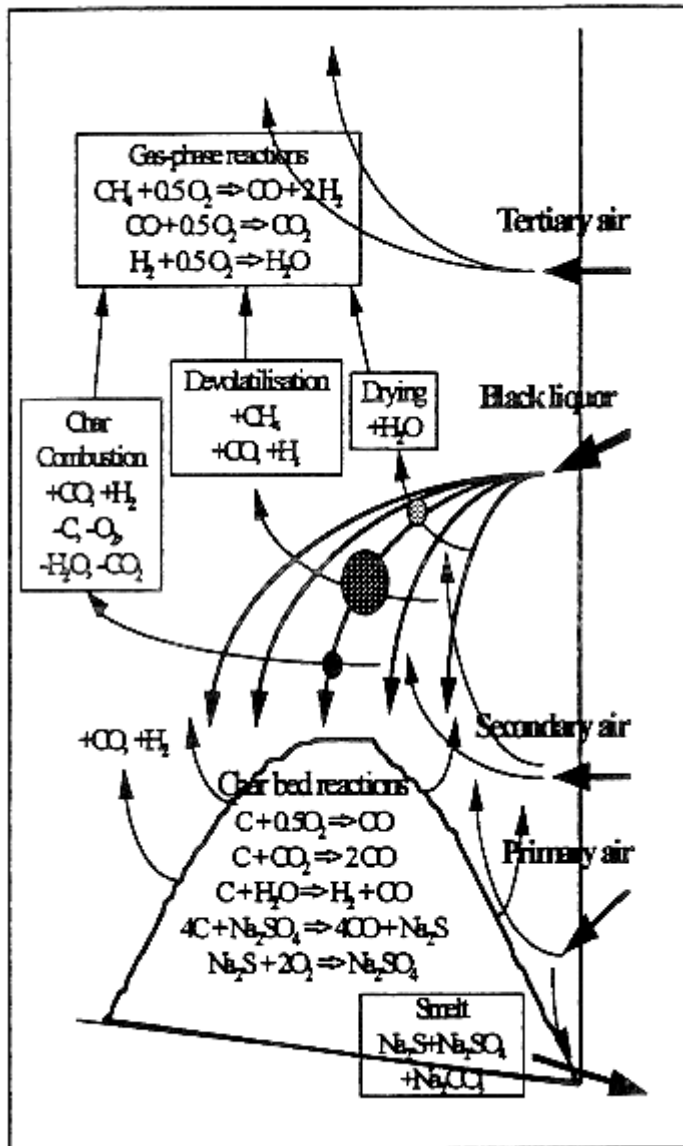


Figure 2: Black liquor combustion processes [Tao et al., 1996].

The green liquor strength is important for smooth operation within the liquor cycle and has to be carefully controlled. The optimal level is a compromise between two factors. A higher concentration of the green liquor increases the inventory of soda chemicals, which will help to level out the operation and improve the capacity against interruptions. But, a lower concentration improves the causticizing efficiency, which will ensure that a lower dead load of non-reactive  $Na_2CO_3$  is carried around the cycle.

#### 4.1.2. Black Liquor

Black liquor is an important resource for steam generation in the pulp and paper industry. It is a substance unique to the pulping process and a fairly available renewable energy source. It is also one of the few fuels that have been locally produced and used in the countries with a pulping industry.

Black liquor is a liquid, but it has two states, fluid and solid. Its main components are inorganic cooking chemicals, lignin and other organic constituents removed from the wood during pulping in the digester, and water. The exact composition of the black liquor depends on the wood species, the pulp yield, and the alkali charge used. Considerable differences exist between liquors from different species, and especially between those from hardwood and softwood.

65% solids and 35% water are common properties of black liquor. The dried product, black liquor solids, consists of approximately 50% dissolved wood and 50% inorganics. *Table 1* shows the chemical species and the elemental composition of black liquors from North American wood species. Five elements are always present: sodium (Na), sulphur (S), carbon (C), hydrogen (H), and oxygen (O). Depending on the type of wood, potassium (K) and chlorine (Cl) can also be present. The organic part is divided between char (20%) and volatiles (30%) during the devolatilization process. Black liquor char, the pyrolysis product, consists mainly of a mixture of carbon, sodium carbonate, sodium sulphide and sodium sulphate [Smook, 1992].

**Table 1** [Adams et al., 1997]

| <b>Chemical species in black liquor, wt%</b> |        | <b>Elemental composition of black liquor</b> |           |
|--|--------|--|-----------|
| Alkali lignin                                | 30-45% | Carbon                                       | 34-39%    |
| Carboxylic acids                             | 25-35% | Hydrogen                                     | 3-5%      |
| Extractives                                  | 3-5%   | Oxygen                                       | 33-38%    |
| Acetic acid                                  | 5%     | Sodium                                       | 17-25%    |
| Formic acid                                  | 3%     | Sulphur                                      | 3-7%      |
| Methanol                                     | 1%     | Potassium                                    | 0.1-2%    |
| Sulphur                                      | 3-5%   | Chloride                                     | 0.2-2%    |
| Sodium                                       | 15-20% | Nitrogen                                     | 0.04-0.2% |
|  |        | Others                                       | 0.1-0.3%  |

## 5. Recovery Boilers

A recovery boiler is both a steam boiler and a chemical reactor. Tubes in the walls, bottom and top of the furnace deliver the steam required by the mill. Sodium sulphate is chemically reduced in the boiler to sodium sulphide. A unique characteristic of recovery boilers is the char bed in the lower furnace. These boilers were developed by Tomlinson, in cooperation with Babcock and Wilcox, in the early 1930s and contributed to the dominance of the Kraft process.

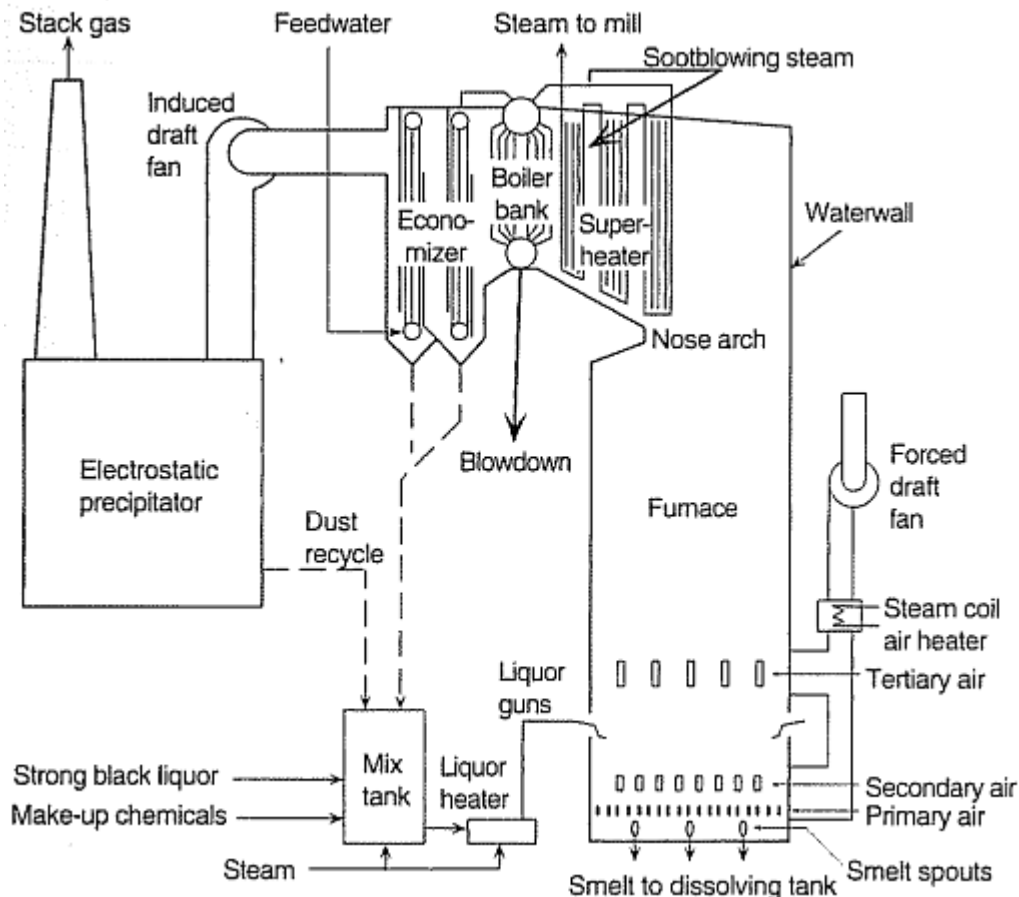


**Figure 3:** Schematic figure of a recovery boiler [Adams et al., 1997].

Recovery boilers have two main sections; a furnace section and a convective heat transfer section. The nose arch is the border line between these two sections. The mixing and combustion of the fuel (black liquor) and the air should be completed in the furnace section. The char bed is required for final combustion of the black liquor char and for separation of the inorganic smelt. Modern recovery boilers achieve this with a liquor spray and by introducing the combustion air at about three or four different levels in the boiler. The necessary heat transfer surface area to extract the heat from the combustion gases is provided by water wall construction of the lower furnace in combination with the convective heat transfer section in the upper furnace. About 40% of the heat from the combustion gas is transferred to the boiler water in the furnace section. The remaining 60% of the heat is transferred in the convective heat transfer section to form high pressure steam. The upper part of the recovery boiler is generally similar to that of other types of furnaces, e.g. bark or oil furnaces.

Despite the physical size of these units, the combustion efficiency is quite good, greater than 99% under most circumstances [Adams et al., 1997]. The last 1% represents, however, a great energy loss on an absolute scale, and this is naturally of environmental concern. The overall energy efficiency, at about 61%, is relatively low, but two of the largest losses, fuel hydrogen loss and sulphur reduction loss, are inherent in the fuel and the Kraft process, and cannot thereby easily be changed [Adams et al., 1997]. The largest single loss is due to water in the black liquor. This can be changed by burning black liquor at higher dry solids contents. Some of the potential benefits of higher solids content are combustion stability, safety, sulphur capture, increased throughput and energy efficiency.

### 5.1. The Lower Furnace

The furnace section can be considered as consisting of three zones as shown in *Figure 4*: a drying zone where the liquor is introduced, a reduction zone at the bottom, and the oxidation zone in the turbulent upper section.

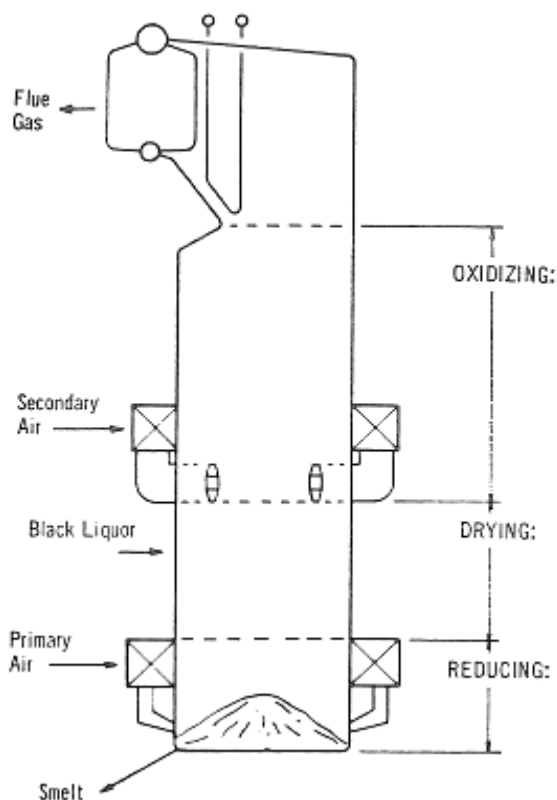


**Figure 4:** The furnace zones [Smook, 1992].

The combustion of the black liquor requires an addition of heat and air (oxygen) to the black liquor droplets. The heat is required to dry and pyrolyse the liquor, while air is required for oxidation of the organic material. The overall process is very similar to that for other fuels burned in boilers. But two unique aspects of recovery boilers are that the air and fuel are introduced entirely separately and that the fuel is not finely divided. The droplets are also larger than those of typical fossil fuels. Some of the reasons for this are the high inorganic

content of the liquor, the need to avoid entrainment and the need to build a bed on the furnace floor for sulphur reduction and smelt removal.

The purpose of the combustion is to release heat. During the combustion hydrogen is converted to water vapour and carbon to either  $\text{CO}_2$  or carbonate. Black liquor droplets are sprayed into the recovery furnace through nozzles. The organic components of the black liquor droplets are then burned to form gaseous products during a series of processes; drying, pyrolysis, char gasification and homogeneous combustion. The droplet releases water to the gas phase during the drying stage. During pyrolysis, the droplet releases combustibles ( $\text{CO}$ ,  $\text{CH}_4$ , etc.) to the gas phase. Burning of the solid char, the residue left after the pyrolysis of the black liquor, occurs mainly on the char bed, which covers the floor of the furnace, but some char is burned in flight. While the carbon in the char is gasified, the inorganic compounds in the char are released and form a molten salt mixture, the smelt, which flows to the bottom of the char bed and leaves the furnace through smelt spouts. The smelt usually consists of about  $2/3 \text{Na}_2\text{CO}_3$  and  $1/3 \text{Na}_2\text{S}$ , but also a small amount of  $\text{Na}_2\text{SO}_4$  occur [Adams et al., 1997]. The smelt is dissolved in water to form green liquor, which is further processed to make fresh cooking chemicals. It is important that at least 90% of the sodium sulphate is reduced to sodium sulphide to avoid dead load in the chemical system.

Air is introduced into the furnace through several sets of ports called the primary, secondary and tertiary air etc., from the bottom upwards. The primary air ports, which are supplying 50-65% of the required air, are located a few metres above the hearth and extend around all four walls of the furnace. The goals of the primary air ports are to push the bed away from the walls, to maintain good bed temperatures, and to maintain a layer of char on top of the smelt in order to ensure good chemical reduction efficiency. Secondary and tertiary air is usually introduced at higher velocities than the primary air to ensure complete mixing and combustion of the unburned gases.

The gas flow pattern within a recovery boiler is very complex. The flow pattern created by the air supply system is strongly influenced by the char bed. The shape of the char bed changes with time in a random way. These changes affect the flow field created by the combustion air system. This time dependent process is relatively slow, but very difficult to predict. Interaction between the char bed and the flow pattern is the main reason for the unstable behaviour of recovery boilers.

The water rising in the wall tubes receives heat indirectly by radiation from the char bed and flames in the furnace through the wall tubes. The furnace walls can represent as much as one half of the heat transfer surface required to produce high pressure steam.

## **5.2. The Convective Heat Transfer Section**

The upper part of the boiler consists of four sections of tube banks: the screen tubes, the superheater, the boiler bank and the economizer. In the economizer the feed water temperature is raised to just below its boiling point before it enters the boiler drum. The screen tubes cool the upward flowing combustion gases before they enter the superheater. The superheater increases the steam temperature from saturation to the superheat temperature. In the boiler bank, along with the furnace walls, the water is evaporated to steam.

Heat transfer from the combustion gas to the tube banks in the upper section of the boiler is mainly by convection, but radiation from flames in the furnace can also contribute largely.

The flows in the upper furnace consist of a mixture of liquid drops, solid particles and gases. The gas temperature is approximately 850 °C at the inlet to the upper furnace and 200 °C at the exit from the economizer, which can cause flue gas density variations as high as 300% [Shen et al., 1995].

The furnace gases, which are formed during combustion in the lower furnace, flow upward and through the convective section of the boiler. They pass over the nose arch, the superheater, the generating bank, and finally the economizer. After the economizer, the remaining sensible heat may be used to evaporate liquor or, less commonly, to heat the incoming air. Otherwise, the gas goes directly to the precipitator, where the dust particles are collected. The flows of feed water/steam and combustion gases are illustrated in *Figure 5*.

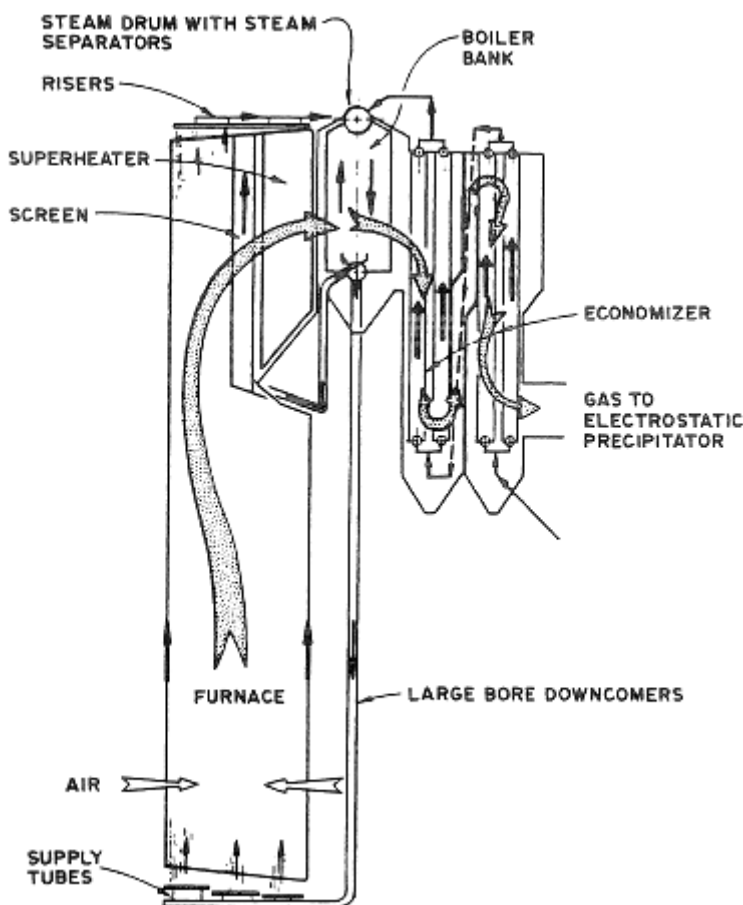
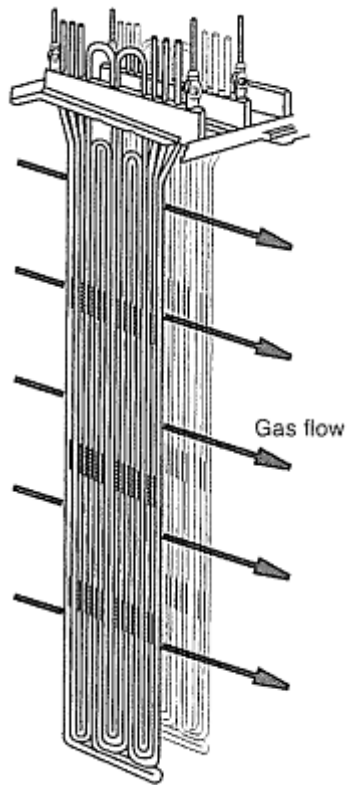


**Figure 5:** Directions of gas and steam flows in a recovery boiler [Smook, 1992].

The flow of combustion gas and boiler water through the convective sections is generally countercurrent, but in some parts of the superheater it may be co-current. The heat transfer in the individual sections can be either cross flow or parallel flow.



In-line arrangement of the tube banks are common because of the ease of tube cleaning and the lower gas-pressure drops across the tube bundles. The boiler bank consists of in-line tubes of typically about 5-7 cm diameter and about 10-12 cm side spacing [Adams et al., 1997]. Greater spacing is often used between the first rows of tubes to reduce plugging. The superheater can either be a bank of in-line tubes or platens with side spacing of approximately 30 cm. Platens are superheater tube sheets with in-line tubes of zero front-to-back spacing. This layout restricts cross flow and deposits are easier to remove from this flat arrangement.

The boiler bank tubes are more closely spaced than the superheater tubes. This is necessary to provide the required heat transfer surface area in the limited space. The tube spacing is a trade off between the risk of plugging and the cost of the boiler. Economizers consist of many small tubes closely spaced to get a sufficient surface area for heat transfer between the low temperature combustion gas entering the economizer and the water in the tubes.

**Figure 6:** Arrangement of two superheater platens [Adams et al., 1997].

The flue gas flow in the upper furnace influences the boiler operation in many aspects. Depositions and fouling on the outside of the tubes are caused by the high temperature and carryover of solid particulates from the furnace, which can result in plugging of gas passages. Carryover originates from physically entrained smelt and/or partially burned black liquor particles, and results in solid material accompanying the combustion gases into the convective section. Carryover particles are strongly influenced by local flue gas mean flow velocity, turbulence intensity and temperature. As a result, boilers sometimes have to be operated at reduced loads. The capacity of recovery boilers is affected mainly by carryover and fume-related plugging. Optimizing such units can increase their capacity, thermal output, and running time between water washes.

The tendency for fouling must be accounted for when the amount of heat transfer surface area needed is determined. By periodically removing the tube deposits with soot blowers, the heat transfer between the combustion gas and the tubes is maximized.

The low thermal efficiency common in many recovery boilers is closely related to the gas flow. According to observations, the design of the upper boiler and the shape of the bull nose could result in a large recirculation flow above the bull nose, which greatly reduces the convective heat transfer.

In *Figure 7* a flow sheet of the upper furnace in a recovery boiler is shown. Some of the constituents of the upper boiler are described below.

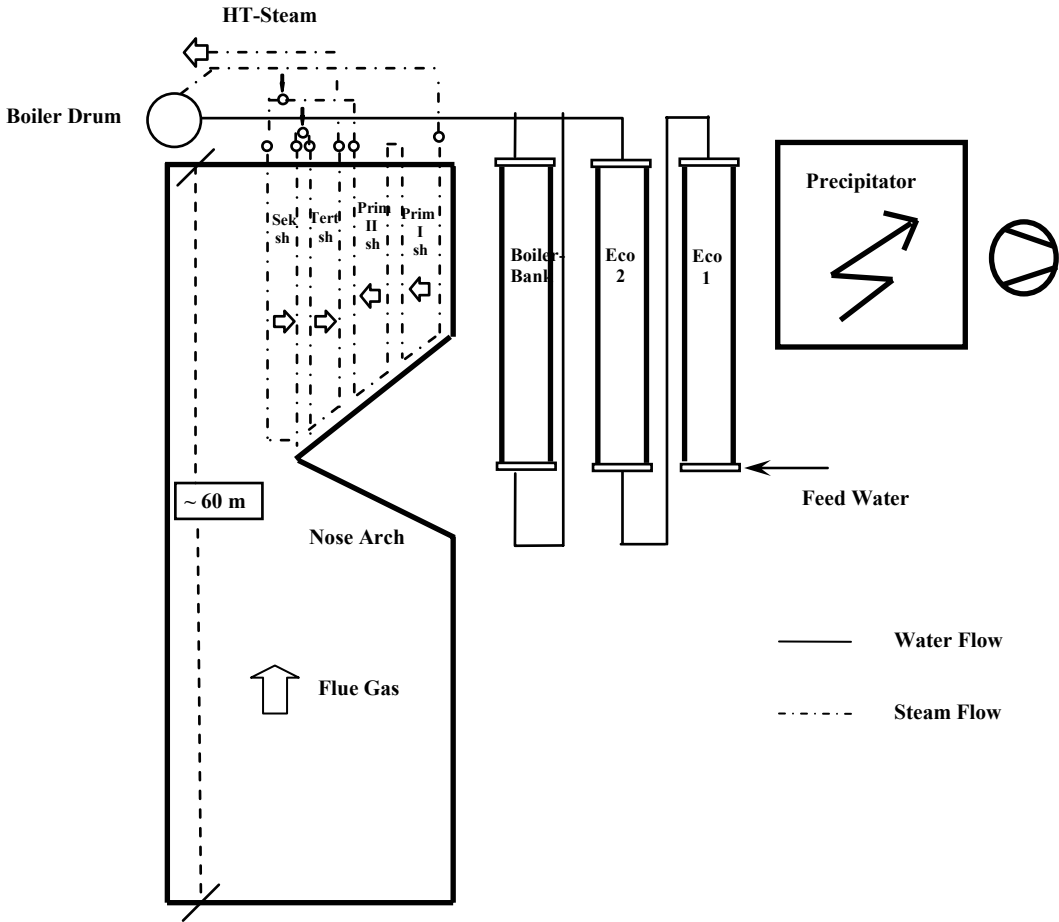


**Figure 7:** Flow sheet of the upper furnace in a recovery boiler.

### 5.2.1. The Nose Arch

The nose arch or bull nose extends out from the back wall of the upper furnace and occupies from 25% to 50% of the furnace cross-section (see *Figure 8*). The size of the bull nose is indicated by the horizontal flow area in the region of the bull nose compared to that of the open furnace area. The purpose of the bull nose is to protect the superheater from direct radiation from the furnace and thereby lower the corrosion rates, and also to guide the combustion gases and produce a uniform flow over the heat transfer surface. Unfortunately, a large nose arch results in poor gas flow characteristics above the nose arch, where a large region of recirculation is formed (see *Figure 9*). This region of recirculation has two negative impacts: it causes reduced heat transfer along the lower portions of the superheaters, and higher velocities around the remaining portion of the superheater which can result in increased fouling. Alternative designs that can reduce this region of recirculation need to be developed further.

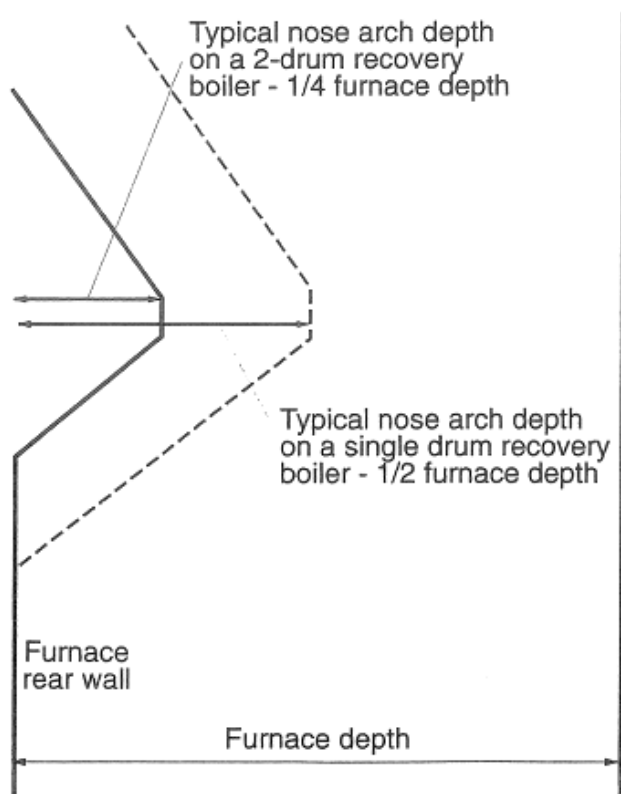


**Figure 8:** The nose arch geometry [Adams et al., 1997].

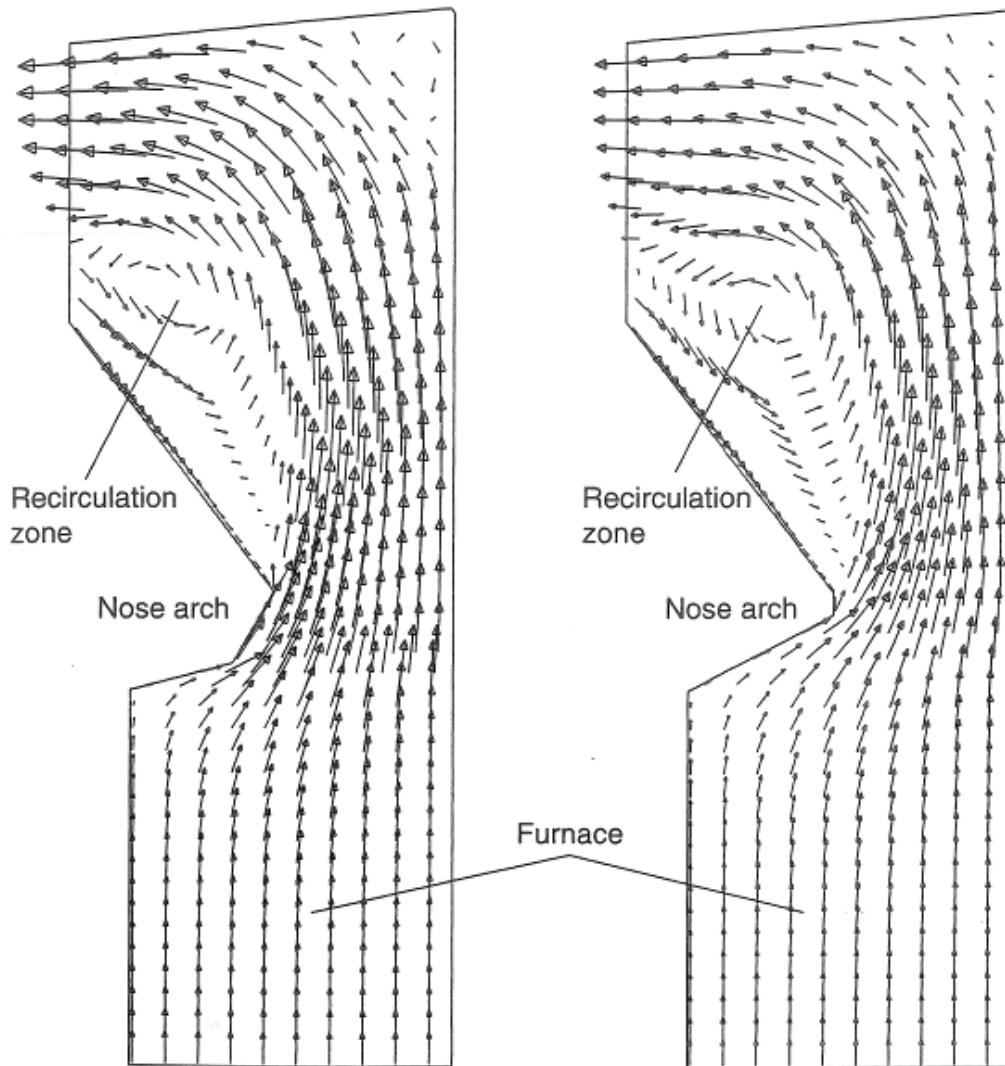


**Figure 9:** Recirculation zone above the nose arch [Adams et al., 1997].

One impact of this recirculation region above the nose arch is that the lower portion of the superheater tends to get less fouled [Adams et al., 1997]. Therefore soot blowing should be concentrated on the upper portions of the superheaters.

A large nose arch also complicates the design because it limits the space available for the superheater. A large superheater may require additional boiler height to fit above the nose arch. This can have a great effect on the boiler structure and cost.

### 5.2.2. The Boiler Drum

A mixture of water and steam is flowing into the drum from the water walls and the generating bank and the role of the boiler drum is to separate the liquid water from the steam. The drum size is based on total steam flow, steam pressure, and required steam purity. The total steam flow determines the drum volume, and the diameter is selected so that the drum length is equal to the furnace width. The pressure and number of connections drilled in the drum determines its thickness. Steam purity is ensured by selecting the correct type and length of steam/water separators.

### 5.2.3. The Screen Tubes

Many recovery boilers, particularly older units, have screen tubes in front of the superheater tubes. Screen tubes are usually water-filled tubes which are part of the steam generating circuit. Their purpose is to cool the combustion gases before they enter the superheater section, to block radiation from the furnace to the superheater section, and to collect some of the particulate carryover from the furnace.

Screens were required on older, lower steam pressure recovery units because the superheater steam temperature, and therefore heat requirement, was lower. Higher pressure recovery boilers have higher superheating requirements and larger superheaters. Screens are not needed in these units. Screens are also a potential safety hazard, because they are usually cooled with saturated water instead of superheated steam. A ruptured screen tube could release water into the furnace directly above the char bed, which could cause a serious safety hazard due to smelt-water contact [Adams et al., 1997].

### 5.2.4. The Superheaters

The flows created in the furnace have a major impact on the gas flow entering the superheaters. The size and geometry of the nose arch and the temperatures are examples of other factors that affect the gas flow. The influence of the design of the superheater on the gas flow is usually quite small because the pressure drop across the superheater is low when the superheater is not severely fouled.

It is very unusual that the superheaters only consist of one single section that receives saturated steam and delivers the superheated steam. Superheaters usually consist of multiple sections: primary, secondary, and so on. The heat transfer in each section varies with the cleanliness of the boiler and the firing rate. To avoid overheating, attemperating water flows between the sections (see *Figure 7*), which provide good control. The heat transfer requirement in the superheater depends on the amount of attemperating flow and the flow of saturated steam from the drum.

The superheater must produce the desired steam temperature and pressure over the normal operating range up to the Maximum Continuous Rating (MCR) of the boiler. It must also result in a generating bank inlet temperature below the point at which the deposits melt. The primary design parameter is the total superheater surface area. The number of sections, their arrangement, and the superheater position with respect to the nose arch all influence the design. A counter-current arrangement would be the most effective from a heat transfer point of view, but would also result in the highest temperature of the tube wall of the superheater. Because the combustion gas mainly flows horizontally, and the steam in the superheaters generally flows up and down, counter-current here means that the primary superheater is the section nearest the generating bank and exposed to the coldest combustion gas. The following sections usually go in order towards the furnace. *Figure 5* shows the directions of the gas and steam flows in a recovery boiler.

The superheater inlet gas temperature is based on the required generating bank inlet temperature and an energy balance around the superheater. The pressure and temperature of the superheated steam delivered by the boiler determine the enthalpy of the superheated steam and, with a correction for the pressure drop across the superheater, the steam saturation

temperature. The overall energy balance for the boiler determines the steam flow rate. The steam flow rate and the change in enthalpy across the superheater determine the rate of heat transfer to the steam in the superheater. The superheater inlet gas temperature is then determined by the energy balance on the gas-side and the generating bank inlet temperature.

**Table 2:** Typical flue gas temperatures at the inlet to the superheaters

|              | Temperature, ° C |
|--------------|------------------|
| Secondary SH | 800              |
| Tertiary SH  | 620              |
| Primary SH   | 535              |

But there are some complications in this superheater energy balance. One is the steam side superheater pressure drop and another is the use of attemperating water flow between the superheater sections. There must always be a significant pressure drop between the boiler drum and the superheated steam outlet. This pressure drop ensures that the flow of steam is distributed uniformly over the individual superheater tubes, and thereby avoiding that the tubes are overheated. The design pressure across the superheaters must be added to the design superheater steam pressure, which is the basis for the saturation properties of the steam entering the superheater.

The superheater tube walls are only cooled by the steam, and can therefore be much hotter than the steam. This can lead to very rapid corrosion. Because of this a counter-current arrangement may not be optimal. A co-current arrangement would yield a lower tube wall temperature, but would also result in a much larger superheater. The impact of the furnace nose arch, which blocks some of the radiation from the furnace, is also complicating the design. The final choice of the total superheater surface area and the arrangement of the sections depend on the final superheater steam temperature, superheater inlet gas temperature, the size of the nose arch, and the expected value of the overall heat transfer coefficient. The last parameter is based on vendor experience along with tube arrangement and superheater cleanliness.

The heat absorption by the superheaters is strongly depending on the uniformity of the gas conditions that flows through the superheater. Design conditions for the superheater assume that the gas that passes through the superheater section is completely uniform. Differences from uniformity in velocity or temperature reduce the heat absorption, which causes low steam temperature and/or excessive gas temperature entering the generating bank.

A design that limits the amount of fouling will minimize the flow channelling that could occur. In an ideal case all the gases flow through the boiler at the same velocity in a so called plug flow. In reality the flow is often channelled, which means that a region of higher velocity is formed in the centre of the channel. To minimize the fouling wide spacing of the sections should be used. Tangent tubes prevent the formation of deposits that completely surround the tubes, and are therefore a better option than spaced tubes (see *Figure 10*).

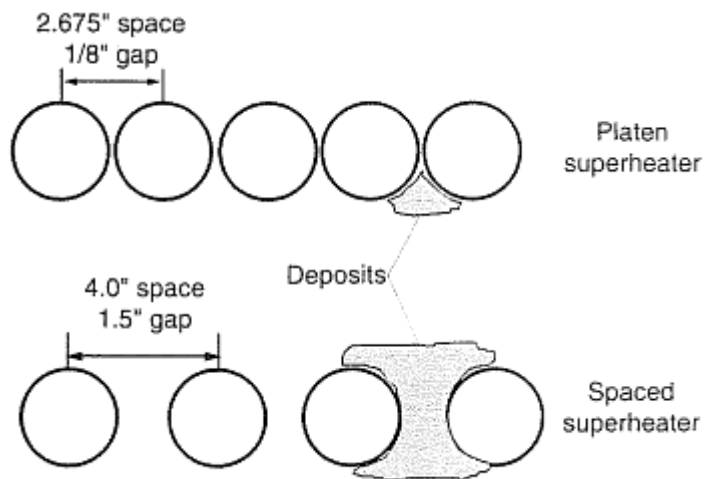


**Figure 10:** Deposit formation on tangent and spaced tube superheaters [Adams et al., 1997].

Typical surface temperatures of superheater tubes vary from 350 to 550 °C. The deposits surrounding the tubes start melting at a temperature of about 560 °C. However, an uneven flue gas temperature distribution may result in hot spots in the superheater region where tube temperatures rise above the temperature where the deposits start melting. Accelerated corrosion caused by the molten deposits may then occur [Shen et al., 1995].

### 5.2.5. The Boiler/Generating Bank

Steam is generated in both the convective steam generating section and the water walls of recovery boilers. The convective steam generating section is also referred to as the boiler bank or the generating bank and is located in the upper furnace between the superheater and the economizer. The purpose of the generating bank is to generate steam, and to lower the gas temperature to avoid steaming in the economizer.

The generating bank inlet gas temperature is typically about 400 to 500 °C, considerably lower than the furnace outlet temperature or superheater inlet gas temperature. Substantially more surface area is required in the generating bank compared to the superheater to lower the gas temperature due to the lower temperature difference and the higher heat transfer requirement in the generating bank. To achieve this large surface area, the tubes have to be closely spaced. The generating bank tubes usually have one-quarter to one half the spacing of the superheater tubes. A typical layout would be tubes of about 5-7 cm diameter and 10-12 cm side spacing [Adams et al., 1997]. This compact spacing increases the surface area per unit volume, but it also increases the gas velocity through the generating bank and decreases the effectiveness of the soot blowers. There is always a trade-off between boiler cost and operating problems. Boiler cost increases with the size of the generating bank, while operating problems, such as erosion and pluggage, decrease with increased boiler tube spacing. When the tube spacing is increased to prevent erosion and pluggage, other complications can occur due to tube vibration. The generating bank is the surface which is most likely to become plugged on a recovery boiler, mostly because of the close spacing of the tubes. To keep the generating bank clean the temperature should be kept low and the carryover that reaches the generating bank should be minimized.

The construction of the generating bank and the gas flow pattern are different for a two-drum boiler and a single-drum boiler [Adams et al., 1997].

### **5.2.6. The Economizer**

The purpose of the economizer is to raise the feed water temperature to a value just below the saturation temperature. The gas temperatures in the economizer are even lower than for the generating bank, so the heat transfer rate is reduced and a very large surface area is required.

The economizer exit gas temperature must never fall below about 150 °C. This temperature is just above the acid dew point where considerable corrosion can occur in the electrostatic precipitator, which captures the dust in the flue gases. These low temperatures could for example be avoided with a bypass in the economizer.

Two common types of economizers are cross-flow and parallel-flow. Most new boilers have parallel-flow economizers. The main operational problems related to gas flow are the same as for boiler banks, namely flow channelling and pluggage. [Adams et al, 1997; Salcudean, 1998; Shen et al., 1995; Smook, 1992]

## 6. Modelling of Recovery Boilers

Knowledge of the flow and combustion in recovery boilers is very difficult to obtain. Detailed measurements in an operating boiler are prohibitive because of the hostile environment. Even cold flow measurements are difficult to obtain due to the large size of the unit and are expensive due to the cost associated with the loss of production during the measurement work. Mathematical modelling of the flow and combustion in a boiler is an attractive alternative as the required details can be obtained and the effects of the operating parameters can be investigated without in-boiler measurements. Modelling provide comprehensive information throughout the entire boiler at relatively low cost, and can evaluate “what if” scenarios to improve operation and design.

The mathematical modelling of flows in recovery boilers is a complex task. The flow is fully three-dimensional as geometric symmetry is not present in all designs. Even when the boiler is geometrically symmetric, flow instabilities and jet interactions can cause major asymmetries in the flow patterns. The flow is often grossly unsteady, which also has been observed in physical models of boilers.

In mathematical modelling, the flow fields are obtained by solving the governing equations representing the conservation of mass, momentum and energy of the gas. Since the flow in recovery boilers is turbulent, conservation equations also have to be solved to simulate the effects of turbulence. To determine the temperatures a radiation model is needed. There is a very complex coupling between chemistry, flow and radiation in recovery boilers.

The gas phase and the black liquor droplets exchange mass, momentum and energy via source terms in the appropriate equation. For example, if a droplet evaporates water while crossing a cell, the water vapour mass is added to the cell mass balance through the source term.

During modelling, the momentum equation for each black liquor droplet is solved. Each droplet undergoes drying, pyrolysis, char burning and smelt reduction phases. Both drying and pyrolysis are assumed to be heat-transfer controlled. The char carbon gasification (burning) is assumed to occur via reactions with  $O_2$  and  $H_2O$ . The char burning rate is assumed to be controlled by the rate of mass transfer of  $O_2$  and  $H_2O$  to the char particle. The combustion is assumed to be controlled by the mixing rate.

One of the challenges is the modelling of turbulence. Despite the recent progress in turbulence simulation, such as more sophisticated models and large eddy simulations, engineers still need to use simpler models which give a reasonably accurate result, and at the same time assuring that the computations are feasible within reasonable time limits. Turbulence equations often have very large source terms compared to convective and diffusive terms in many practical situations.

Another issue in the modelling of the physics is establishing the boundary conditions. This is by no means a simple task in complex engineering problems.

When modelling transport phenomena in recovery boilers, two critical issues commonly observed are the need for high local resolution, for example at the air port levels, and the slow convergence of the solution algorithms, mainly due to the large domain of the boiler. It is important to reduce the computational time for complex problems. Calculations must

converge reasonably otherwise it is impractical to use CFD as a design and optimization tool. Using so called multigrid methods provides very good improvements of the convergence rate for a large number of cases. Multigrid methods solve on successively coarser grids and then transfer corrections to the solution back up to the original fine grid, and thereby increasing the speed of the convergence [FLUENT user guide].

Many large problems contain a wide range of scales, and therefore much denser grids should be used in regions in which strong gradients are present, and this high local resolution could be attained by using a block-structured segmented grid [FLUENT user guide]. The grid distribution is optimized using this technique, as the majority of the grid nodes can be concentrated in regions of interest. It should be noted that the complexity of the computer code increases significantly to provide such flexibility in defining the grid.

There is a lack of understanding of the radiation properties of the particles and of deposition in the heat exchanger region. The heat exchanger region is very complex and, therefore, a simplified treatment based on the assumption of porous medium is often necessary.

The limitation of computer power is another bottleneck in the recovery boiler fluid flow calculations. The improving models and computers increase the efficiency and reliability of the results from CFD modelling. But it is difficult to fully control and get enough knowledge about some recovery boiler phenomena.

CFD has been established as a major tool in process simulation and optimization. There are great challenges in computing real engineering processes with respect to setting up reasonable physical models as well as in carrying out the computations. The computations are demanding and require good understanding of the physical processes. The non-linearity of the equations, the complexity, the three-dimensionality, the turbulence and other associated transport phenomena of heat and species, result in a very complex problem which requires a sophisticated analyst. [Salcudean, 1998]

## **6.1. Modelling Fluid Flow in a Porous Medium**

Available results of numerical simulations for industrial boilers often focus on the physical and chemical processes in the lower furnace despite the importance of the fluid flow and heat transfer through the tube banks in the upper furnace. Accurate predictions of the superheater steam temperature is important both for evaluating the performance of the boiler and for estimating the possibility of fouling and corrosion of the superheater.

The small size of the components that build up the tube banks causes difficulties when modelling the upper furnace region. The grid usually has to be much coarser than the dimensions of the individual tubes to get a substantial solution within a reasonable time limit.

An alternative method for modelling the superheaters was developed by Patankar and Spalding [1974]. The method acknowledges the fact that fine geometric details of the tube banks cannot be captured by the grid commonly used in CFD simulations. Instead, modifications applying the porosity and distributed resistance concepts are introduced in the governing equations to simulate the effects due to the tube banks. A porosity factor based on the amount of flow blockage is introduced to take into consideration the flow acceleration

through obstructed passages. Distributed resistances are introduced as source terms in the momentum equations to simulate the pressure loss due to the tube bank obstructions.

This approach has several major advantages. One is that the grid can be much coarser than the dimensions of the individual tubes. Another advantage is that the same CFD solution algorithm can be applied in the entire domain since only the terms in the governing equations are modified. In this method experimental data for the pressure drop through the tube banks could be used [Tse et al., 1996].

## **7. Modelling of the Superheater**

In this chapter the models used to study the superheater are described. The models have been created by using the commercial code FLUENT. The computational mesh was created in GAMBIT.

### **7.1. The Purpose of the Modelling**

Observations of the superheater section in a couple of existing recovery boilers indicate that the flow pattern is not optimal from a heat exchange point of view. A zone of recirculation flow is likely to occur at the lower portions of the superheater, which reduces the heat transfer between the flue gas and the steam. This means that the resulting steam temperature is reduced. Optimizing the gas flow and thereby the heat transfer to the steam could result in a significant economical profit for the pulp mill.

The purpose of this study is to model the flue gas flow through the superheater in a recovery boiler and to investigate if this suspected recirculation zone exists and how it can be minimized.

The gas flow pattern in the upper furnace is influenced by many parameters, for example the geometry of the char bed and the design of the combustion air system. The construction of the superheater and the size and shape of the bull nose as well as the temperature and velocity of the gas also affect the gas flow.

### **7.2. Modelling in Fluent**

CFD is an engineering tool for modelling fluid flow, heat and mass transfer and chemical reactions in complex geometries by solving the set of governing mathematical equations. The code used in this work was FLUENT 6.2 from Fluent Inc.

In any CFD model it is necessary to make certain assumptions and the predicted results have thereby some limitations. The size of the grid elements and the suitability of their layout for the geometry being studied is an uncertainty with all CFD studies. The accuracy of the mathematical description of turbulence is another. More specific to current investigation is the uncertainty in the inlet flow conditions to the region of interest.

CFD solutions only represent a steady-state situation since unsteady-state modelling is extremely computational intensive. Real systems are, however, always time dependent, which should be kept in mind when evaluating the results.

The most important features of the models are described below. Geometry, material and boundary conditions are presented as well as turbulence and radiation models used.

## 7.2.1. Geometry and Materials

The region modelled in this study is the upper region of a boiler extending from the bull nose, which in this case is located about 40 m above the furnace bottom, to the outlet of the boiler bank (see *Figure 11*). This region is characterized as one with a single inlet and exit, and no significant chemical reaction and heat release.

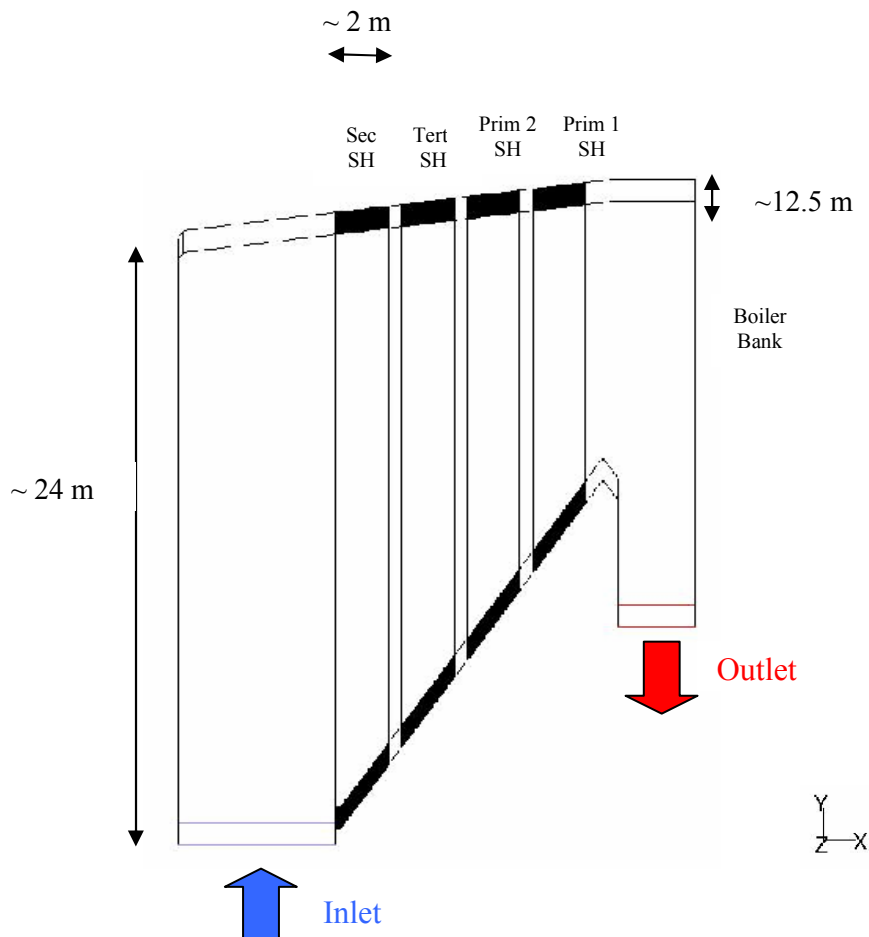


**Figure 11:** The region modelled.

In *Table 3* some characteristic data for the superheater sections of the boiler being modelled are shown.

**Table 3:** Characteristic data for the superheater sections of the boiler.

|                                   | Secondary SH | Tertiary SH | Primary SH 2 | Primary SH 1 |
|-----------------------------------|--------------|-------------|--------------|--------------|
| Number of platens, -              | 39           | 39          | 39           | 39           |
| Number of tubes in each platen, - | 38           | 38          | 20           | 20           |
| Tube outer diameter, m            | 0.050        | 0.050       | 0.050        | 0.050        |
| Tube thickness, m                 | 0.0063       | 0.0071      | 0.0063       | 0.0056       |
| Tube spacing longitudinal, m      | 0.053        | 0.053       | 0.100        | 0.100        |
| Tube spacing transverse, m        | 0.312        | 0.312       | 0.312        | 0.312        |
| Heating surface, m <sup>2</sup>   | 5396         | 4625        | 3852         | 3079         |

**Table 4:** Example of typical steam and flue gas temperatures and absorbed heat in the different superheater sections [Lundborg, 2005].

|                           | Secondary SH | Tertiary SH | Primary SH 2 | Primary SH 1 |
|---------------------------|--------------|-------------|--------------|--------------|
| Flue gas temp. before, °C | 801          | 619         | 534          | 455          |
| Flue gas temp. after, °C  | 618          | 536         | 459          | 410          |
| Steam temp. before, °C    | 318          | 386         | 304          | 285          |
| Steam temp. after, °C     | 465          | 450         | 354          | 307          |
| Absorbed heat, MW         | 32.79        | 14.34       | 12.85        | 7.53         |

Table 4 illustrates typical values of the steam and flue gas temperatures and the amount of heat absorbed in the different superheater sections from a boiler operating at a black liquor firing rate of 2100 t dry solids (DS)/ 24 h with a heating value of 14.1 MJ/kg DS.

In the upper boiler heat is transferred from the hot flue gas to the steam. The objective is to make use of the energy of the hot flue gas and produce superheated steam and possibly generate electricity. The flue gas is flowing through the boiler from the char bed where it is produced over the nose arch, the superheater, the boiler bank, and finally the economizer. The steam is flowing up and down inside the superheater tubes, while the flue gas is flowing outside the tubes.

A flow sheet of the upper furnace is shown in Figure 12. The saturated steam from the boiler drum flows through the primary superheater 1, the primary superheater 2, the secondary superheater and finally the tertiary superheater. The steam flow is parallel to the flue gas flow in the secondary and tertiary superheaters, while it runs counter to the flue gas flow in the primary superheaters. There are two attemperators located between the secondary and tertiary superheaters, and between the secondary and 2nd primary superheaters, which purpose is to avoid overheating any section.

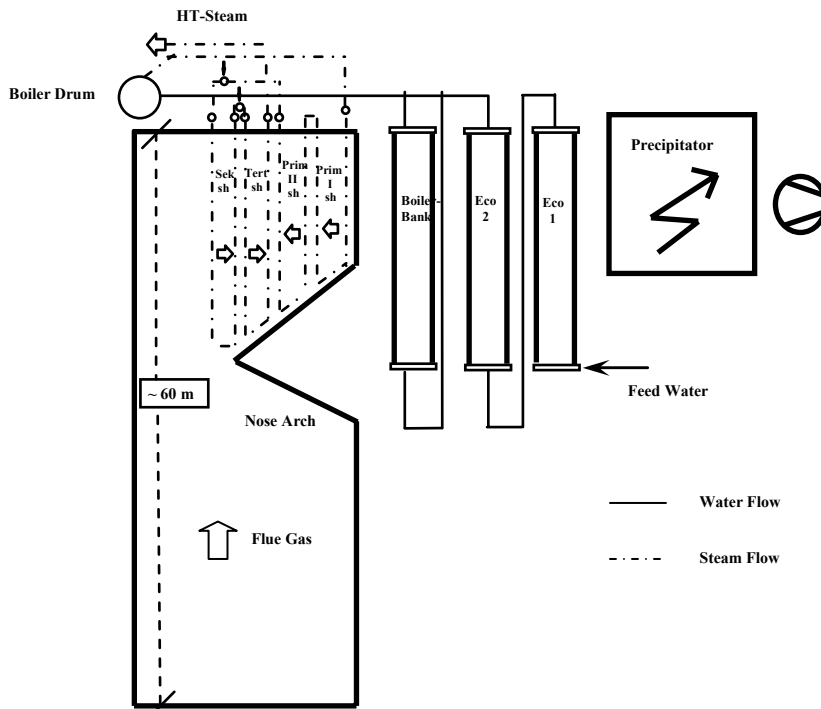


**Figure 12:** Flow sheet of the upper furnace in a recovery boiler.

The flow in the upper boiler consists of a three phase system. In this study the combustion gases in the upper furnace are approximated as air, which is assumed to be an incompressible ideal gas.

The superheater tubes are vertical and laid out in rows aligned with the gas flow path. The superheater consists of four groups of parallel platens of closely spaced in-line tube bundles. The parallel platens are installed with constant spacing, separating the gas flow into a number of channel-like flows bounded by the platens. This layout restricts cross flow.

The size of the bull nose is indicated by the horizontal flow area in the region of the bull nose compared to that of the open furnace area. This ratio for the recovery boiler modelled is about 50%, which corresponds to a relatively large bull nose.

In this work a couple of different cases were studied, which included both geometries in 2D and 3D. At first, a two-dimensional plane of the upper boiler was studied; both with the superheater tubes modelled as single cylindrical tubes (see *Figure 13*) and as rectangular packages (see *Figure 14*). The purpose was mainly to investigate if the tubes could be approximated as rectangular packages, which would simplify the calculations greatly.



**Figure 13:** The 2D plane with the superheater tubes modelled as cylindrical tubes.

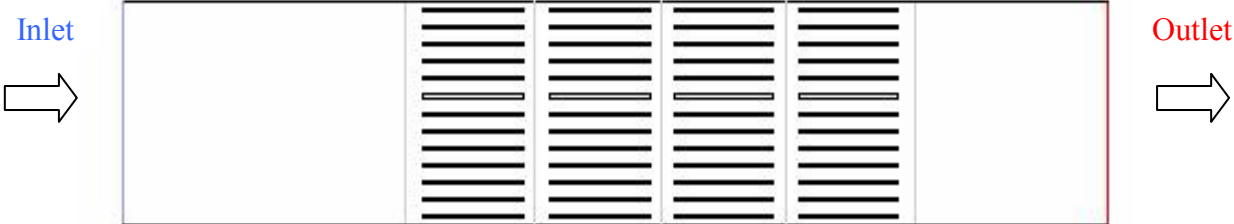


**Figure 14:** The 2D plane with the superheater tubes modelled as rectangular packages.

The main objective of this work was, however, the 3D modelling. A result of the 2D calculations is that modelling the superheater tubes as rectangular packages is an acceptable approximation. At first, the entire domain was studied. It is, however, desirable to increase the number of cells in the superheater area, but this is not possible when studying the entire domain since the number of cells is already large, about 1 million. To achieve an increased cell concentration, a smaller three-dimensional domain was studied. This is possible because assuming symmetry of the region.

## 7.2.2. Boundary Conditions

The boundary conditions have to be specified when setting up the model. They strongly influence the predicted results and should therefore be defined carefully.

The inlet was defined as a velocity inlet and the outlet as a pressure outlet. The walls of the boiler as well as the boiler bank were defined as wall boundary conditions.

The inlet flow conditions to the region being modelled are those of the upper region of the recovery furnace. These flow conditions depend strongly on the geometry of the char bed, and the number, layout, and velocity of the combustion air jets. The inlet conditions to the 3D domain in this study were determined by outlet flow profiles of the lower furnace from calculations performed at AF-Process AB [Jacoby, 2005].

In order to test the impact of the inlet flow profile on the model predictions, the results when using different profiles were compared. To investigate the influence of the shape of the bull nose, it can be changed by changing the angle of the upstream face of the bull nose. The inlet flow profiles represent different shapes of the bull nose.

The superheaters were modelled as porous zones. This means that the pressure drop due to the superheaters is simulated by introducing empirical coefficients of flow resistance as source terms in the momentum equations. The coefficients of flow resistance depend on the geometry, the tube diameter, the tube spacing and the flue gas velocity. In the flow direction and the transverse direction the coefficients were calculated by using the following relation [Tse et al., 1996]:

$$C_2 = \frac{4f'}{S_L} \cdot \left( \frac{S_T}{S_T - D} \right)^2 \quad [\text{m}^{-1}]$$

where

$$f' = \left\{ 0.044 + \frac{0.08 S_L / D}{[(S_T - D) / D]^{[0.43 + 1.13 D / S_L]}} \right\} \text{Re}_{D, \max}^{-0.15}, \text{ which is the empirical friction factor [Jakob, 1938].}$$

$$\text{Re}_{D, \max} = \rho U_{\max} D / \mu$$

D = tube diameter, m

S<sub>L</sub> = longitudinal tube separation, m

S<sub>T</sub> = transverse tube separation, m

In the axial direction the coefficients were calculated by using the following relation [Tse et al., 1996]:

$$C_2 = 0.184 \cdot \text{Re}_{L_H}^{-0.2} / L_H \quad [\text{m}^{-1}]$$

where

$$\text{Re}_{L_H} = \rho |U_3| L_H / \mu$$

$$L_H = \frac{4}{\pi} \cdot \frac{S_T \cdot S_L - \pi D^2 / 4}{D}, \text{ which is the hydraulic diameter, m.}$$

See Appendixes D and E for detailed description and calculation of the coefficients of flow resistance. *Table 5* shows a summary of the coefficients of flow resistance for the different superheater sections. For an illustration of the flow directions of the flue gas see *Figure 26*.

**Table 5**

| <b>Coefficients of Flow Resistance</b> |                                 |                                       |                                  |
|--|---------------------------------|---------------------------------------|----------------------------------|
|  | Flow Direction, m <sup>-1</sup> | Transverse Direction, m <sup>-1</sup> | Axial Direction, m <sup>-1</sup> |
| Secondary SH                           | 1.70                            | 4360                                  | 0.105                            |
| Tertiary SH                            | 1.72                            | 7300                                  | 0.136                            |
| Primary SH 2                           | 1.31                            | 14.1                                  | 0.0406                           |
| Primary SH 1                           | 1.31                            | 11.4                                  | 0.0356                           |

The temperatures of the gas and the walls of the boiler vary with time and location in the boiler. The average gas temperature is approximately 750 °C at the inlet to the upper furnace being modelled and approximately 350 °C at the exit from the generating bank.

Because the main purpose of this study was to investigate the gas flow pattern in the superheater region, and not the heat transfer, the surface temperature was specified as a constant value for each superheater section and the walls of the boiler.

### 7.2.3. Turbulence and Radiation Models

All CFD codes attempt to provide a numerical solution of the Navier-Stokes equations and the energy equation. For turbulent flows, a description of the turbulent transport of energy and momentum is required. Despite the development of more sophisticated turbulence models it is still common to use simpler models which give reasonable results within shorter calculation time.

In Fluent several turbulence models are available, which are all suited for different flow problems. The well-known k-ε model is often used. In this study the realizable k-ε model [FLUENT user guide] was used because experiences at AF-Process AB show that this model is preferred when simulating recirculation flows. This turbulence model consists of two equations, which means that it is not especially computational intensive. In the 2D model another turbulence model, the Spalart-Allmaras model, was used. This simple model only consists of one equation, which means that a shorter calculation time is required compared to the k-ε model.

A radiation model is needed to simulate the radiation occurring inside the boiler and to determine the temperatures. The model used in this study was the P1 model [FLUENT user guide] because it is relatively simple and well known.

#### 7.2.4. Mesh

The computational mesh was created in Gambit 2.2.

The mesh (or grid) consists of cells and the solution to a flow problem (velocity, pressure, temperature etc.) is defined at nodes inside each cell.

The accuracy of the solution and its cost in terms of necessary computer hardware and calculation time are dependent on the fineness of the grid. A large number of cells give, in general, better solution accuracy. Optimal meshes are often non-uniform; finer in areas where large variations occur from point to point and coarser in regions with relatively little change.

In this study the grid of the 2D models consists of quadrilateral cells. In the case where the superheaters are modelled as circular tubes the grid contains approximately 340 000 cells compared to 90 000 cells when they are modelled as rectangular packages. In the first case the cells near the boundary of the tubes are adapted to increase the concentration of cells where high accuracy is most important (see *Figure 16*).

In the 3D models the grid mainly consists of hexahedral cells, but also tetrahedral cells. In the model of the entire domain the grid contains approximately 1 015 000 cells and in the model of the smaller sub-domain approximately 1 550 000 cells, which represents a great increase in cell density.

# 8. Results

## 8.1. 2D Modelling

In the first two-dimensional case the superheater tubes were modelled as single circles and in the second case they were modelled as rectangular packages. The main purpose of the modelling in 2D was to investigate if the tubes could be approximated as rectangular packages, which would simplify the calculations greatly.

In the 2D models the velocities at the inlet to the domain were estimated compared to in the 3D models where the inlet profiles were taken from actual calculations. Since the objective of the 2D modelling was to compare the results of case 1 and case 2, the chosen values of these velocities are not particularly important as long as they are identical for the two cases. However, when choosing the velocity vectors one should remember that the purpose is to investigate if flow in the transverse direction exists. In *Figure 15* the chosen velocity vectors at the inlet are shown.

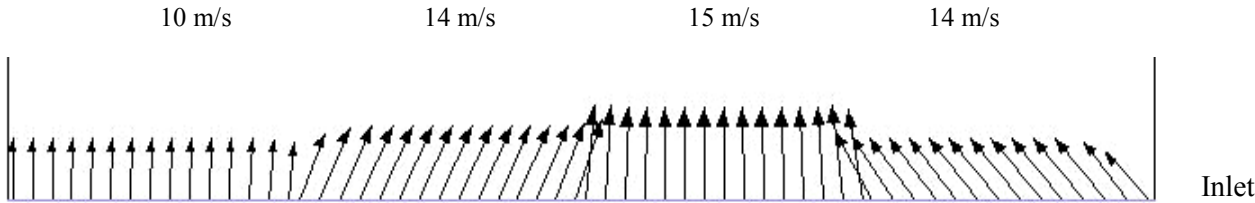


*Figure 15: The inlet velocity vectors to the 2D geometry.*

### 8.1.1. Case 1: The Superheaters as Cylindrical Tubes

The mesh consists of approximately 340 000 cells. *Figure 16* shows the structure of the mesh, which has been refined near the boundary of the tubes where high gradients are present.

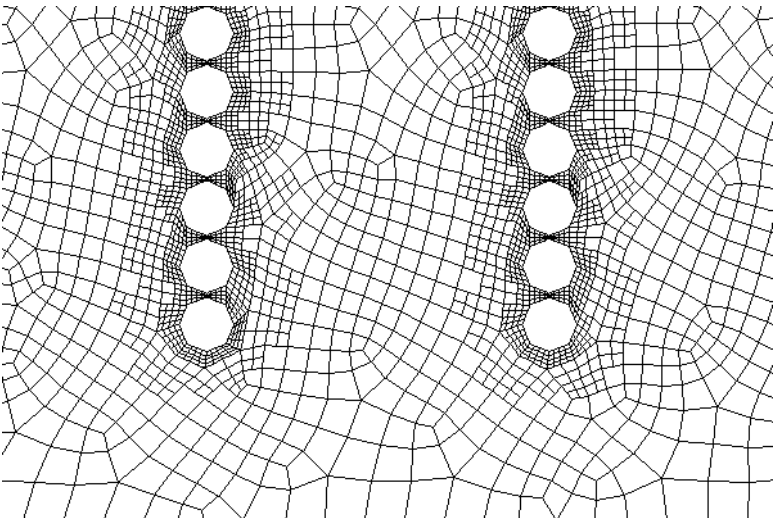


*Figure 16: 2D mesh – the superheaters as cylindrical tubes.*

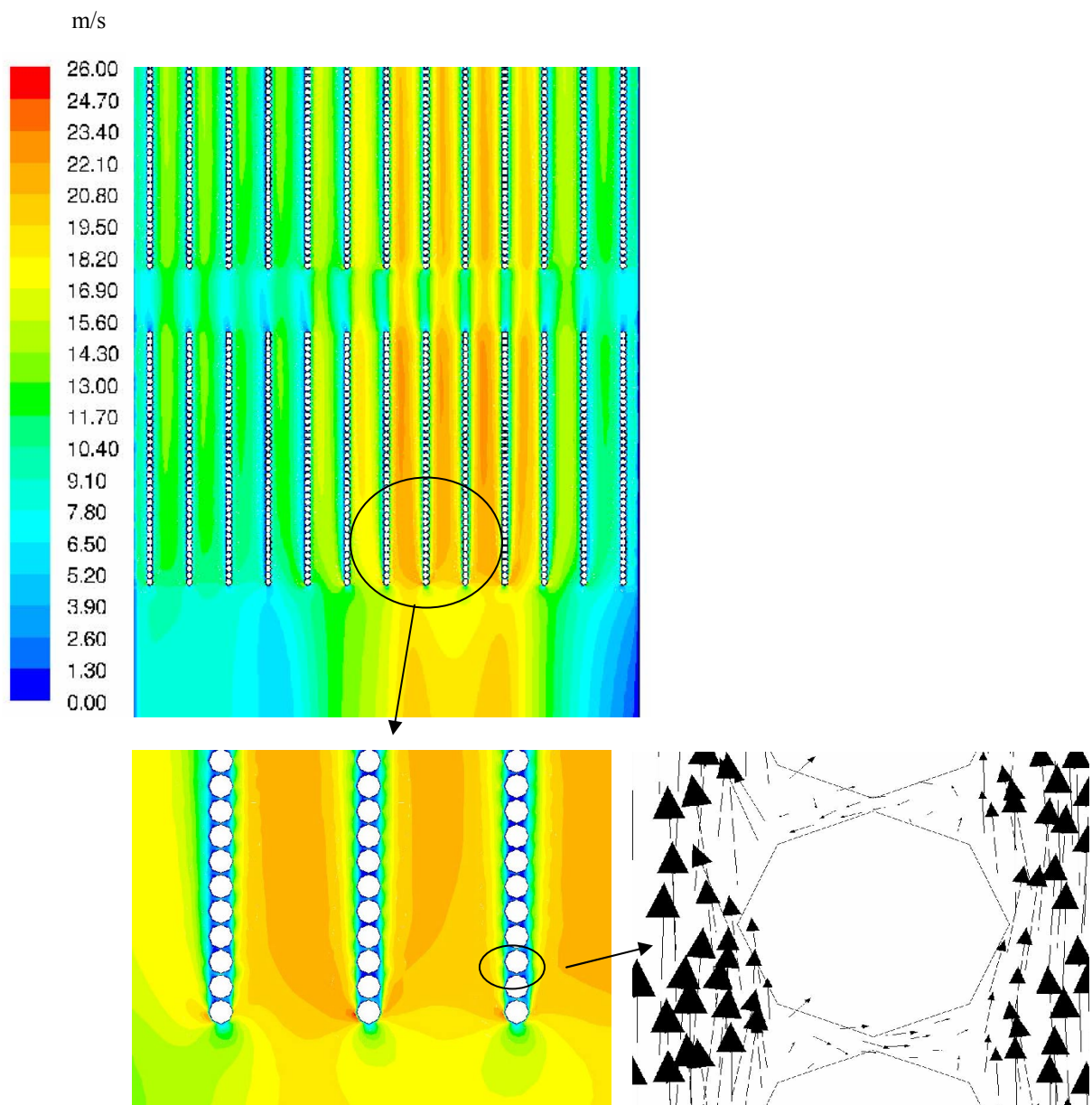


**Figure 17:** Velocity profile – case 1

One interesting task to investigate when modelling the tubes as circles was if the gas would flow between the tubes. Considering that the tubes are very closely spaced one could suspect that the gas flow would be minimal through these small passages. The velocity profile obtained from the calculations is shown in *Figure 17*. From these figures it can be stated that part of the gas is flowing between the tubes. However, the gas is flowing at a very low velocity between the tubes compared to the mean velocity of the gas. This means that the mass flow through the small passages in between the tubes in the transverse direction of the flow is small.

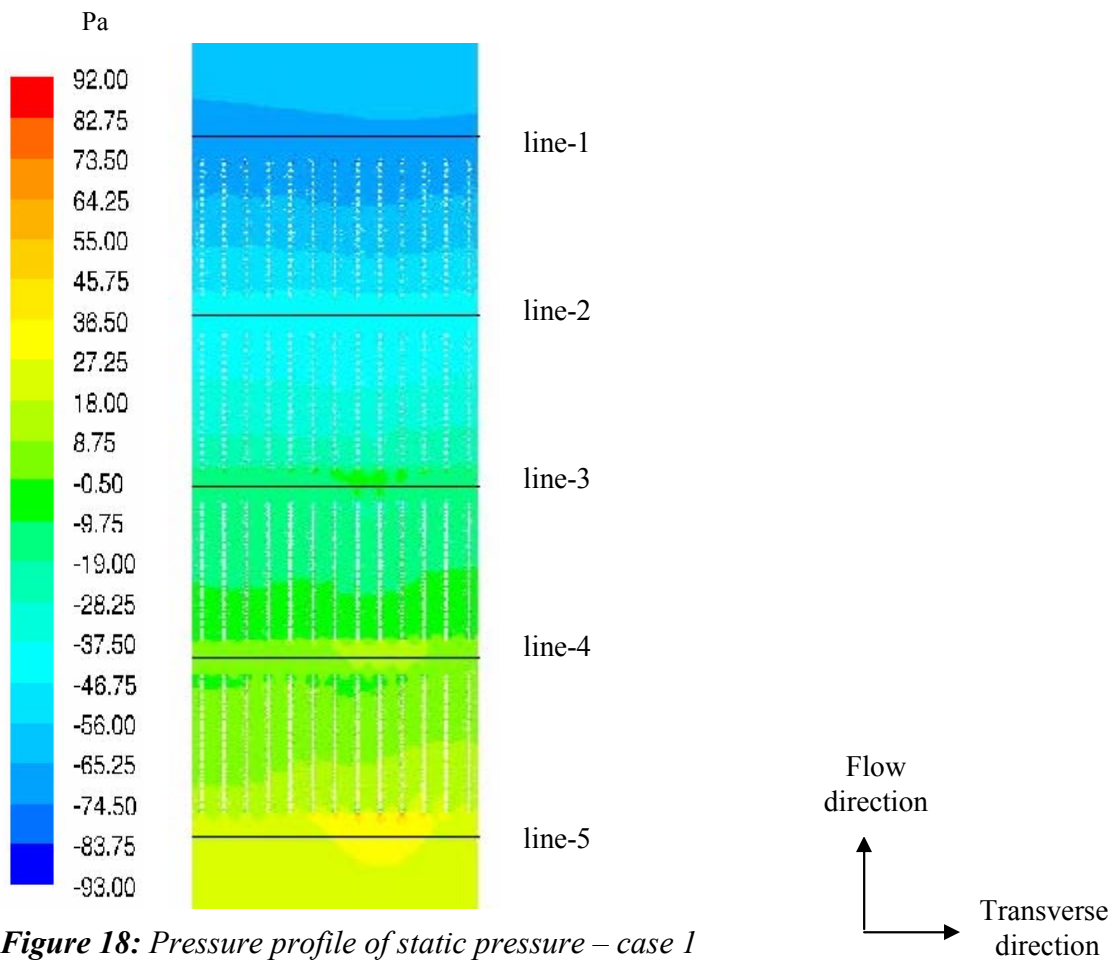


**Figure 18:** Pressure profile of static pressure – case 1

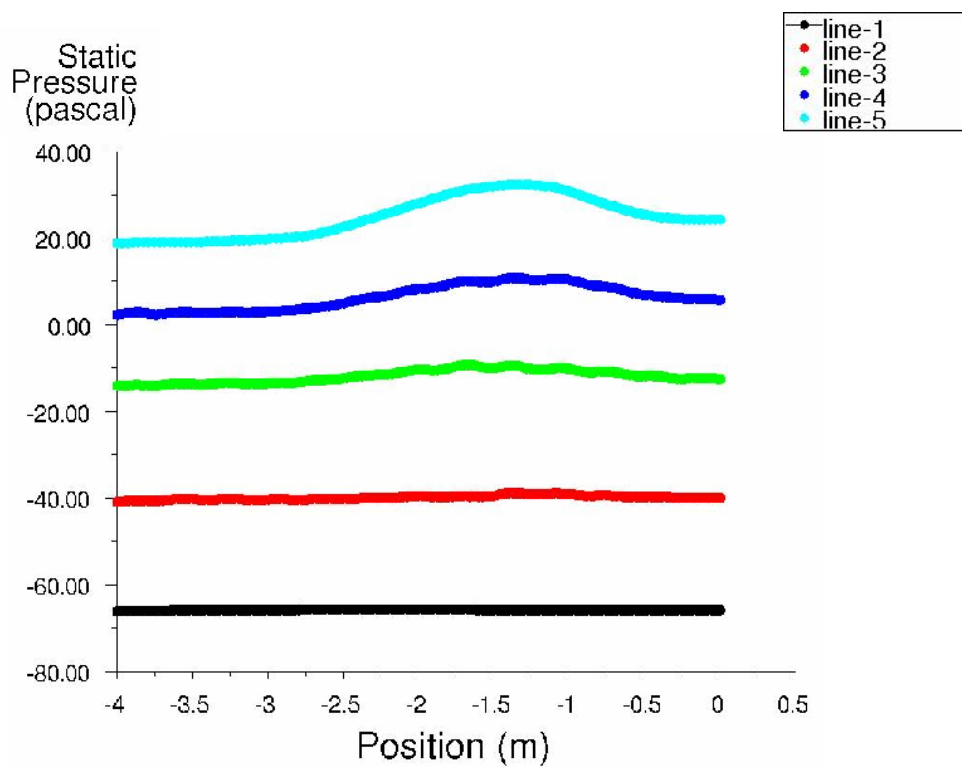


**Figure 19:** Pressure plot – case 1

The pressure plot shown in *Figure 19* illustrates the pressure drops across the superheaters in the flow direction. The position-axis represents the position along the transverse direction of the flow. The positions of the lines 1 to 5 where the pressures are evaluated are shown in *Figure 18*.

From the pressure plot above it can be stated that the pressure drops across the superheaters in the flow direction of the gas are small. The largest pressure drop across one of the superheaters is about 30 Pa. As one can see in the plot, the pressure drop is greater at positions between -1 m and -1.5 m. This is caused by the inlet velocity profile and represents a location in the geometry where gas flowing in different directions collides. In the transverse direction of the flow there is very little variation in pressure.

### 8.1.2. Case 2: The Superheaters as Rectangular Packages

The mesh consists of approximately 90 000 cells. *Figure 20* shows the structure of the mesh.

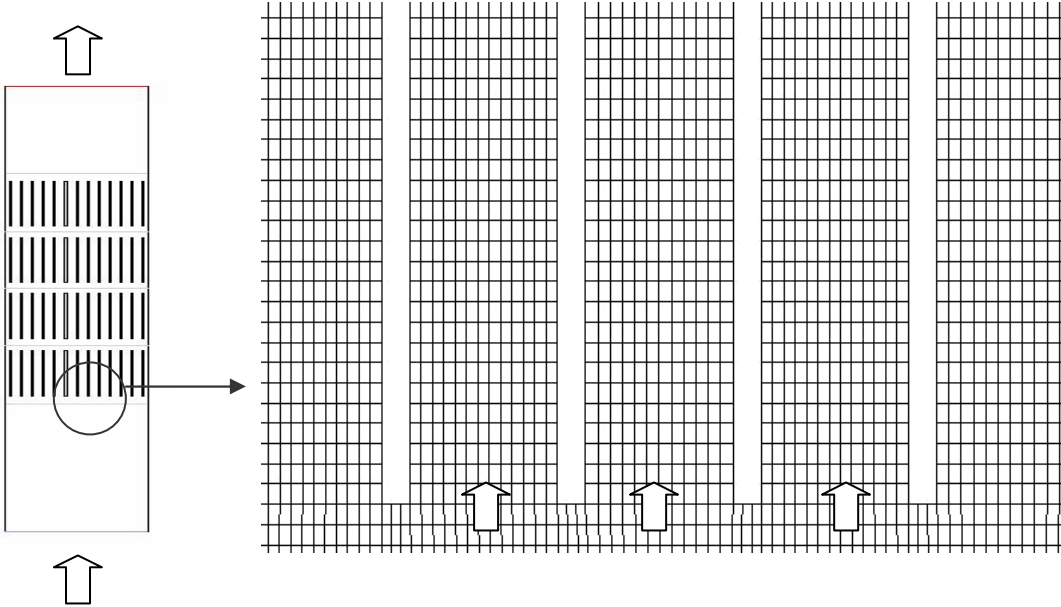


**Figure 20:** 2D mesh – the superheaters as rectangular packages. The arrows show the direction of the flow.

The velocity profile of case 2, where the superheater tubes are modelled as rectangular packages, is shown in *Figure 21*.

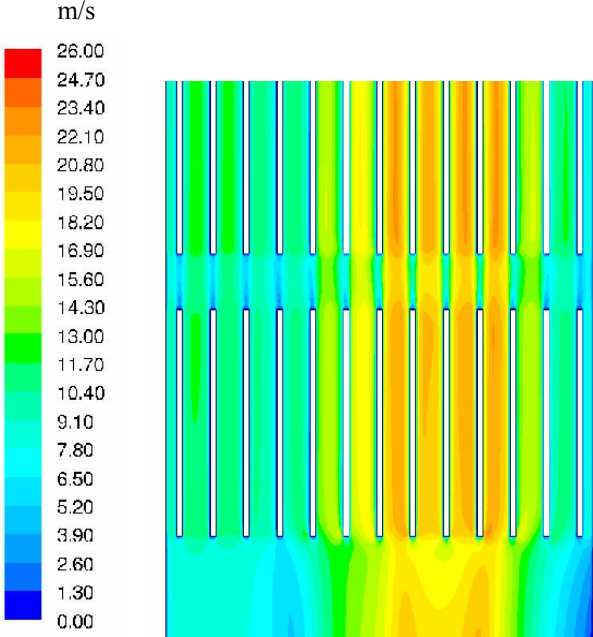


**Figure 21:** Velocity profile – case 2

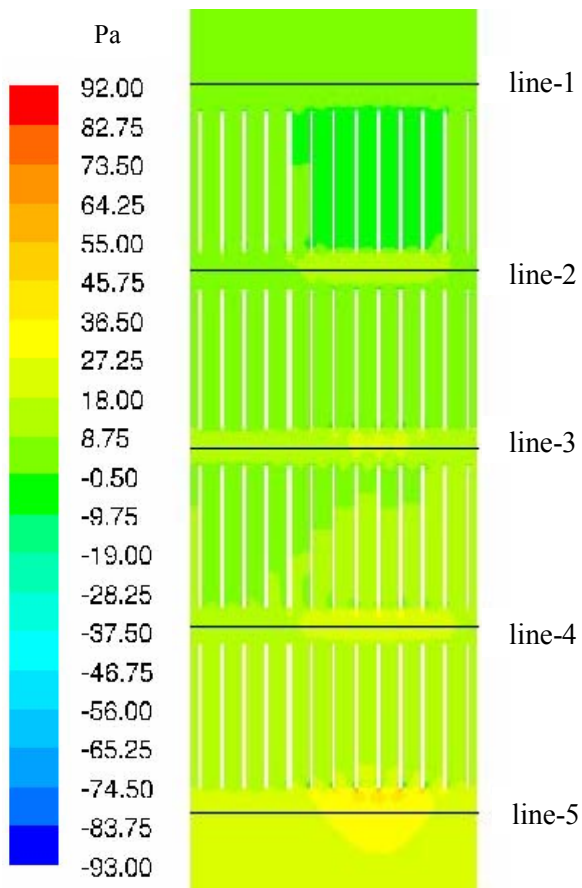


**Figure 22:** Pressure profile of static pressure – case 2

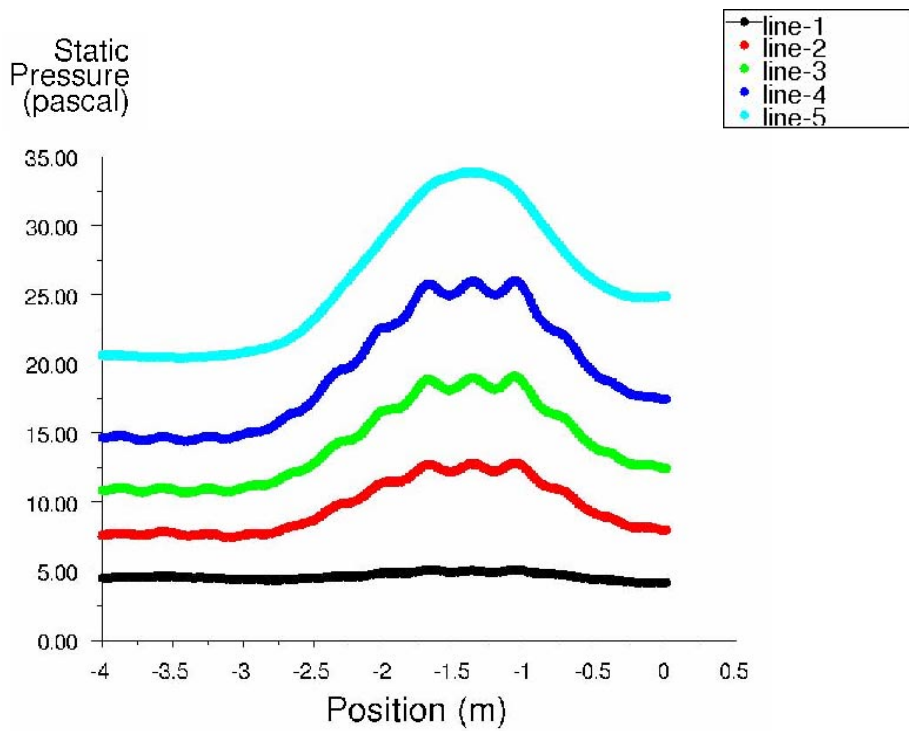


**Figure 23:** Pressure plot – case 2

The plot above shows that the pressure drop across the superheaters is very small when modelling them as rectangular packages. The largest pressure drop is about 8 Pa. Since the inlet velocity vectors are the same as in case 1 the pressure drop is greater at positions between -1 m and -1.5 m also in this case. In the transverse direction of the flow there is very little variation in pressure.

### 8.1.3. Conclusions from the 2D Modelling

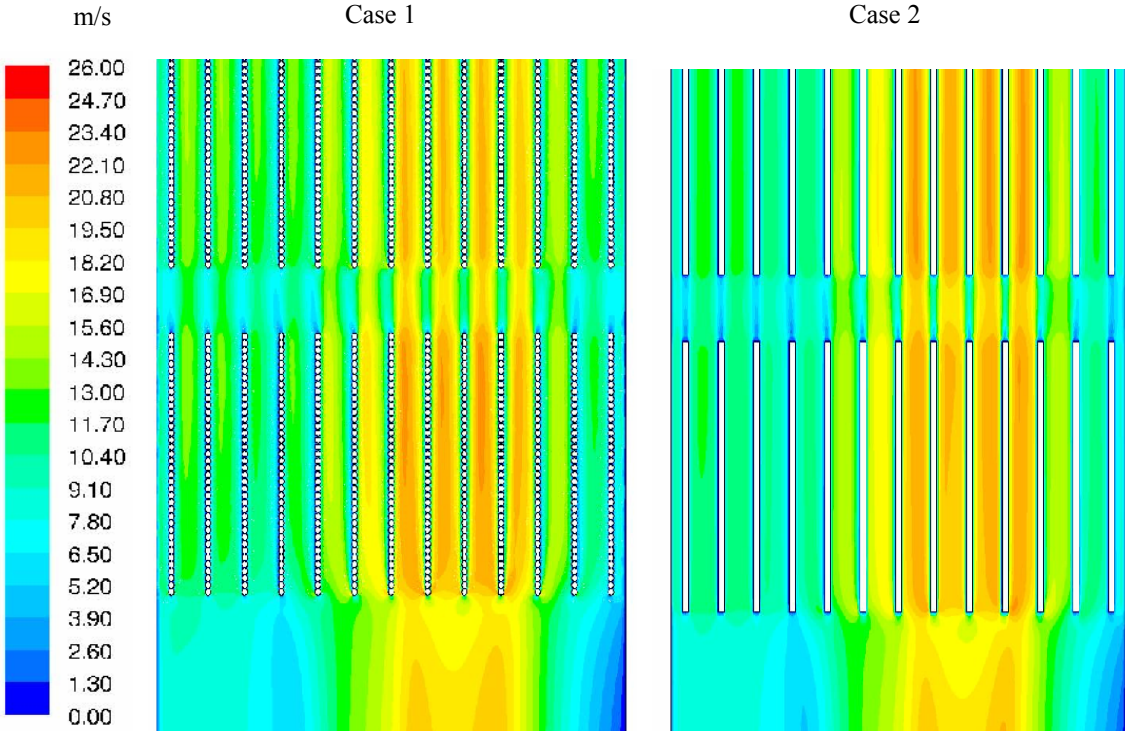


Figure 24: Comparison of the velocity profiles of case 1 and case 2.

When comparing the velocity contours of the two cases some differences can be observed. The superheaters have an equalizing effect on the velocities along the flow direction of the gas. As shown in Figure 24, the higher velocities observed around the middle of the geometry decrease and the lower velocities observed near the walls increase along the flow direction. This effect is more developed in case 1. In case 2 the velocity is almost constant in the direction of the flow. When modelling circular tubes turbulent eddies occur in the flow to a greater extent than when the tubes are modelled as rectangular packages where the flow is more channel like. These eddies claim energy which result in greater changes in velocity and pressure along the direction of the flow. Another difference between the two cases is that the gas flow channels in between the superheaters are more weakened in case 1 compared to in case 2. As discussed above and shown in Figure 17 part of the gas is flowing in between the tubes when modelling the superheaters as single tubes. When the tubes are modelled as rectangular packages these flows in the transverse direction naturally do not exist.

When examining the pressure plots of the two cases (see Figure 19 and Figure 23) the most important conclusion is that the pressure drops across the superheaters are very small in both cases. The pressure drops are larger in case 1 compared to in case 2 due to the modelling of

the tubes as single, cylindrical tubes, which results in a more complex flow pattern with flow in the transverse direction and formation of eddies.

The fact that the pressure drops across the superheaters are small and that the differences in pressure drops between the two cases are small, together with the fact that the gas is flowing at very low velocity in the transverse direction in between the tubes, indicate that the arrangement of the tubes can be simplified as rectangular packages. The most important result from the 2D calculations is that modelling the superheater tubes as rectangular packages is an acceptable approximation. Because of this conclusion the superheater tubes are modelled as rectangular packages of porous zones in the 3D simulations.

### 8.2. 3D Modelling

In the three-dimensional models the superheaters were modelled as rectangular packages of porous zones. Two different geometries were modelled; the entire domain and a smaller part of the domain, a sub-domain. *Figure 25* illustrates the geometry of the domain. The sub-domain consists of a smaller part of the domain, about  $\frac{1}{4}$ , in the direction of the z-axis. Two different flow inlet profiles, called 1 and 2, were investigated.

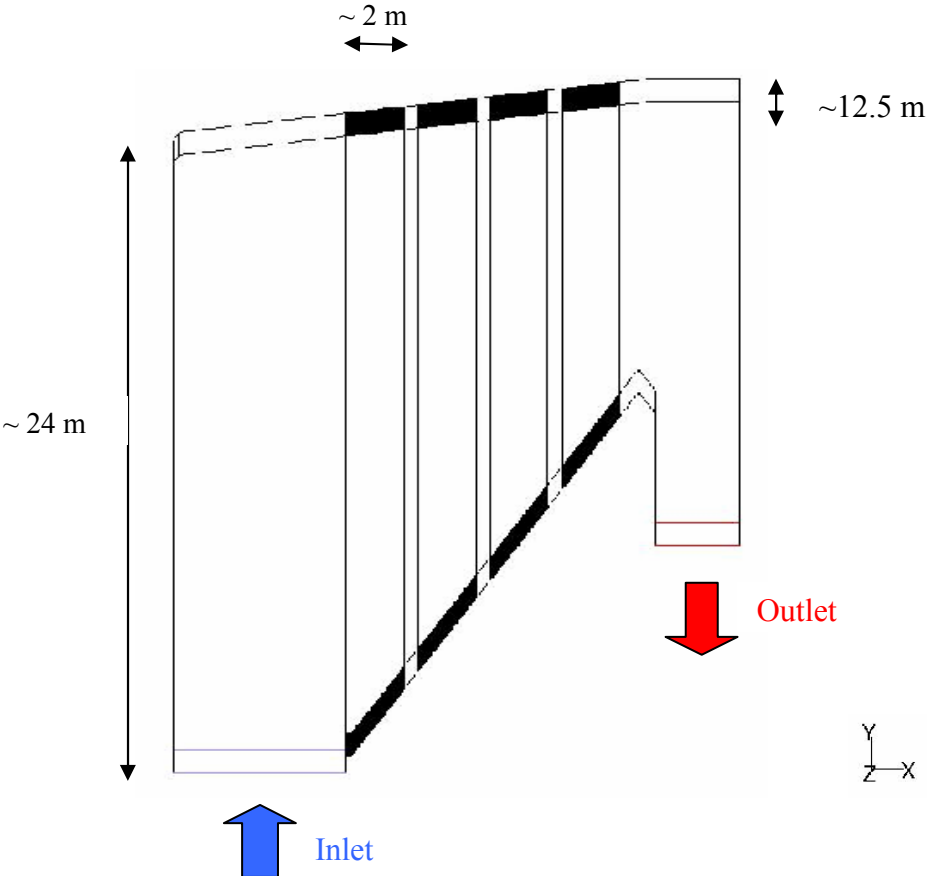


**Figure 25:** The 3D domain.

Figure 26 illustrates the nomenclature of the flow directions of the flue gas.

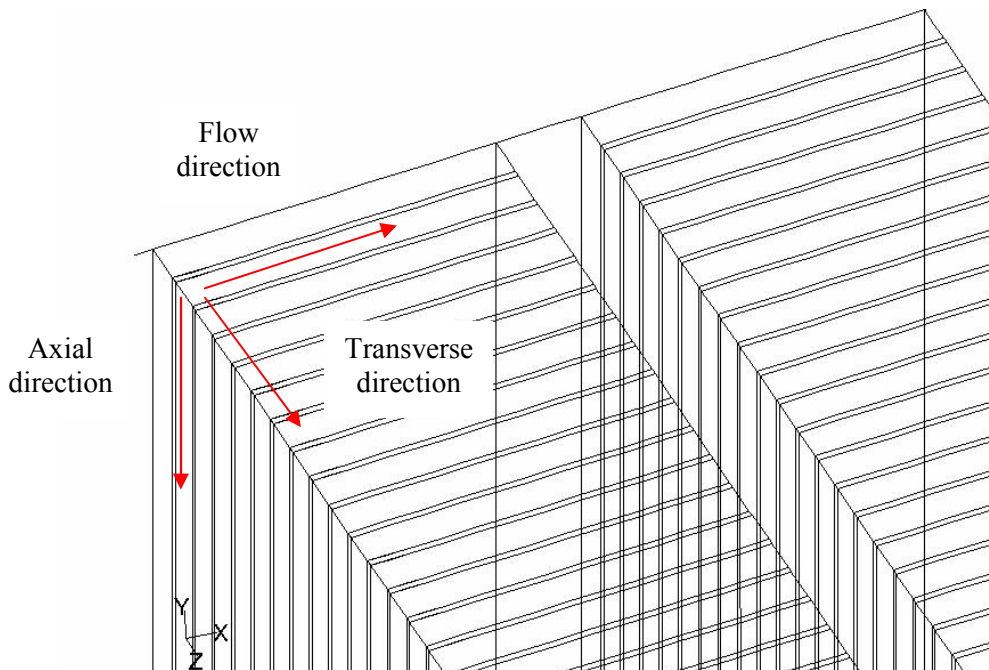


Figure 26: The flow directions of the flue gas.

### 8.2.1. Case 3: Modelling the Entire Domain, Inlet Flow Profile 1

The mesh consists of approximately 1 015 000 cells. Figure 27 shows the structure of the mesh, which consists of both hexahedral and tetrahedral cells. When constructing the mesh the priority is to achieve a high cell concentration in the superheater area. In this case tetrahedral cells are used to join areas of different cell concentrations.

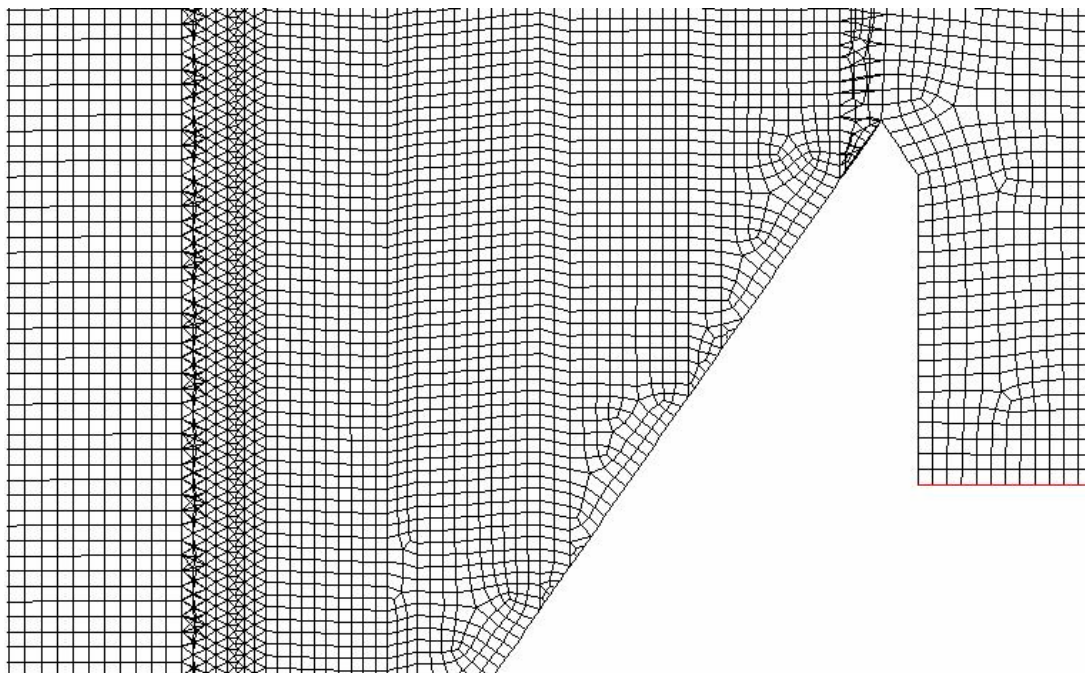
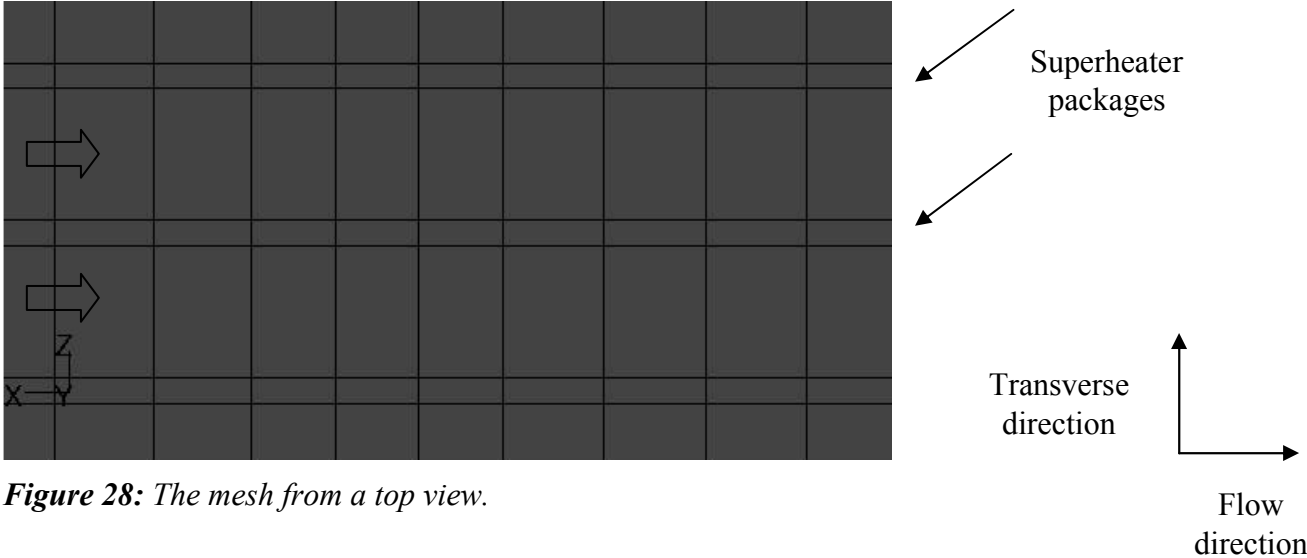


Figure 27: The structure of the mesh from a side view.

In *Figure 28* part of the mesh from a top view of the boiler is shown. Observe that the mesh only consists of one cell in the transverse direction of the superheater packages. The desire is to have a higher concentration of cells in this area, but in this case the total number of cells is already large.



**Figure 28:** The mesh from a top view.

Inlet profile 1 is shown in *Figure 29*. This profile represents a sloping bull nose of rounded shape (see *Figure 30*). The purpose of the bull nose is both to protect the superheaters from radiation, and to guide the combustion gases and produce a uniform flow over the heat transfer surface.

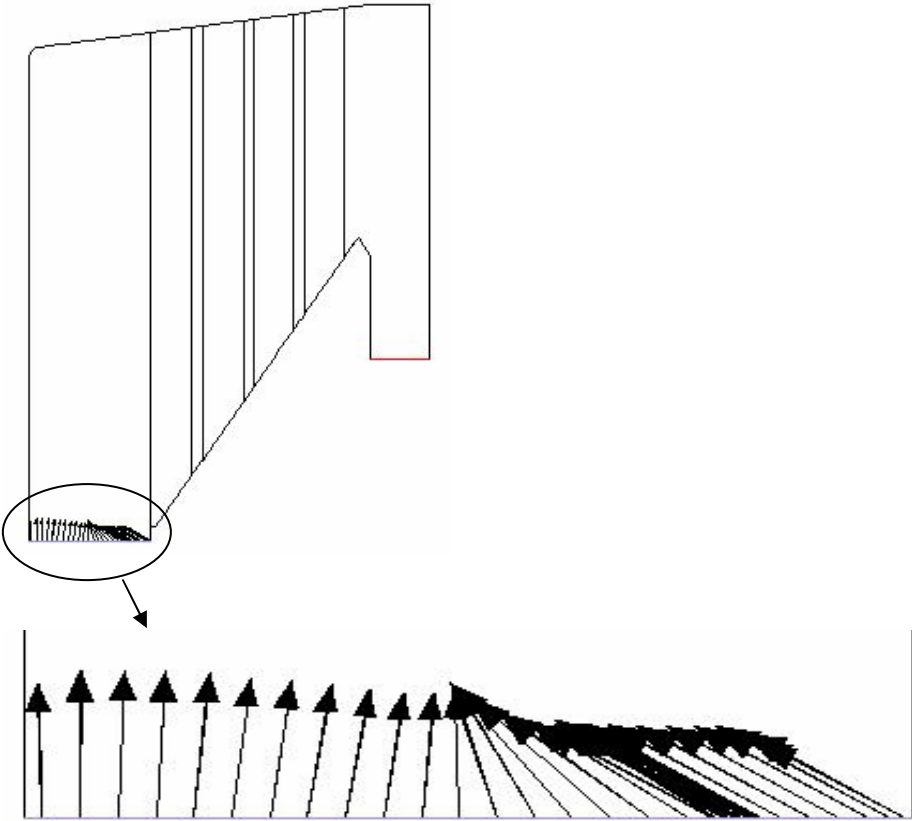


**Figure 29:** Inlet flow profile 1.

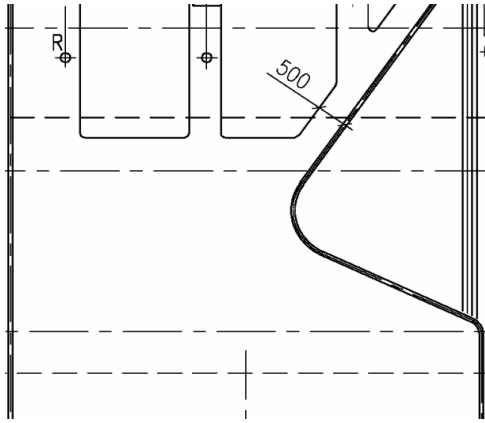


**Figure 30:** Illustration of a rounded, sloping bull nose.

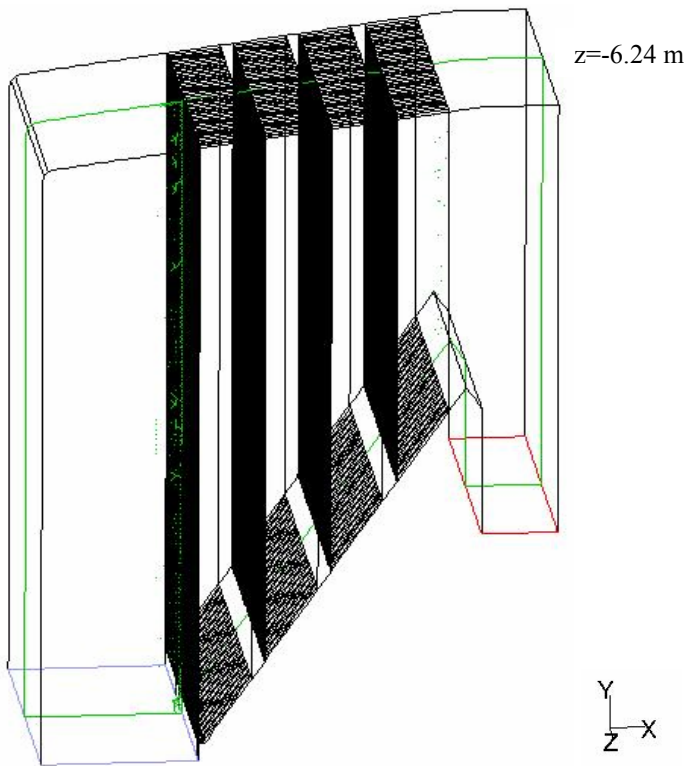


**Figure 31:** A cross-section in the middle of the domain at  $z=-6.24$  m.

The contours of velocity magnitude of a cross-section in the middle of the domain (see *Figure 31*) are shown in *Figure 32*. A channelled flow is obtained where the mean velocity of the flue gas is higher. The velocity generally decreases along the path, with the exception of an increase at the outlet of the boiler bank caused by the sudden contraction. The velocity contours indicate that the flow accelerates at the location of the bull nose then rises well above the bull nose before turning toward the boiler bank. A large zone of recirculation is observed located at the lower part of the superheaters as shown in *Figure 33*. As discussed earlier, this recirculation could result in reduced heat transfer between the gas and the steam or even negative heat transfer. The temperature of the gas could fall below the temperature of the steam when unfavourable conditions exist in the boiler, which would cause heat transfer

from the steam to the gas. In this area of recirculation the velocity of the gas is very low; the gas is nearly standing still, which results in a long residence time in the boiler. Another zone of recirculation is observed in the upper left-hand corner of the boiler.

Design conditions for the superheater assume that the gas that passes through the superheater section is uniform. Differences from uniformity in velocity or temperature reduce the heat absorption, which causes low steam temperature and/or excessive gas temperature entering the generating bank. In an ideal case the flue gas flows through the boiler at the same velocity in a so called plug flow. In reality the flow is often channelled, which means that a region of higher velocity is formed in the centre of the channel. The desire is to minimize the flow channelling, which for example could be attained by using a wide spacing of the superheater sections. It is also favourable to use superheater platens instead of spaced tubes. Furthermore, the ideal flow pattern would not contain any zone of recirculation flow.

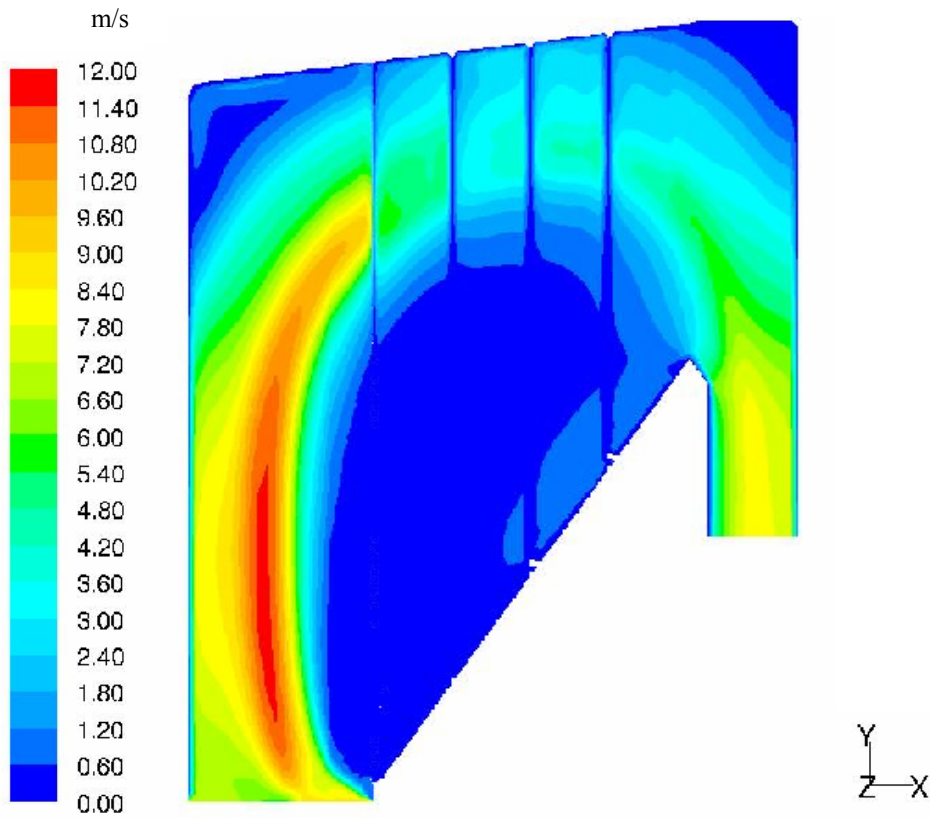


**Figure 32:** The velocity contours of case 3.

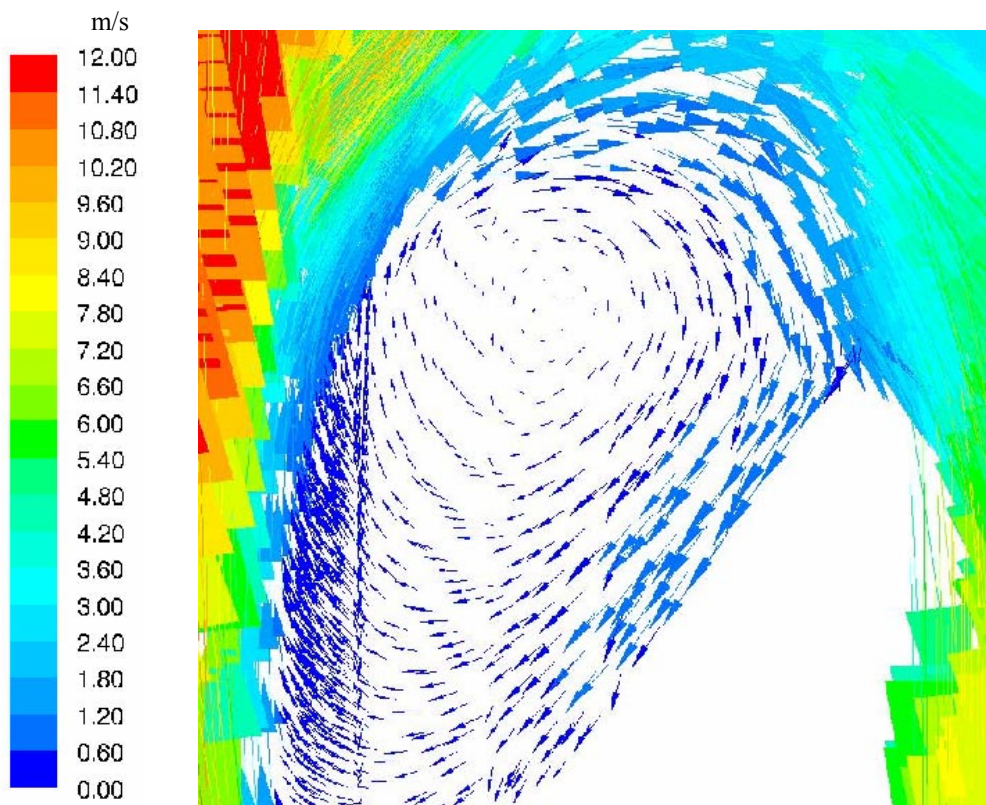


**Figure 33:** The zone of recirculation – case 3.

A profile of the temperature of the flue gas is shown in *Figure 34*. The view is from the top of the boiler of a plane at  $y=15$  m. The temperature is decreasing along the path of the gas. This is expected since the flue gas is supposed to transfer heat to the steam flowing in the tubes.

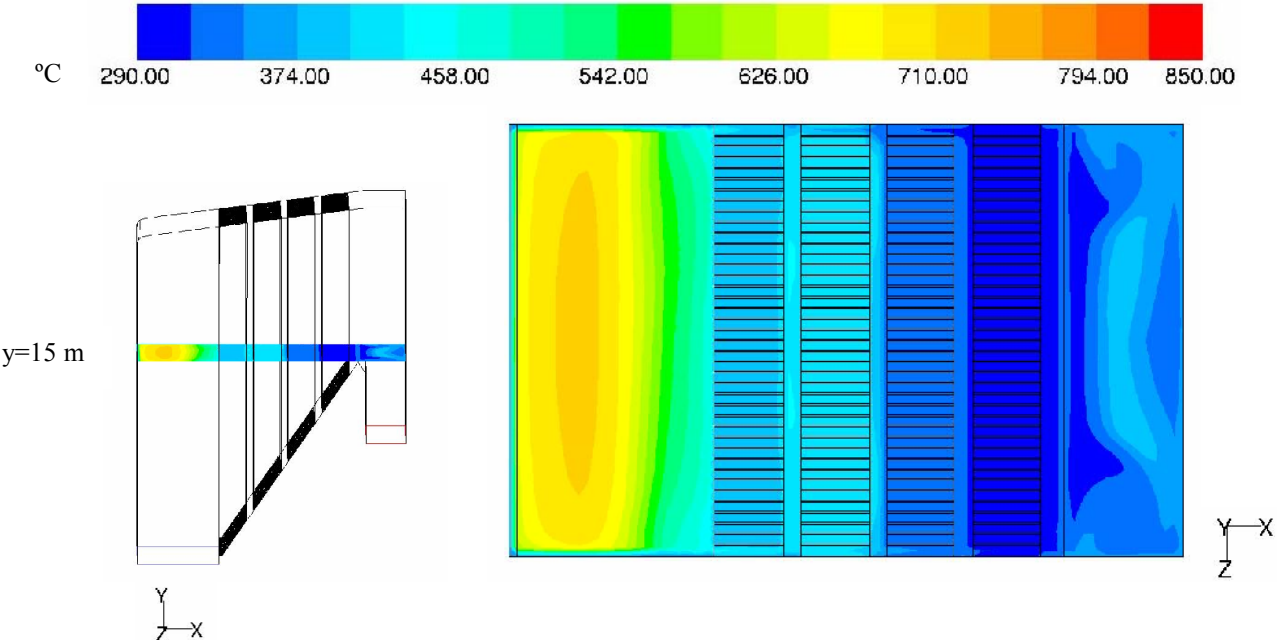


**Figure 34:** The temperature profile at  $y=15$  m – case 3.

In *Figure 35* a profile of the pressure is shown. The pressure drops across the superheaters are very small both in the direction of the flow and in the transverse direction.

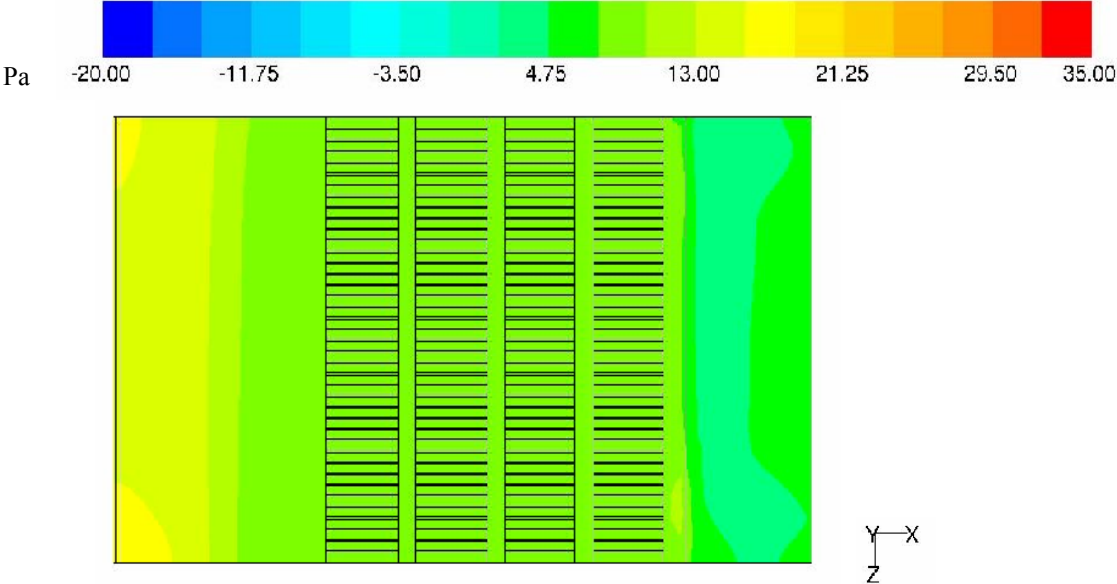


**Figure 35:** Pressure profile of static pressure at  $y=15$  m – case 3.

**8.2.2. Case 4: Modelling the Entire Domain, Inlet Flow Profile 2**

The structure of the grid is the same as in case 3 (see *Figure 27*).

Inlet profile 2 is shown in *Figure 36*. This profile represents a bull nose of more abrupt and angular shape (see *Figure 37*) compared to the rounded, sloping nose in case 3.

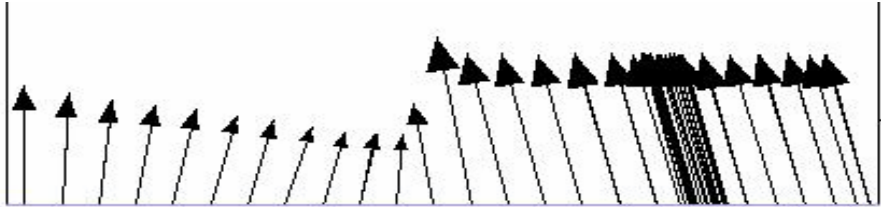


*Figure 36: Inlet profile 2.*

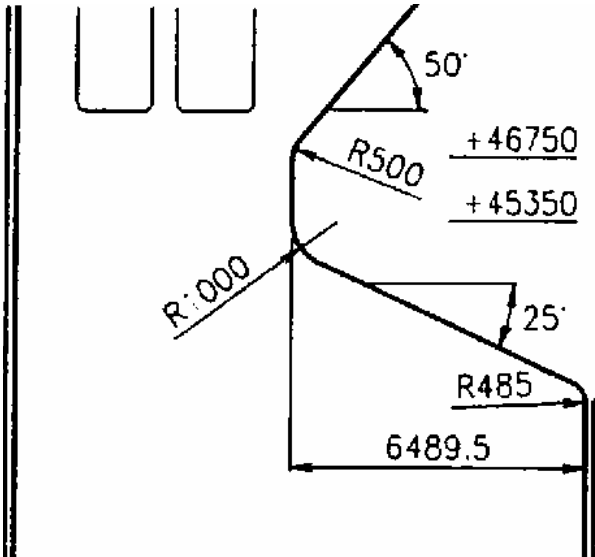


*Figure 37: Illustration of an abrupt and angular bull nose.*

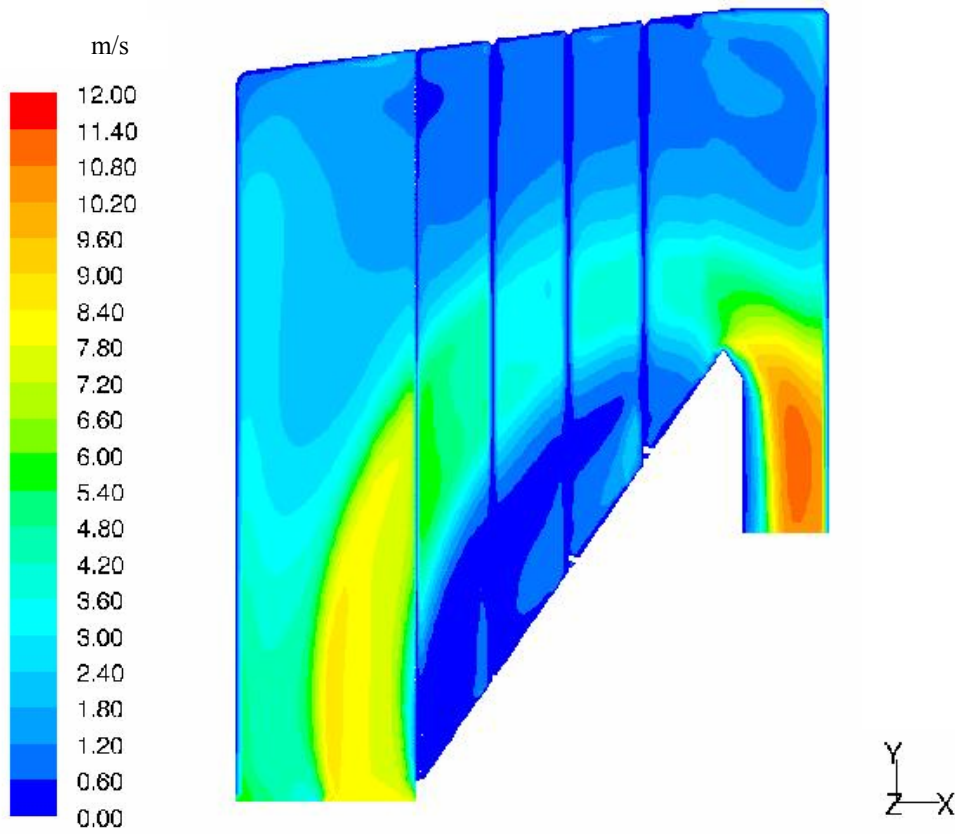


**Figure 38:** The velocity contours of case 4.

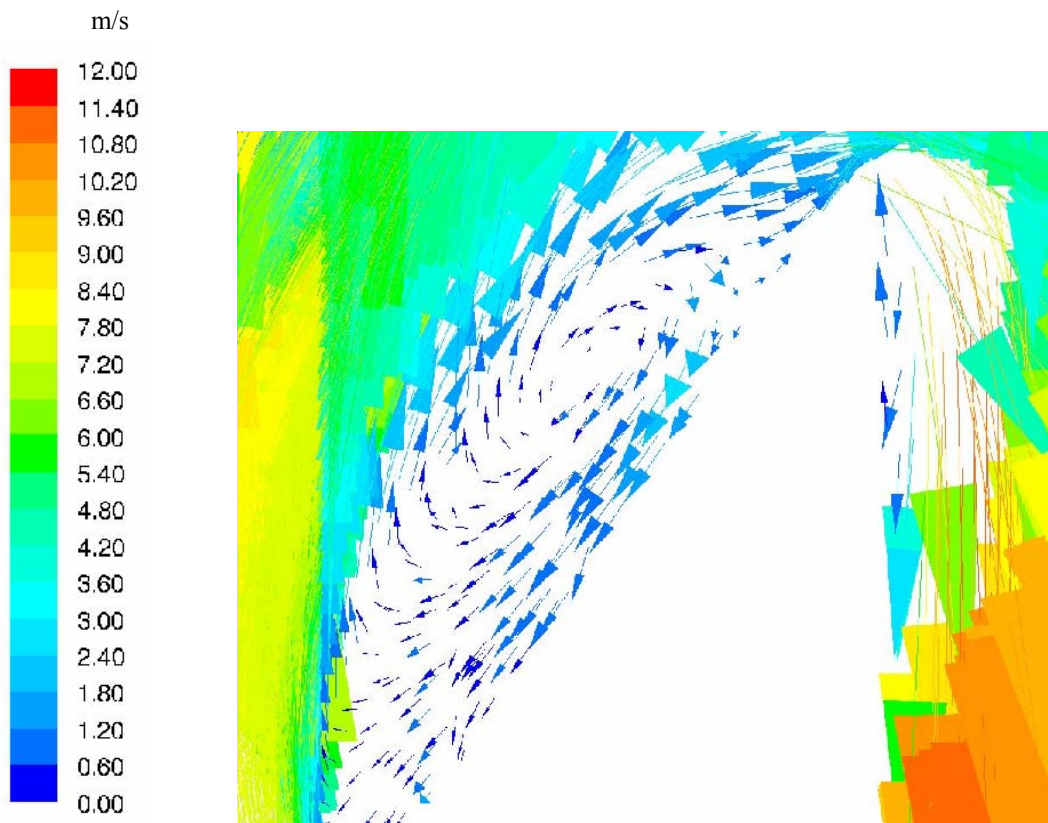


**Figure 39:** The zone of recirculation – case 4.

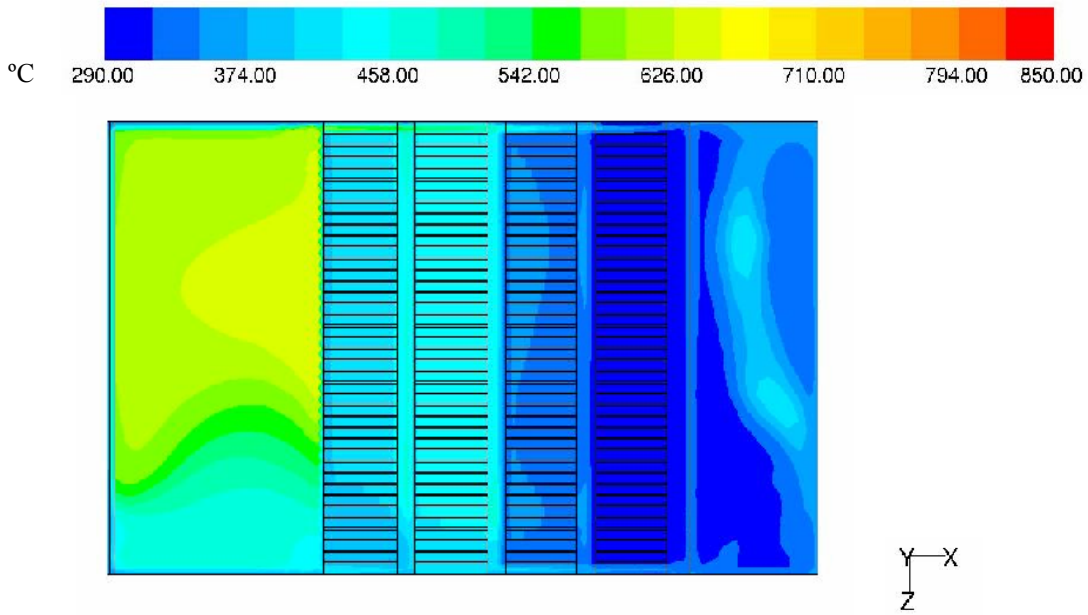


**Figure 40:** The temperature profile at  $y=15$  m – case 4.

A temperature profile from the top view of the boiler of a plane at  $y=15$  m is shown in *Figure 40*. The temperature is decreasing along the flow direction of the gas as expected.

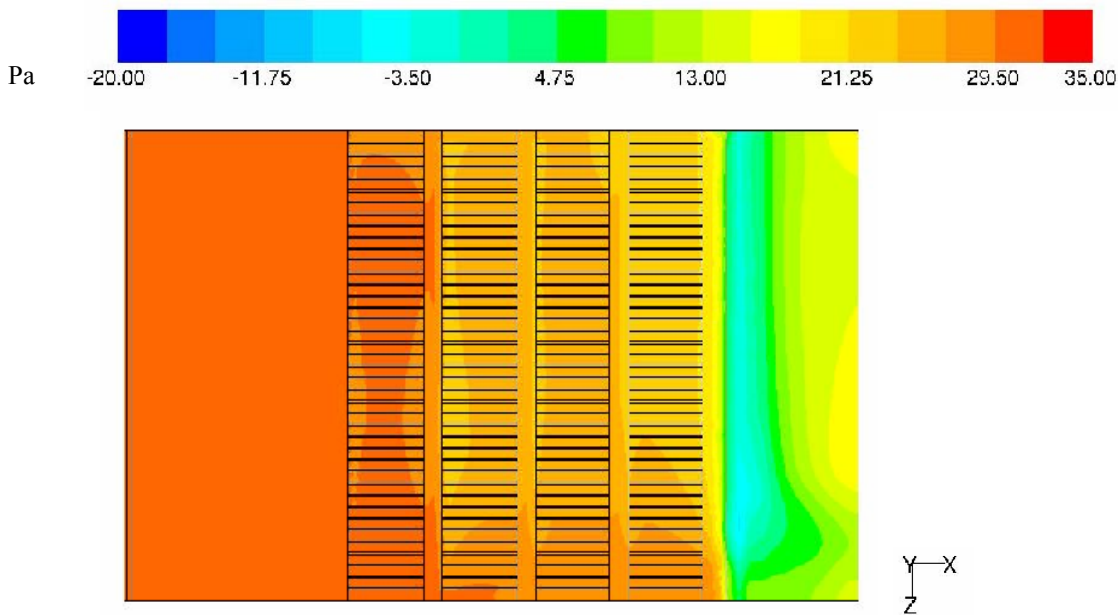


**Figure 41:** Pressure profile of static pressure at  $y=15$  m – case 4.

In *Figure 41* a profile of the pressure is shown. The pressure drops across the superheaters are small both in the direction of the flow and in the transverse direction.

### 8.2.3. Case 5: Modelling a Sub-Domain, Inlet Flow Profile 1

Because of the arrangement of the superheaters as platens, which restricts cross flow, and the uniform side-to-side spacing of the superheater platens in each section, a significant simplification of the flow model is possible. Instead of modelling the full side-to-side width of the boiler, only a width equivalent to 10 side-to-side platens could be modelled, which contains all the geometric features of the upper region of the boiler. When modelling a smaller part of the domain it is possible to increase the concentration of cells around the superheater packages. This is desirable since the accuracy of the flow field will be increased.

When modelling the sub-domain only the two primary superheaters are modelled as porous zones. The secondary and tertiary superheaters are modelled as wall boundary conditions based on the assumption that no transverse flow exists since the tubes are very closely spaced.

The mesh consists of approximately 1 550 000 cells. In *Figure 42* the mesh around the superheater packages is shown from a top view of the boiler. The mesh in the transverse direction of the superheater packages consists of two cells, while the mesh in between the superheater packages consists of five cells. Compared to the mesh in cases 3 and 4 this mesh should result in a higher resolution and accuracy of the flow field.

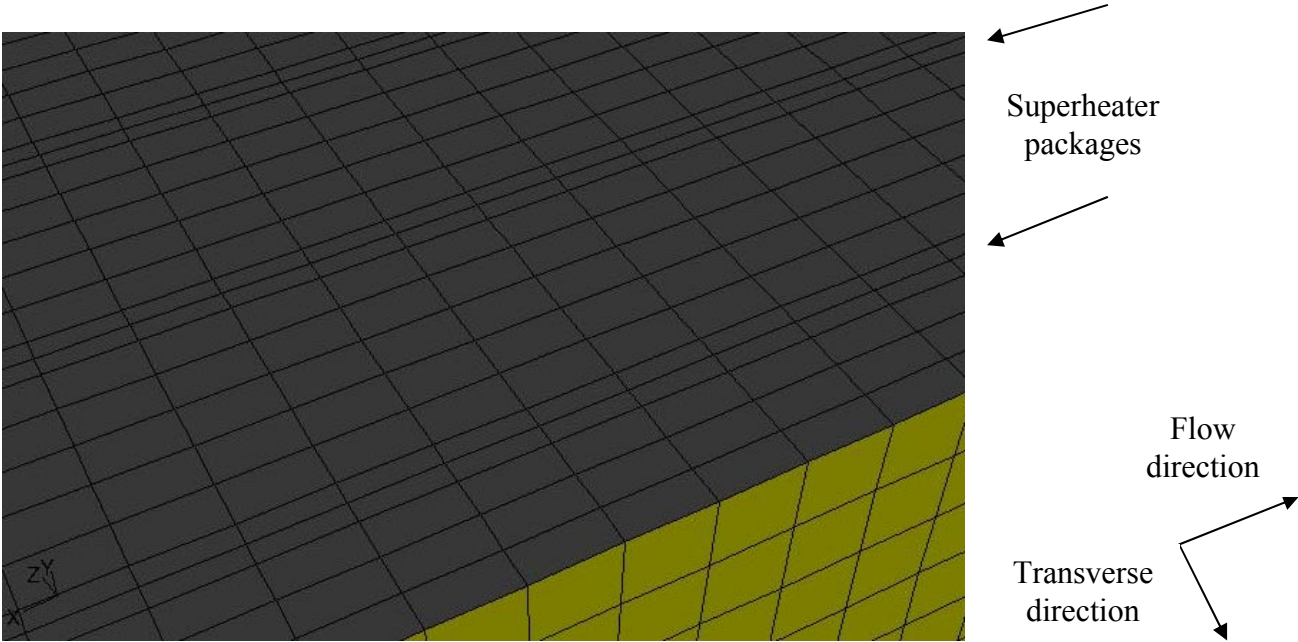


**Figure 42:** The mesh from a top view.

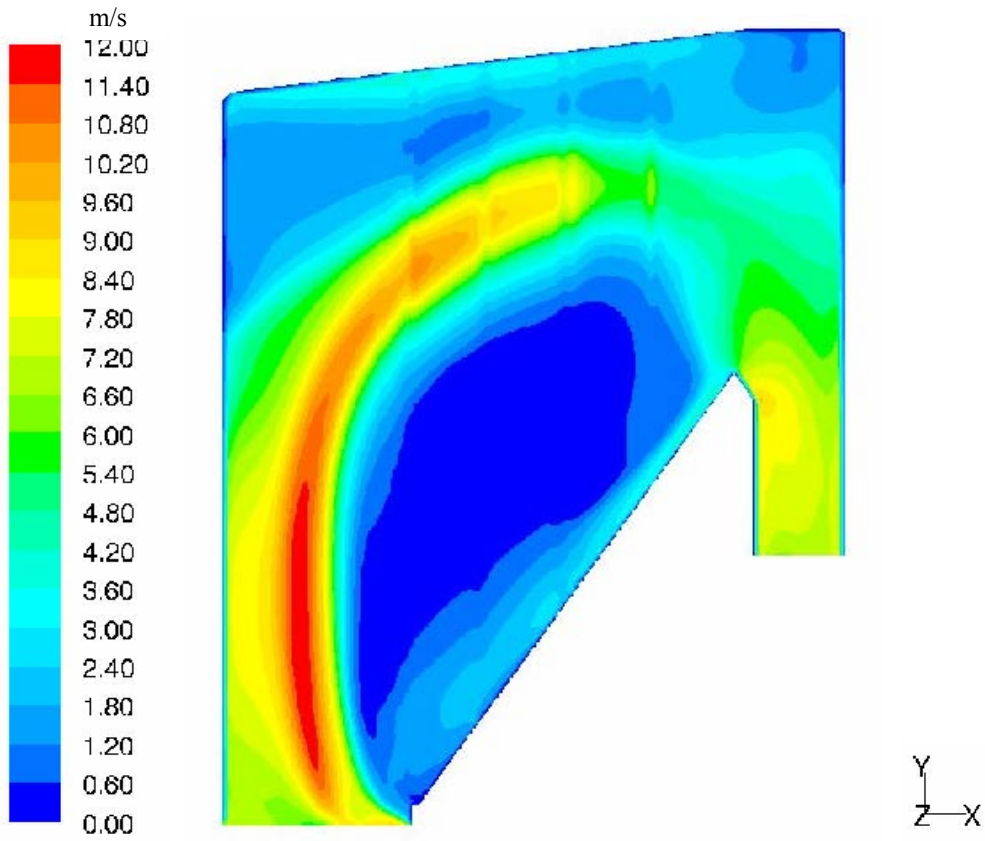


**Figure 43:** The velocity contours of case 5.

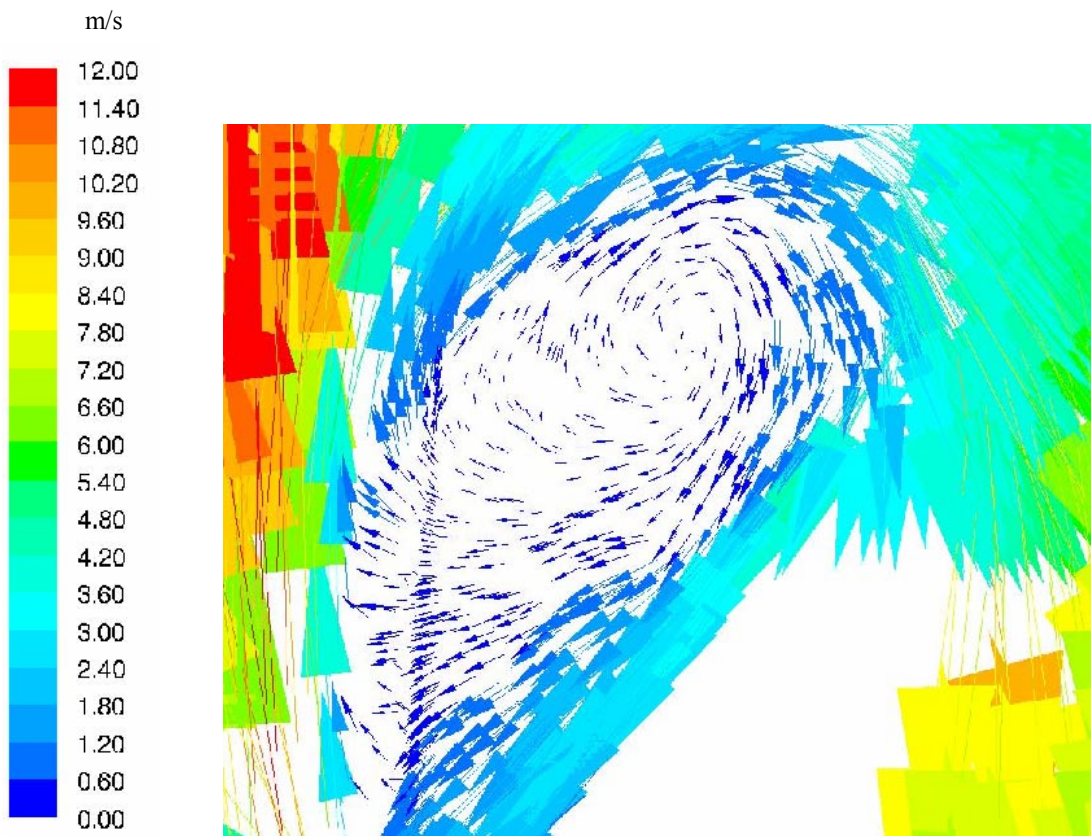


**Figure 44:** The zone of recirculation – case5.

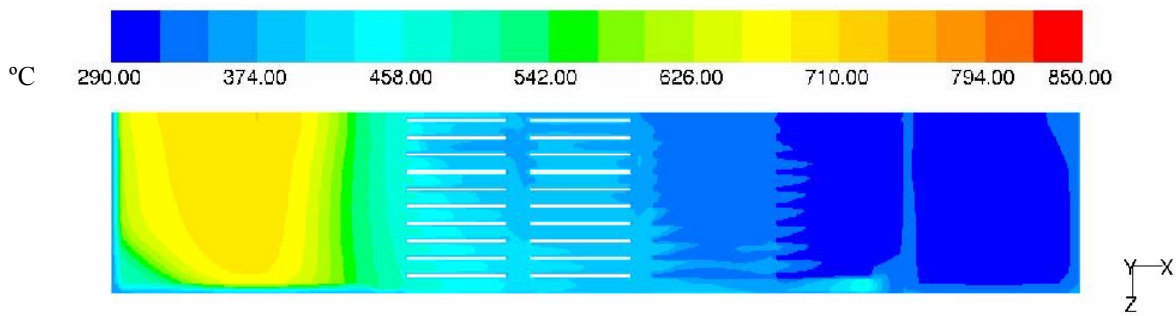


**Figure 45:** The temperature profile at  $y=15\text{ m}$  – case 5.

As shown in *Figure 45* the temperature is decreasing along the path of the gas.

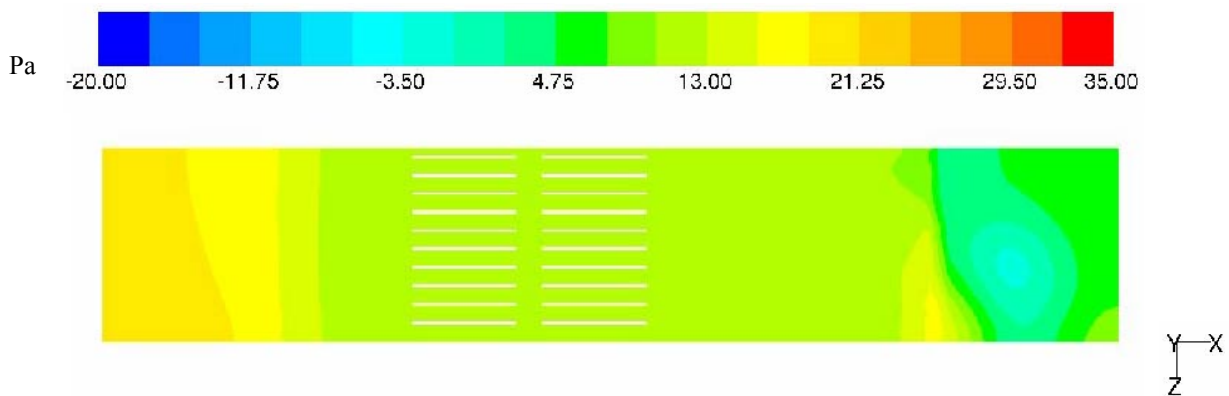


**Figure 46:** Pressure profile of static pressure at  $y=15\text{ m}$  – case 5.

The pressure profile in *Figure 46* shows that the pressure drops across the superheaters are very small both in the flow direction and in the transverse direction.

**8.2.4. Case 6: Modelling a Sub-Domain, Inlet Flow Profile 2**

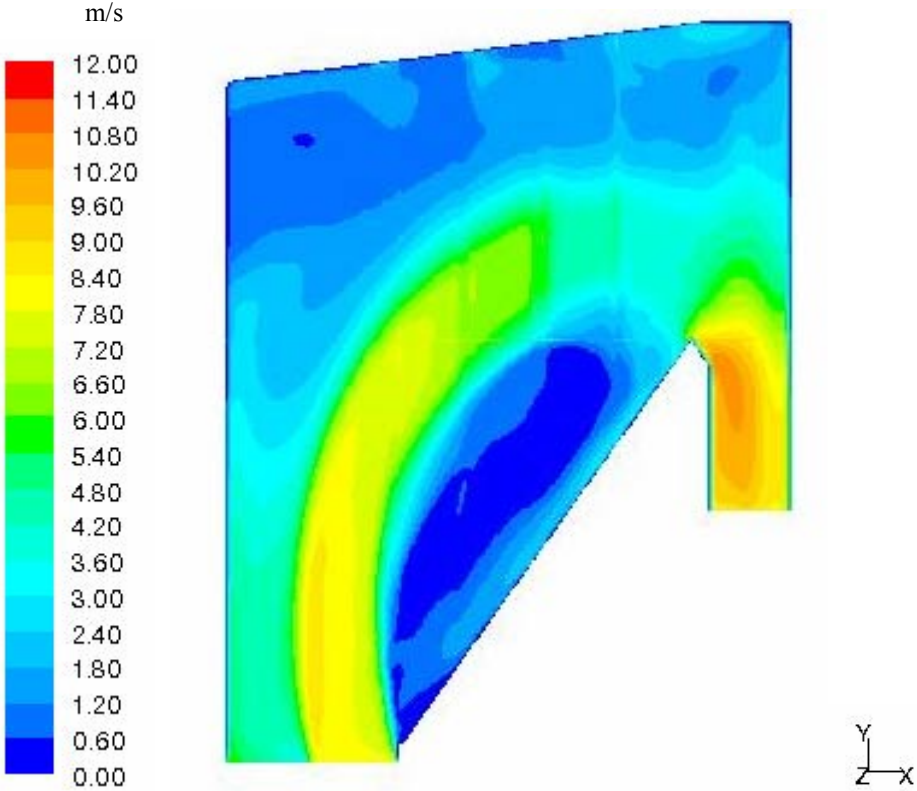


*Figure 47: The velocity contours of case 6.*

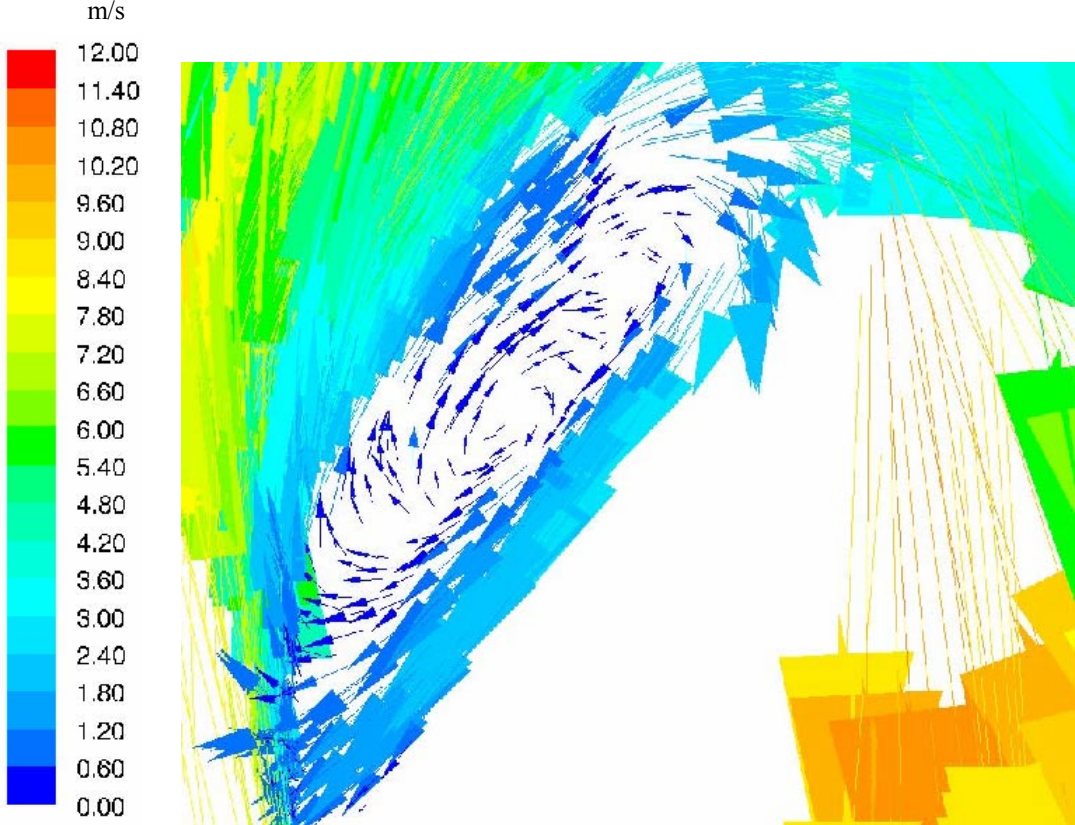


*Figure 48: The zone of recirculation – case 6.*

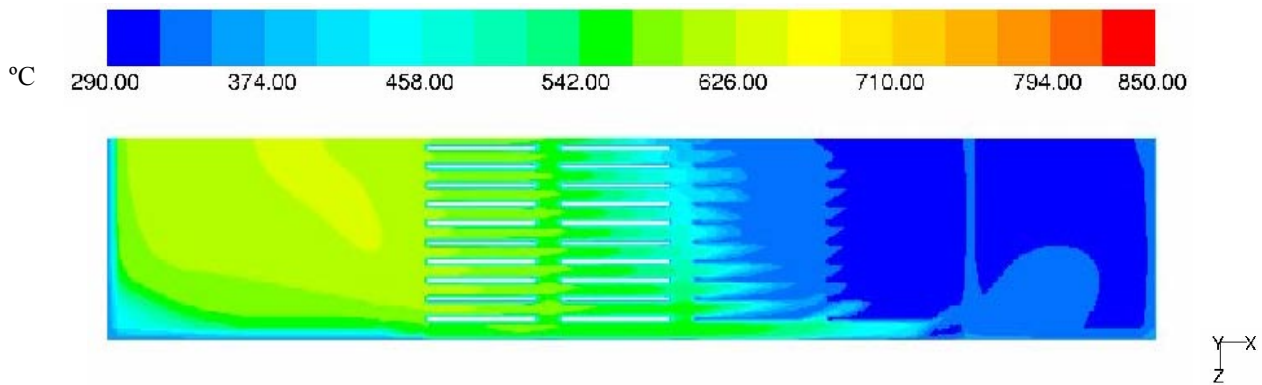


**Figure 49:** The temperature profile at  $y=15$  m – case 6.

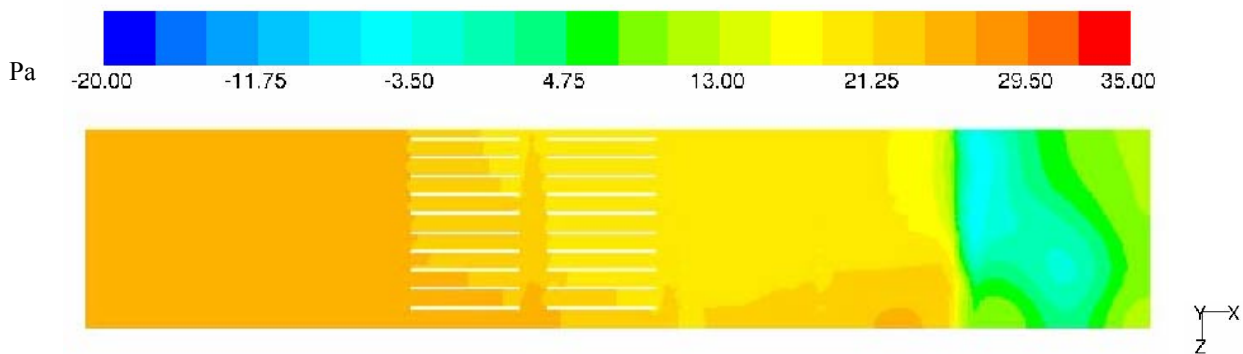


**Figure 50:** Pressure profile of static pressure at  $y=15$  m – case 6.

### 8.2.5. Influence of Inlet Flow Profile

Two different inlet flow profiles were used in the models to investigate the influence of the profile on the predicted results. The inlet profiles are shown in *Figure 29* and *Figure 36*.

None of the flow patterns of cases 3 and 4 are ideal, but the pattern of case 4 is the better one from a heat exchange point of view. When comparing the velocity contours of case 3 (see *Figure 32*) and case 4 (see *Figure 38*) one can see that the zone of recirculation flow is much larger in case 3 compared to case 4. Other observations are that the flow does not rise as high above the bull nose before turning toward the boiler bank in case 4 as in case 3 and the velocities of the channelled flow are lower. In case 4 the gas flow that passes the superheaters is more uniform than in case 3. These effects can partly be explained by the change of inlet profile to one corresponding to a bull nose of more abrupt and angular shape in case 4 compared to the rounded, sloping nose in case 3. Since a large zone of recirculation reduces the heat transfer between the flue gas and the steam one conclusion is that a bull nose of abrupt shape is better from a heat exchange point of view than a bull nose of sloping shape. However, the flow pattern in the upper boiler depends for example both on the shape and size of the bull nose and the conditions in the boiler. One must not forget that the ideal flow pattern would not contain any recirculation zone at all and the flow passing the superheaters would be completely uniform.

A comparison of the velocity contours of case 5 (see *Figure 43*) and case 6 (see *Figure 47*) shows the same pattern. The zone of recirculation flow is much greater when using inlet profile 1 compared to inlet profile 2.

The contours of temperature show a consistent steady decrease in gas temperature along the path of the gas in all cases. This is the expected result since the objective of the upper boiler is to transfer heat from the flue gas.

The contours of static pressure show that the pressure drops across the superheaters are small in the direction of the flow in all cases. In the transverse direction the pressure drops are almost zero. The pressures are generally higher in cases 4 and 6 than in cases 3 and 5.

### **8.2.6. Modelling the Entire Domain vs. a Sub-Domain**

There are some advantages of modelling only a smaller part of the domain. For example, a higher concentration of cells can be used in the areas of most interest, which give a higher resolution and accuracy of the flow field. However, information in the transverse direction of the flow can be lost when only modelling a part of the boiler width.

When comparing the results of case 3 (see *Figure 32*) and case 5 (see *Figure 43*) some differences can be observed. The recirculation zones are approximately of equal size, but the velocities of the flue gas in this area are even lower in case 3 than in case 5. In case 3 a smaller zone of recirculation flow is obtained in the upper left corner of the boiler, which cannot be discovered in case 5. The velocities along the channelled flow are even higher in case 5 and the gas flow through the superheaters is less uniform compared to in case 3.

A comparison of the results of case 4 (see *Figure 38*) and case 6 (see *Figure 47*) also shows some differences. In case 6 the flow rises higher above the bull nose before turning toward the boiler bank compared to in case 4. The velocities along the path of the channelled flow are higher in case 6 compared to in case 4 and the gas flow through the superheaters is less uniform. The zone of recirculation flow is somewhat greater in case 6.

The flow patterns of cases 5 and 6 probably give a more realistic illustration of the flow field than cases 3 and 4. An observation is that the velocities are more smoothly changed along the direction of the flow in cases 5 and 6 compared to in cases 3 and 4 where the velocities changes more abruptly especially when passing the superheaters. This can be explained by the finer grid and thereby the higher accuracy of the flow field in cases 5 and 6.

No significant differences occur when comparing the contours of temperature and static pressure from the modelling of the entire domain and the sub-domain.

Differences between the predicted results when modelling the entire domain vs. a sub-domain can be explained by the fineness and construction of the grid.

## 9. Discussion

### 9.1. Economical consequence of a recirculation flow in the superheater

One interesting task to investigate is the economical consequence of a recirculation flow in the superheater section. According to a study performed by Lundborg [2005] the flue gas recirculation results in a significant economical loss associated with the reduced electricity production in the steam turbine. This chapter is a summary of the study of Lundborg with the purpose to estimate the effect of the recirculation flow and to show the importance of optimizing the gas flow through the superheater section.

The following example illustrates the economical loss caused by the recirculation flow. It is based on measurements on a recovery boiler with a dry solids input of 3300 t DS/ 24 h. Since the superheater was practically clean in this case, the reduced heat absorption has to be due to the flue gas recirculation, which decreases the temperature difference between the steam and the flue gas.

The following relation describes the amount of heat absorbed by the steam:

$$Q = U \cdot A \cdot \theta_{\text{lm}}$$

where

$Q$  = absorbed heat by the steam, W

$U$  = heat transfer coefficient, W/m<sup>2</sup>, °C

$A$  = area available for heat absorption, m<sup>2</sup>

$\theta_{\text{lm}}$  = logarithmic temperature difference between the steam and the flue gas, °C

In this example the expected steam temperature to the mill should have been 515 °C, but from measurements it has been showed to be as low as 470 °C, i.e.  $\Delta T_{\text{steam}} = 45$  °C. This decrease in steam temperature results in a reduced electricity production.

Two different cases were considered; oil and bark based electricity. There are some economical benefits associated with using bio fuel, for example renewable electricity certificates, CO<sub>2</sub> tax, and CO<sub>2</sub> allowances, which has been considered in the calculations.

The turbine in this example has a high isentropic efficiency, 89%. In this case steam is extracted at two different pressures; 12 bars and 4.5 bars. The cost of the electricity consumption of the feed water pump has been considered.

For a detailed description of the calculations see Appendix F. The calculations are not described completely, but the basic conditions are stated.

The calculations show that the value of the lost electricity production due to the recirculation flow in this case is 15 MSEK/year for the oil based electricity and 29 MSEK/year for the bark based electricity.

A conclusion is that optimizing the gas flow and thereby the heat transfer between the flue gas and the steam probably result in a significant economical profit for the pulp mill.

## ***9.2. Methods to improve the flue gas flow and heat transfer through the superheater***

From the modelling performed in this work it can be stated that the gas flow pattern through the superheater section is far from ideal from a heat exchange point of view. Methods to improve the gas flow pattern need to be investigated to improve the heat absorption and make use of the available heat exchanger area.

A possible method to improve the flow pattern could be to place metal strips in front of the bull nose to guide the flue gas through the boiler. This method is, however, expensive and could be difficult to implement in reality.

One can change the flow pattern by placing screen tubes in front of the superheater, which cool the upward flowing flue gases before they enter the superheater, protect the superheater from radiation, and collect some of the particulate carryover from the furnace. The screen tubes have an equalizing effect on the velocities along the flow direction of the flue gas.

The size and shape of the bull nose have great impact on the flow pattern. From the calculations performed in this study it can be stated that an abrupt and angular bull nose is preferred compared to a round, sloping bull nose from a heat exchange point of view.

Another option could be to place high pressure steam soot blowers at the location of the bull nose to create a desired flow path of the flue gas. A great benefit when using this method is that the boiler does not have to be re-constructed.

## 10. Conclusions

Observations of the superheater section in a couple of existing recovery boilers indicate that the flow pattern is not optimal from a heat exchange point of view. The CFD modelling performed in this study confirms that the flow profile is far from ideal.

2D calculations were performed to investigate if the superheater tubes could be modelled as rectangular packages, which would greatly simplify the calculations. Since the mass flow through the small passages in between the tubes in the transverse direction of the flow is shown to be very small an acceptable approximation is to model the tubes as rectangular packages.

In the 3D models the superheaters were modelled as rectangular packages of porous zones, which mean that the pressure drop due to the superheaters is simulated by introducing empirical coefficients of flow resistance as source terms in the momentum equations. The coefficients of flow resistance depend on the geometry, the tube diameter, the tube spacing and the flue gas velocity. A coefficient of high value means that the flow resistance for the flue gas is significant. *Table 5* shows a summary of the coefficients of flow resistance for the different superheater sections.

When studying the flow profiles of the 3D models a channelled flow is observed along the higher portions of the superheater, where the velocities are high, and a recirculation flow is obtained along the lower portions of the superheater, where the velocities are very low. In an ideal case the flue gas would flow through the superheater at the same velocity in a uniform flow.

The recirculation flow causes reduced heat transfer between the flue gas and the steam, which means that the resulting steam temperature is reduced. In the zone of recirculation the velocity of the gas is very low, which results in a long residence time in the boiler. Even heat transfer from the steam to the gas could occur if the temperature of the gas falls below the temperature of the steam. The high velocities obtained in the upper part of the superheater section could cause increased fouling of the superheater.

Two cases with different inlet profiles have been investigated to evaluate the influence of the inlet conditions to the geometry on the predicted results. When comparing the flow profiles of cases 5 (see *Figure 43*) and 6 (see *Figure 47*) some differences can be observed. In case 6 the zone of recirculation flow is smaller and the velocities of the channelled flow are lower compared to in case 5. This means that the flow through the superheater is more uniform in case 6, which results in a more effective heat exchange between the flue gas and the steam. Since the inlet flow profiles of cases 5 and 6 represent different bull nose shapes, a conclusion is that an abrupt and angular bull nose (see *Figure 30*) is better than a round and sloping nose (see *Figure 37*) from a heat exchange point of view.

## **Acknowledgements**

The work in this Master of Science thesis has been performed at AF-Process AB in Stockholm, Sweden, in the year of 2005.

I would like to thank my supervisors, particularly Jürgen Jacoby at AF-Process AB for being very helpful and enthusiastic, and Lars J. Pettersson at the Department of Chemical Engineering and Technology, KTH-Royal Institute of Technology, for showing a great interest in the project.

I also would like to thank my father, Sten Lundborg, for his support and for making this project possible.

## References

- Adams T.N., Frederick W.J., Grace T.M., Hupa M., Iisa K., Jones A.K., and Tran H., *Kraft recovery boilers*, American Forest & Paper Association, Tappi Press, Atlanta, 1997, ISBN 0-9625985-9-3.
- Adams T.N., and Frederick W.J., *Kraft recovery boiler physical and chemical processes*, American Paper Institute, New York, NY, 1988.
- Backman R., Hupa M., and Hyöty P., *Tappi J.*, 67 (12): 60-64, 1984.
- Björklund H., Warnquist B., Pettersson B., *Inside a Kraft recovery boiler – combustion of (high sulfidity) black liquor at high solids content*, Tappi/CPPA 1989 International Chemical Recovery Conference Proceedings, Tappi Press, Atlanta, pp. 177-182, 1989.
- Blasiak W., Vaclavinek J., and Collin, R., *Investigation of the flow conditions in a recovery boiler with respect to gases, droplets and dust*, Project number: 1192, Department of Heat and Furnace Technology, Royal Institute of Technology, 1992.
- Coulson J.M., and Richardson J.F., *Chemical engineering, Volume 1; Fluid flow, heat transfer and mass transfer*, 6<sup>th</sup> edition, The Bath Press, Bath, Great Britain, 2000.
- FLUENT user guide, Fluent inc., 2001.
- Grace T.M., Lien S., Schmidl W., Tse D., Abdullah Z., and Salcudean M., *Validation of CFD-based recovery furnace models*, International Chemical Recovery Conference, 1998.
- Grimison E.D., *Correlation and utilization of new data on flow resistance and heat transfer for cross flow of gases over tube banks*, Trans. ASME, 59: 583-594, 1937.
- Hupa M., Backman R., Skrifvars B.-J., *Tappi J.*, 73(6): 185-189, 1990.
- Idelchik I.E., *Handbook of hydraulic resistance*, 3<sup>rd</sup> ed., Begell House, 1996, ISBN 1-56700-074-6.
- Jacoby J., AF-Process AB, personal communication, 2005.
- Jakob M., *Heat transfer and flow resistance in cross flow of gases over tube banks*, Trans ASME, 60: 384, 1938.
- Kawaji M., Shen X.H., Tran H.N., Esaki S., and Dees C., *Prediction of heat transfer in the Kraft recovery boiler superheater region*, *Tappi J.*, 78(10): 214-221, 1995.
- Lundborg S., AF-Process AB, personal communication, 2005.
- Patankar S.V., and Spalding, *Heat exchangers: design and theory sourcebook*, Scripta Book Co., Washington, D.C., pp.155-176, 1974.

Salcudean M., *Modelling of industrial processes using computational fluid dynamics*, Canadian Metallurgical Quarterly, 37(3-4): 251-263, 1998.

Saviharju K., Pakarinen L., Wag K., and Välipakka I., *Numerical modelling feedback in recovery boilers*, International Chemical Recovery Conference, 2004.

Shen X.H., Kuhn D.C.S., Tran H.N., Mostaghimi, J., and Dees C., *Simulation of flue gas flow in the upper furnace of a recovery boiler*, Pulp & Paper Canada, 96(5): T171-T175, 1995.

Smook G.A., *Handbook for pulp & paper technologists*, 2<sup>nd</sup> edition, Angus Wilde Publications, 1992.

Tao L., and Blasiak W., *Numerical simulation of a Kraft recovery boiler using rotation firing method*, Modelling of Kraft recovery boilers - collection of publications (1), Division of Heat and Furnace Technology, Royal Institute of Technology, 1996.

Tran H.N., Tappi J., 69 (11): 102, 1986.

Tse D., Matys P., Nowak P., Abdullah Z., Salcudean M., and Gartshore I., *Flow and heat transfer modelling in the upper furnace of a Kraft recovery furnace*, Department of Mechanical Engineering, University of British Columbia, Vancouver, B.C., Canada, 1996, in the 1998 final year report of *Black liquor combustion validated recovery boiler modelling*, the Institute of Paper Science and Technology, Oregon State University, the University of British Columbia and Babcock & Wilcox Company.

Vakkilainen E.K., Adams T.N., and Horton R.R., *The effect of recovery furnace bullnose designs on upper furnace flow and temperature profiles*, Proc. of 1992 International Chemical Recovery Conference, J101-J112, Seattle, USA, 1992.

Vakkilainen E.K., Nikkanen S., Hautamaa J., and Anttonen T., *Flows in the upper region of recovery boilers*, AIChE Forest Products Symposium, 1991, pp. 125-134.

Versteeg H.K. & Malalasekera W., *An introduction to computational fluid dynamics – the finite volume method*, Addison Wesley Longman Limited, 1995, ISBN 0-582-21884-5.

## List of Figures

|  |    |
|--|----|
| <i>Figure 1: The Kraft liquor cycle.</i>   | 16 |
| <i>Figure 2: Black liquor combustion processes [Tao et al., 1996].</i>   | 18 |
| <i>Figure 3: Schematic figure of a recovery boiler [Adams et al., 1997].</i>                                     | 20 |
| <i>Figure 4: The furnace zones [Smook, 1992].</i>  | 21 |
| <i>Figure 5: Directions of gas and steam flows in a recovery boiler [Smook, 1992].</i>                           | 23 |
| <i>Figure 6: Arrangement of two superheater platens [Adams et al., 1997].</i>                                    | 24 |
| <i>Figure 7: Flow sheet of the upper furnace in a recovery boiler.</i>   | 25 |
| <i>Figure 8: The nose arch geometry [Adams et al., 1997].</i>  | 26 |
| <i>Figure 9: Recirculation zone above the nose arch [Adams et al., 1997].</i>                                    | 27 |
| <i>Figure 10: Deposit formation on tangent and spaced tube superheaters [Adams et al., 1997].</i>                | 30 |
| <i>Figure 11: The region modelled.</i>   | 36 |
| <i>Figure 12: Flow sheet of the upper furnace in a recovery boiler.</i>  | 37 |
| <i>Figure 13: The 2D plane with the superheater tubes modelled as cylindrical tubes.</i>                         | 38 |
| <i>Figure 14: The 2D plane with the superheater tubes modelled as rectangular packages.</i>                      | 38 |
| <i>Figure 15: The inlet velocity vectors to the 2D geometry.</i>   | 42 |
| <i>Figure 16: 2D mesh – the superheaters as cylindrical tubes.</i>   | 42 |
| <i>Figure 17: Velocity profile – case 1</i>  | 43 |
| <i>Figure 18: Pressure profile of static pressure – case 1</i>   | 44 |
| <i>Figure 19: Pressure plot – case 1</i>   | 44 |
| <i>Figure 20: 2D mesh – the superheaters as rectangular packages. The arrows show the direction of the flow.</i> | 46 |
| <i>Figure 21: Velocity profile – case 2</i>  | 46 |
| <i>Figure 22: Pressure profile of static pressure – case 2</i>   | 47 |
| <i>Figure 23: Pressure plot – case 2</i>   | 47 |
| <i>Figure 24: Comparison of the velocity profiles of case 1 and case 2.</i>                                      | 48 |
| <i>Figure 25: The 3D domain.</i>   | 49 |
| <i>Figure 26: The flow directions of the flue gas.</i>   | 50 |
| <i>Figure 27: The structure of the mesh from a side view.</i>  | 50 |
| <i>Figure 28: The mesh from a top view.</i>  | 51 |
| <i>Figure 29: Inlet flow profile 1.</i>  | 51 |
| <i>Figure 30: Illustration of a rounded, sloping bull nose.</i>  | 52 |
| <i>Figure 31: A cross-section in the middle of the domain at <math>z=-6.24</math> m.</i>                         | 52 |
| <i>Figure 32: The velocity contours of case 3.</i>   | 54 |
| <i>Figure 33: The zone of recirculation – case 3.</i>  | 54 |
| <i>Figure 34: The temperature profile at <math>y=15</math> m – case 3.</i>                                       | 55 |
| <i>Figure 35: Pressure profile of static pressure at <math>y=15</math> m – case 3.</i>                           | 55 |
| <i>Figure 36: Inlet profile 2.</i>   | 56 |
| <i>Figure 37: Illustration of an abrupt and angular bull nose.</i>   | 56 |
| <i>Figure 38: The velocity contours of case 4.</i>   | 57 |
| <i>Figure 39: The zone of recirculation – case 4.</i>  | 57 |
| <i>Figure 40: The temperature profile at <math>y=15</math> m – case 4.</i>                                       | 58 |
| <i>Figure 41: Pressure profile of static pressure at <math>y=15</math> m – case 4.</i>                           | 58 |
| <i>Figure 42: The mesh from a top view.</i>  | 59 |
| <i>Figure 43: The velocity contours of case 5.</i>   | 60 |
| <i>Figure 44: The zone of recirculation – case 5.</i>  | 60 |
| <i>Figure 45: The temperature profile at <math>y=15</math> m – case 5.</i>                                       | 61 |

|  |    |
|--|----|
| <i>Figure 46: Pressure profile of static pressure at <math>y=15</math> m – case 5.</i>   | 61 |
| <i>Figure 47: The velocity contours of case 6.</i>   | 62 |
| <i>Figure 48: The zone of recirculation – case 6.</i>  | 62 |
| <i>Figure 49: The temperature profile at <math>y=15</math> m – case 6.</i>   | 63 |
| <i>Figure 50: Pressure profile of static pressure at <math>y=15</math> m – case 6.</i>   | 63 |
| <i>Figure 51: Flow sheet of chemical pulping [Smook, 1992].</i>  | 74 |
| <i>Figure 52: Flow sheet of the Kraft mill liquor cycle [Smook, 1992].</i>   | 75 |
| <i>Figure 53: The equilibrium composition of the smelt and the lower furnace gases as a function of air/fuel ratio at a temperature of 1000 °C and a molar S/Na<sub>2</sub> in black liquor solids of 0.3 [Adams et al., 1997].</i>  | 78 |
| <i>Figure 54: The equilibrium composition of the smelt and the lower furnace gases as a function of temperature at an air/fuel ratio of 0.7 and a molar S/Na<sub>2</sub> in black liquor solids of 0.3 [Adams et al., 1997].</i>   | 79 |
| <i>Figure 55: The reactions of sulphur and sodium in the recovery furnace and flue gases on a molar basis. The upper figure illustrates a cold bed with S/Na<sub>2</sub>=1.5 in the flue gases, and the lower figure illustrates a hot bed with S/Na<sub>2</sub>=0.8 in the flue gases [Adams et al., 1997].</i> | 82 |
| <i>Figure 56: Flow past a tube bank [Tse et al., 1996].</i>  | 86 |
| <i>Figure 57: A steam turbine.</i>   | 90 |

## List of Tables

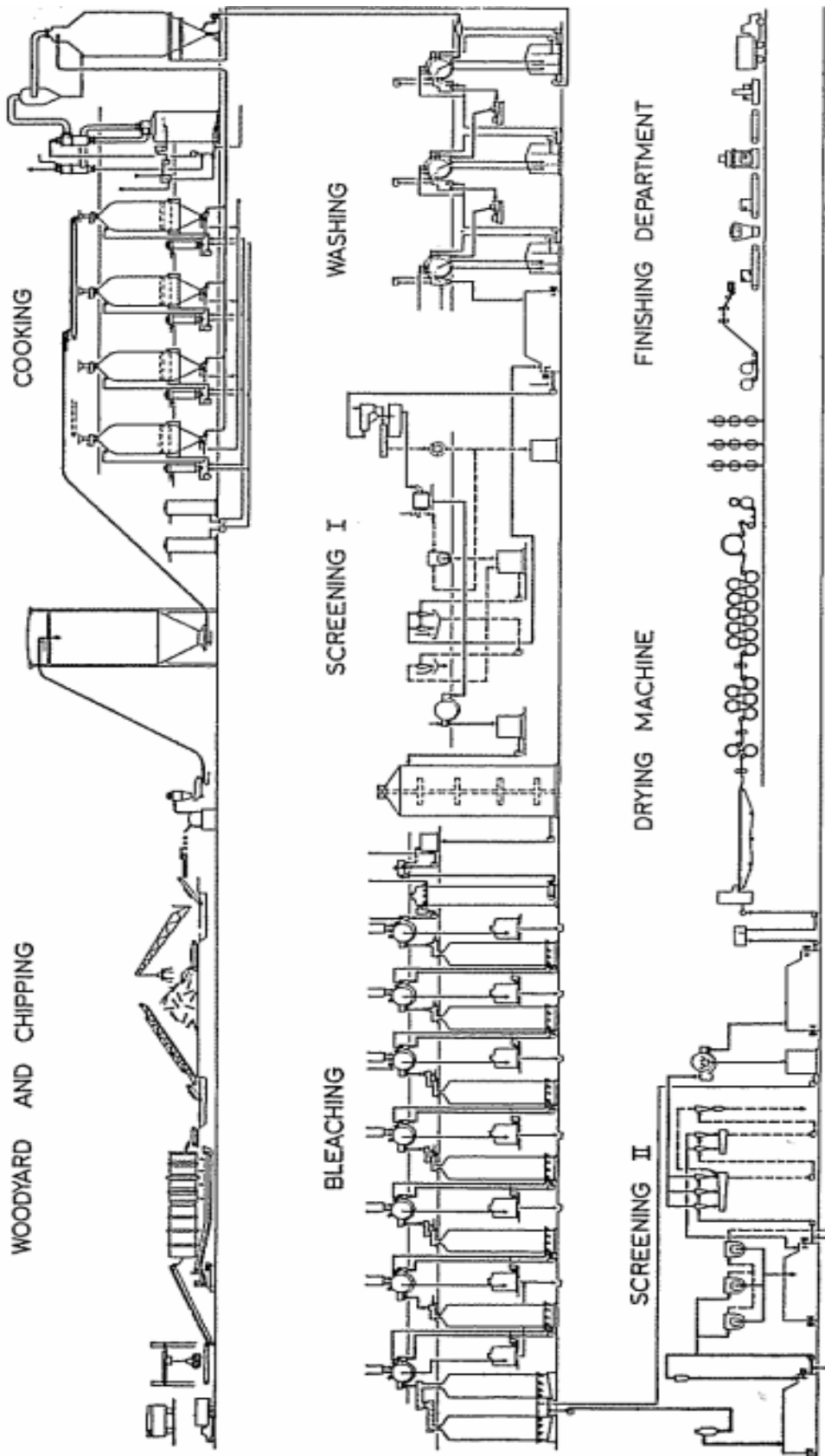
|  |    |
|--|----|
| <i>Table 1 [Adams et al., 1997]</i>  | 19 |
| <i>Table 2: Typical flue gas temperatures at the inlet to the superheaters</i>   | 29 |
| <i>Table 3: Characteristic data for the superheater sections of the boiler.</i>  | 36 |
| <i>Table 4: Example of typical steam and flue gas temperatures and absorbed heat in the different superheater sections [Lundborg, 2005].</i> | 37 |
| <i>Table 5</i>   | 40 |
| <i>Table 6 [Adams et al., 1997]</i>  | 76 |

## Nomenclature

|                 |   |
|-----------------|---|
| T               | Temperature, K  |
| Q               | Heat transfer rate, W   |
| k               | Thermal conductivity, W/m K   |
| U               | Heat transfer coefficient, W/m <sup>2</sup> K   |
| A               | Area, m <sup>2</sup>  |
| C <sub>p</sub>  | Specific heat, kJ/kg K  |
| F <sub>i</sub>  | Additional momentum sink term to the standard fluid flow equation for porous medias, Pa/m or kg/m <sup>2</sup> s <sup>2</sup> |
| α               | Permeability coefficient, kg/m <sup>3</sup> s   |
| u               | Velocity, m/s   |
| P               | Pressure, Pa  |
| f'              | Empirical friction factor, -  |
| ρ               | Density, kg/m <sup>3</sup>  |
| μ               | Dynamic viscosity, kg/m s   |
| D               | Tube diameter, m  |
| S <sub>L</sub>  | Longitudinal tube separation, m   |
| S <sub>T</sub>  | Transverse tube separation, m   |
| C <sub>2</sub>  | Coefficient of inertial resistance, m <sup>-1</sup>   |
| L <sub>H</sub>  | Hydraulic diameter, m   |
| θ <sub>lm</sub> | Logarithmic temperature difference, °C  |

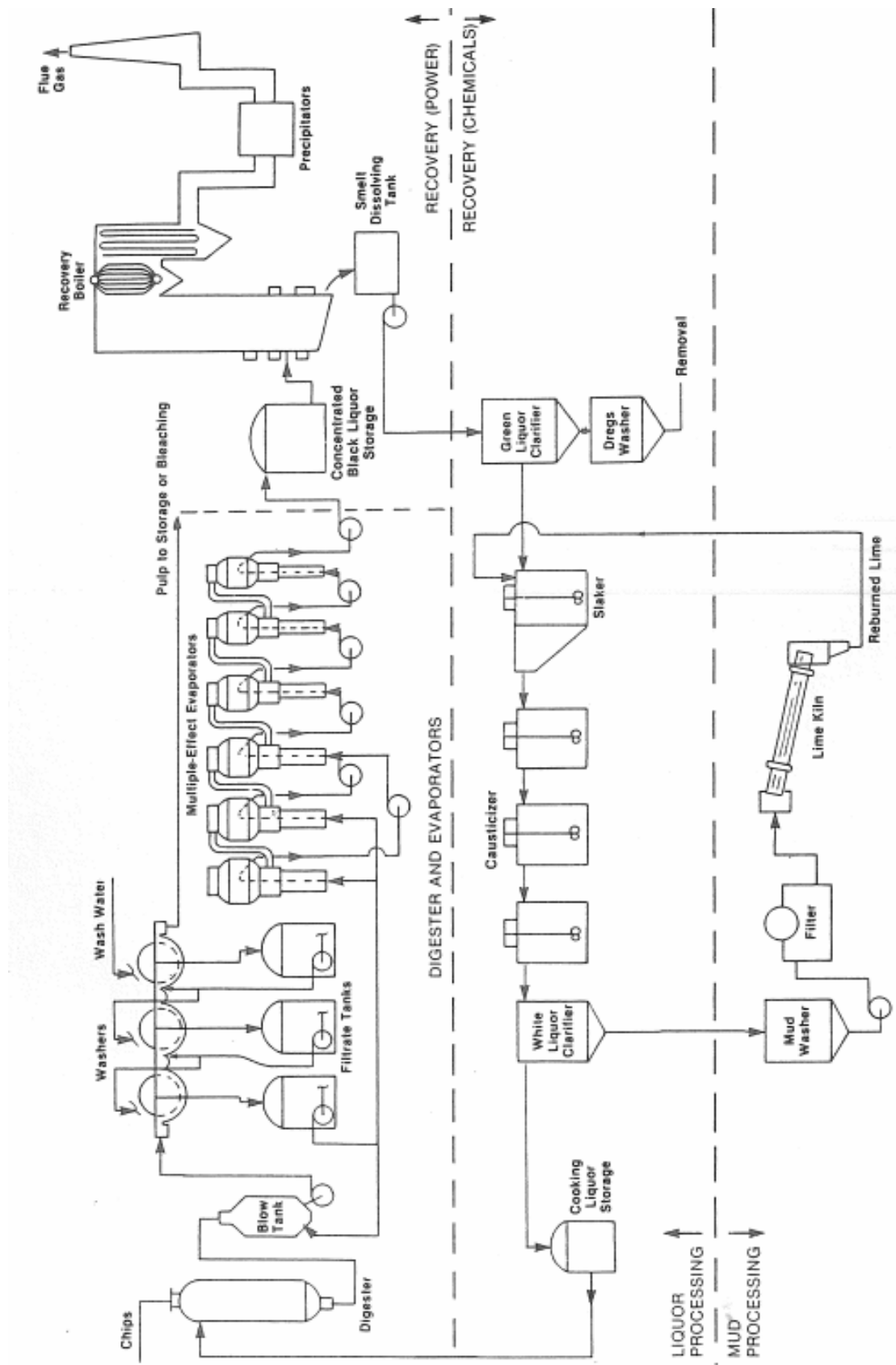
# APPENDIX A

Figure 51: Flow sheet of chemical pulping [Smook, 1992].



# APPENDIX B

Figure 52: Flow sheet of the Kraft mill liquor cycle [Smook, 1992].



## APPENDIX C Recovery Boiler Chemistry

In the recovery boiler furnace several physicochemical processes take place simultaneously:

- Air injection and mixing with the furnace gases
- Black liquor spraying and formation of droplets
- Drying of the black liquor droplets
- Pyrolysis of the black liquor and combustion of the pyrolysis gases
- Gasification and combustion of the char residue
- Reduction of the sulphur compounds to sulphide
- Tapping the molten salt mixture of sodium sulphide and sodium carbonate from the furnace bottom

An undesired side effect during combustion is the vaporization of sodium and sulphur compounds (and to a lesser extent of chlorine and potassium compounds). These vapours escape with the flue gases.

The molar ratio of sodium to sulphur in black liquor determines the chemistry of the sulphur and sodium in the flue gas of a recovery boiler. There is a great difference in this sulphur-sodium ratio between different boilers. In Scandinavia the S/Na<sub>2</sub> range is typically between 0.35 and 0.5, but in North America this range is typically between 0.2 and 0.35. The S/Na<sub>2</sub> ratio is increased when the sulfidity in pulping is high and/or the concentration of Na<sub>2</sub>SO<sub>4</sub> and Na<sub>2</sub>SO<sub>3</sub> are high in the recovery cycle.

In *Table 6*, the chemical composition of the solids in typical black liquor is shown [Adams et al., 1997].

**Table 6** [Adams et al., 1997]

|        | <b>% in Dry Solids</b> |
|--------|------------------------|
| C      | 38.2%                  |
| H      | 3.4%                   |
| O      | 31.1%                  |
| N      | 0.1%                   |
| S      | 5.2%                   |
| Na     | 19.8%                  |
| K      | 1.9%                   |
| Cl     | 0.1%                   |
| Others | 0.2%                   |

$$S/Na_2 = 0.38 \text{ mol/mol}$$

### **C1. Sodium and Sulphur Chemistry**

In an ideal recovery boiler process, all sulphur and sodium compounds would be transformed to sodium sulphide (Na<sub>2</sub>S) and sodium carbonate (Na<sub>2</sub>CO<sub>3</sub>), and they would be contained in the smelt leaving the furnace bottom.

In a real recovery boiler the process is more complicated. For example, the sulphur occurs in the smelt as both sulphide and sulphate. The reduction, or molar ratio  $(\text{Na}_2\text{S})/(\text{total S})$  in the smelt, is typically about 90-95% [Adams et al., 1997]. A considerable part of the sulphur and sodium is carried by the combustion gases, mainly as sodium sulphate dust and gases containing sulphur. These compounds cause problems, such as fouling of heat transfer surfaces and corrosion.

Dust is fine particles condensed from vapour and varies in size from 0.1 to 1 mm. Most of the sodium and sulphur dust leaves the flue gases and is captured by the electrostatic precipitator or the dust hoppers. This dust is fed back into the boiler by mixing it with the incoming black liquor. Roughly 10% of the sodium contained in black liquor is circulating.

Some sodium and sulphur leaves the boiler as flue gas emissions. The main emissions are  $\text{Na}_2\text{SO}_4$ , sulphur dioxide gas ( $\text{SO}_2$ ), and reduced sulphur gases such as hydrogen sulphide ( $\text{H}_2\text{S}$ ) and methyl mercaptan ( $\text{CH}_3\text{SH}$ ). About 20 to 40% of the sulphur is carried by the combustion gases and fume [Adams et al., 1997]. The emissions depend strongly on the operating conditions of the boiler and the equipment for cleaning the flue gas.

The lower furnace and the char bed are crucial for the entire recovery boiler process. The conditions in the lower furnace determine largely how sulphur and sodium are distributed. Especially the temperatures of the lower furnace and the char bed have a major impact on this distribution. These temperatures are mainly determined by the liquor spraying technique and the introduction of air into the furnace. Also the black liquor properties, particularly its dry solids content, affect the temperatures in the furnace.

The composition at the bottom of the furnace is shown in *Figure 53* and *Figure 54*, both as a function of the air/fuel ratio and as a function of temperature. The figure at the bottom describes the composition of the bed, and the top figure the composition of the gas phase near the bed. These figures are based on theoretical thermodynamic equilibrium calculations, which assume an isothermal process with perfect mixing, where all chemical reactions reach equilibrium. Although this is not the case in any recovery boiler furnace, some useful conclusions can be made.

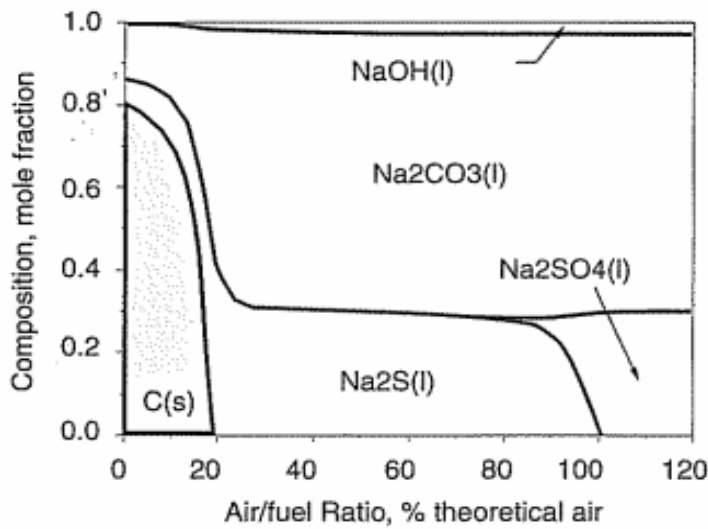
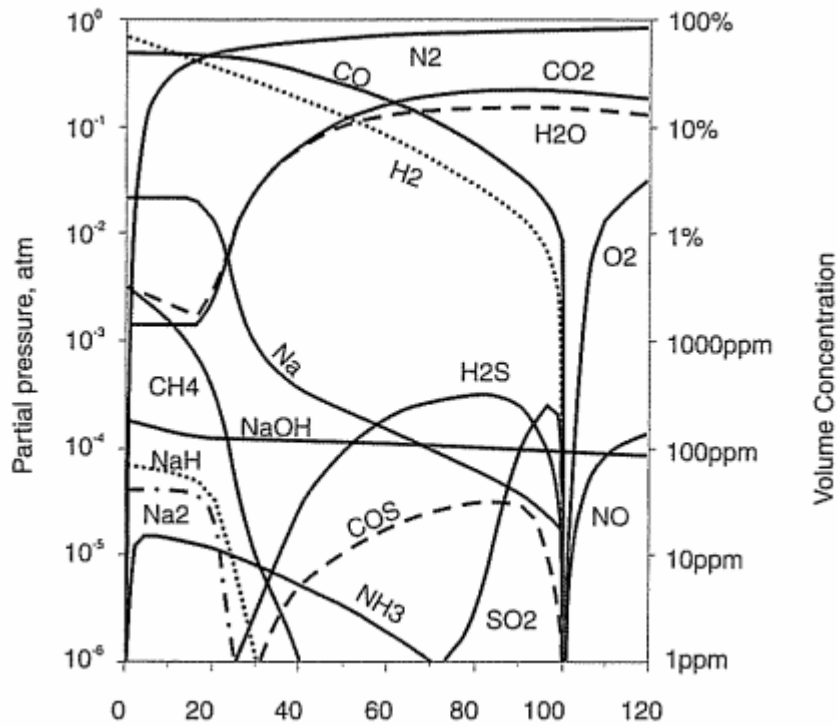


**Figure 53:** The equilibrium composition of the smelt and the lower furnace gases as a function of air/fuel ratio at a temperature of 1000 °C and a molar S/Na<sub>2</sub> in black liquor solids of 0.3 [Adams et al., 1997].

These figures show all the significant chemical compounds that may occur in the lower furnace. Apart from sodium sulphide, sodium carbonate, and sodium sulphate, solid elemental carbon (C) may be present in the bed under extreme conditions. Figure 54 shows that solid compounds begin to form in the bed when the temperature drops below approximately 800°C.

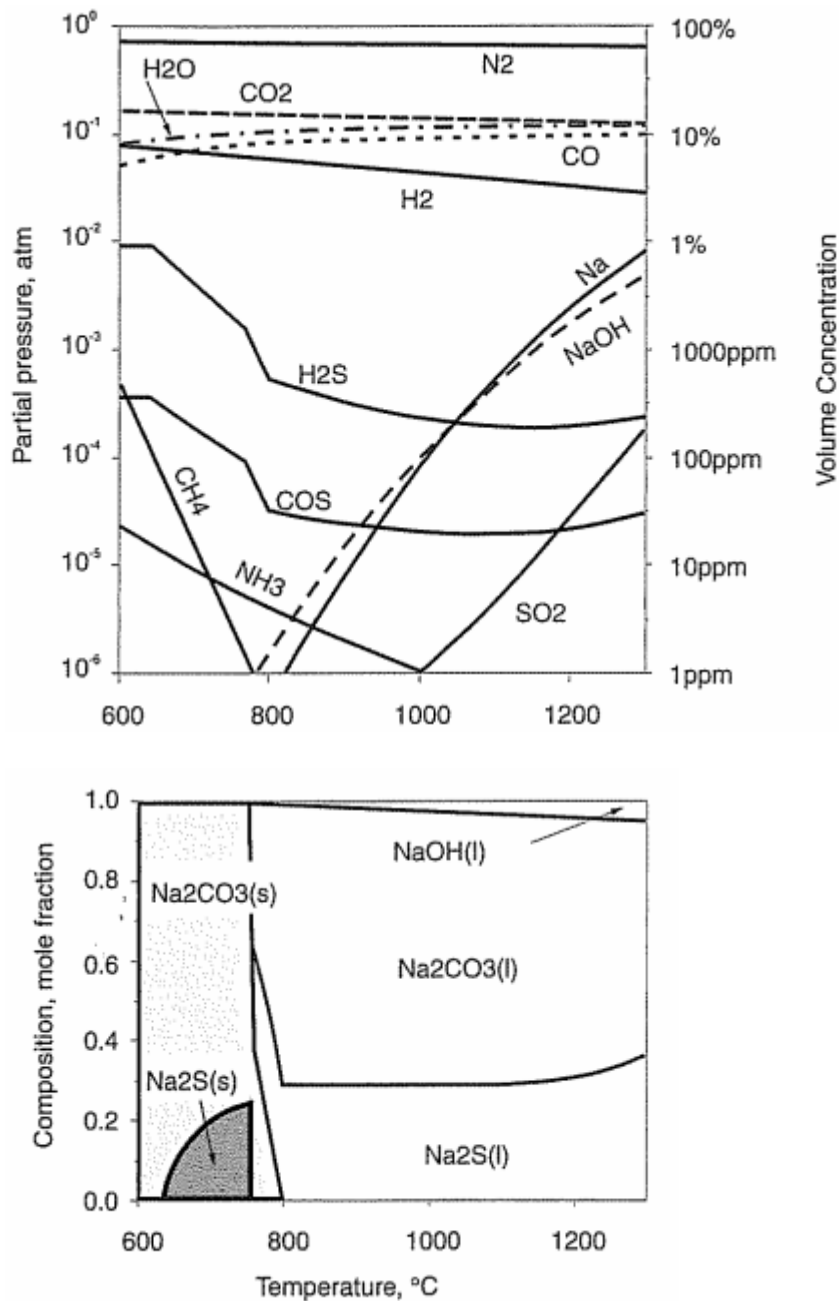


**Figure 54:** The equilibrium composition of the smelt and the lower furnace gases as a function of temperature at an air/fuel ratio of 0.7 and a molar S/Na<sub>2</sub> in black liquor solids of 0.3 [Adams et al., 1997].

The main components of the flue gases are nitrogen (N<sub>2</sub>), carbon monoxide (CO), carbon dioxide (CO<sub>2</sub>), hydrogen (H<sub>2</sub>), and water (H<sub>2</sub>O). Sulphur occurs as hydrogen sulphide (H<sub>2</sub>S), carbonyl sulphide (COS), and, at high air/fuel ratios, as sulphur dioxide (SO<sub>2</sub>). The most important gaseous sodium compounds are sodium hydroxide (NaOH) and metallic sodium (Na).

Figure 53 shows that, under equilibrium conditions, almost perfect smelt reduction may be obtained when the air/fuel ratio remains below approximately 80%. In an actual boiler complete reduction is not obtained because of a limited reduction rate.

Several studies have been performed on the reduction rate of the char bed. The sulphate contained in a black liquor droplet may be reduced by the reducing gases (CO or H<sub>2</sub>) or the solid carbon (char) in the bed. One study [Adams et al., 1988] shows that the reduction of sulphate by char is about two orders of magnitude faster than the reduction with reducing gases. Gas reduction become dominant after 99% of the char in the smelt bed has been consumed. At this stage the whole reduction process is very slow and insignificant for practical purposes.

This means that for efficient smelt reduction, a sufficient amount of char is continuously needed on the surface of the bed. Therefore black liquor should be sprayed in such a way that a significant part of the droplets reach the bed while the char burning is still incomplete. To avoid unwanted growth of the bed, the capacity of the bed to burn the char has to be considered.

The temperature of the bed is another important factor in smelt reduction. The rate of the reduction is strongly dependent on temperature and is roughly doubled if the temperature increases from 50 to 60°C.

Part of the sodium and sulphur is transferred into the flue gases and does not return to the char bed. The most important sulphur compounds in the combustion gases are H<sub>2</sub>S and COS. For sodium, the most important compounds are gaseous Na and NaOH. The vaporization of sulphur and sodium compounds depends mainly on the temperature. *Figure 54* shows that the concentration of gaseous sodium compounds increases sharply with increasing temperature, while the concentration of sulphur compounds decreases with increasing temperature.

These trends have also been observed in operating boilers. It is generally known that when a boiler is operated at a low temperature the flue gases contain higher concentrations of sulphur gases. This low temperature can for example depend on low heat value of black liquor. It is also known that when increasing the furnace temperature; by increasing the dry substance content of the black liquor for example, the rate of sodium vaporization increases, and thereby increasing the rate of dust circulation in the combustion gases and reducing the concentration of sulphur gases.

Observations of real recovery boilers deviate from the results of the equilibrium calculations primarily in two aspects. One is that the vaporization of sodium and sulphur is about 3 or 4 times higher than the equilibrium calculations show. This cannot be explained by carryover of black liquor droplets since the precipitator dust consists of smaller particles.

Another observation is that the concentration of sodium in the flue gas does not change so dramatically with the temperature as expected from the equilibrium curves.

These differences have not been completely explained, but measurements indicate that very little sodium is vaporized in the early stages of combustion, during pyrolysis. On the other hand, a great amount of sodium vapour is released during the char burning. Sodium volatilization during the char burning seems to be due to reactions between the inorganic salts, mainly sodium carbonate, and the char carbon at a temperature where the salts are in a molten state. The reactions yield sodium in vapour form, and gaseous oxides of carbon. These reactions are kinetically controlled so sodium release increases with higher particle temperature and longer reaction time. Measurements indicate that these reactions become

significant when the particle temperatures exceed 900 °C. These reactions can take place either in-flight or on the char bed.

Sulphur release has also been studied, and a result is that sulphur is released by a completely different mechanism than sodium. In unoxidized liquor, there is a significant fraction of sulphur in the form of sulphide. This sulphur reacts with the organic material in the liquor, which results in the release of mercaptans. These reactions are kinetically controlled and take place at a temperature range around 300-400 °C during liquor droplet heating. The longer time the droplet is within this temperature range, the more mercaptans will be released. This mechanism appears to be the most important source of sulphur release for unoxidized liquors, though some organosulphur gases (methyl mercaptan, dimethylsulphide, etc.) are released due to volatilization of organic sulphur.

In oxidized liquors the sulphide in the liquor has been converted to thiosulphate, which does not react in the same way as sulphide. Thiosulphate releases some sulphur during the early stages of droplet combustion, and some organosulphur gases are produced by the volatilization of organic sulphur.

These mechanisms mean that sodium and sulphur in the flue gases can originate from three different regions in the furnace. They can be vaporized in the lower furnace from the char bed. They can be released from black liquor droplets during in-flight combustion. For boilers with substantial wall drying, they can also be released from the char band that is formed on the walls of the furnace. Sulphur is released only during pyrolysis of the black liquor droplets in all three locations. Sodium is released only during char burning.

The following conclusions may be stated:

- Sulphur is vaporized in the furnace mainly as hydrogen sulphide and organosulphur gases, whereas sodium is vaporized as sodium hydroxide and metallic sodium.
- The concentration of sulphur in the flue gas decreases with increasing furnace temperature while the concentration of sodium increases.
- The ratio of sulphur and sodium concentration in the flue gas largely controls the flue gas and dust chemistry. The molar sulphur-to-sodium ratio in the flue gas varies from one boiler to another in the range from 0.8 to 1.5. The ratio is lower at higher furnace temperatures and at lower sulphur-to-sodium ratios in the black liquor.

Under the reducing conditions in the lower furnace, sulphur occurs as hydrogen sulphide, and sodium occurs mainly as metallic sodium and sodium hydroxide. When the lower furnace gases rise to the upper furnace and their combustion is completed, the sulphur and sodium compounds are transformed and they react with each other. The final flue gas dust compounds and the sulphur emissions compounds are produced in these reactions which take place in the upper furnace and in the superheater.

*Figure 55* illustrates the main reactions of sulphur and sodium in the flue gas, beginning with sodium vapours and hydrogen sulphide formed in the lower part of the furnace. The figures are based partly on theoretical calculations and partly on results of field measurements.

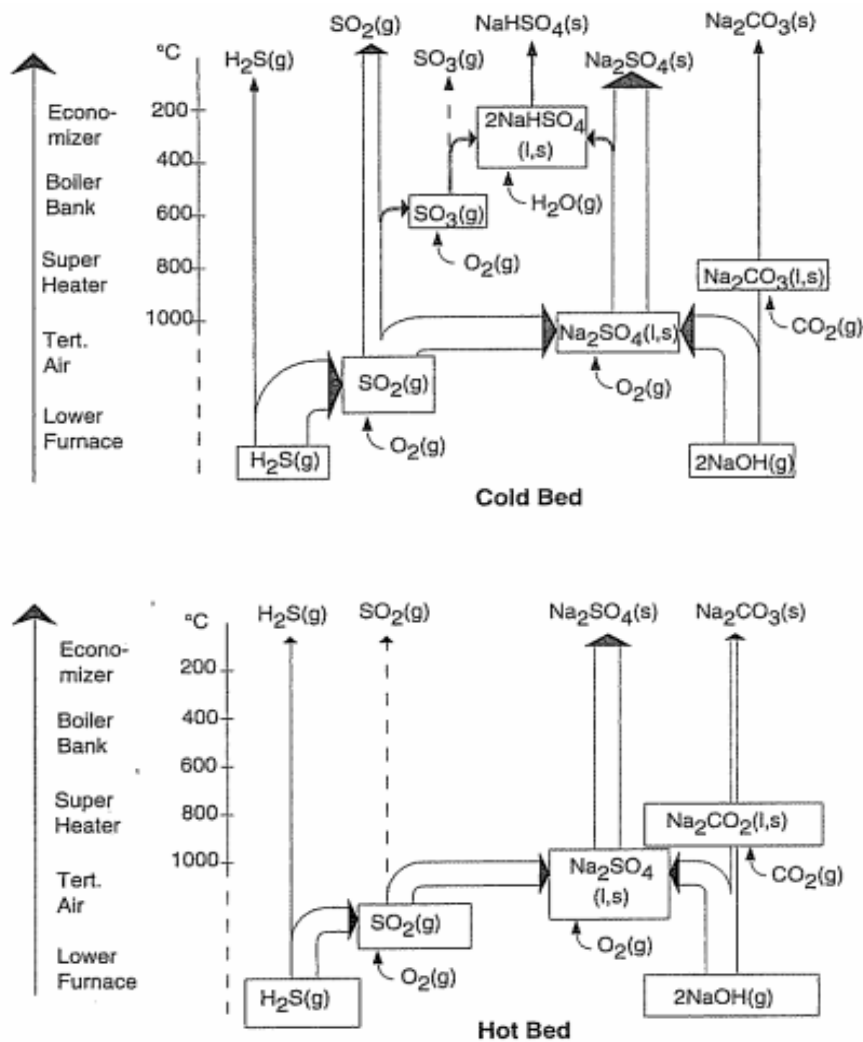


**Figure 55:** The reactions of sulphur and sodium in the recovery furnace and flue gases on a molar basis. The upper figure illustrates a cold bed with  $S/Na_2=1.5$  in the flue gases, and the lower figure illustrates a hot bed with  $S/Na_2=0.8$  in the flue gases [Adams et al., 1997].

The figure shows the final sulphur and sodium compounds in the flue gas at the entrance to the electrostatic precipitator, which captures the dust. The boxes in the figure indicate one or more chemical reactions. The reactants enter the boxes through the bottom or the sides. The reaction product is indicated as the label of the box. The product leaves the box through the top. The width of the line is proportional to the magnitude of the flow.

The reactions in the flue gases depend on the molar ratio of total sulphur and total sodium in these gases. In Figure 55, the reactions for two extreme conditions are shown separately. The upper part of the figure describes the reactions when the  $S/Na_2$  ratio in the flue gases is very high, exceeding unity. These conditions exist in boilers where the furnace temperature is low and/or the black liquor sulfidity is high. The lower part of the figure describes the opposite case, where the furnace temperature is high and/or the black liquor sulfidity is low. Actual boilers usually operate somewhere between these two extremes.

The first reaction is the oxidation of hydrogen sulphide into sulphur dioxide, and takes place at the tertiary air level. How complete this oxidation is depends on the mixing of the air with the combustion gases. Any hydrogen sulphide not oxidized at this point will remain as a

constituent of the flue gas and form the main component of the TRS (total reduced sulphur) emissions of the boiler.

The sulphur dioxide produced during the oxidation of hydrogen sulphide reacts with the sodium compounds in the oxidizing upper furnace and produce sodium sulphate. In this part of the furnace, sodium sulphate will be in a molten state, but will solidify as the combustion gases cool. After this reaction, the chemistry of the furnace gases depends on whether they originally contained an excess of sulphur or sodium.

In the case with a low furnace temperature (cold bed), almost all the sodium becomes sodium sulphate, and a surplus of sulphur dioxide remains. This sulphur dioxide often causes pluggage in the economizer. A surplus of sulphur dioxide may change the sulphate dust into sticky, acidic sulphate (bisulphate). Acidic sulphates may cause rapid fouling of the economizer and corrosion of the boiler bank [Backman et al., 1984]. This excessive sulphur dioxide usually ends up in the atmosphere as a stack emission.

In the case with a high furnace temperature (hot bed), the reaction that produces sodium sulphate consume almost all sulphur dioxide and the surplus sodium reacts with  $\text{CO}_2$  to form sodium carbonate dust. The sulphur dioxide emission from the boiler will be very low in this case and acidic sulphates are not produced. These conditions exist, for example, at high dry solids content. These often favourable conditions can be achieved with extremely high dry solids content even when the black liquor sulfidity is high [Björklund et al., 1989].

## ***C2. Potassium and Chlorine Chemistry***

In addition to the main chemicals, sodium and sulphur, many other elements participate in the recovery boiler process, for example chlorine and potassium. Other minor elements in the process are calcium, silicon, aluminium, and iron, but they are usually insignificant.

Chlorine is present in wood, but may also originate from wood floated in sea water, in makeup chemicals, or in pulp bleaching filtrates. The chlorine content in black liquor is usually quite low, typically 0.1 to 0.8% of the liquor dry solids content.

Potassium enters the process mainly as a natural mineral component of wood. The potassium content in black liquor is typically 1 to 3% of the liquor dry solids content.

### ***C2.1. Alkali Chlorides***

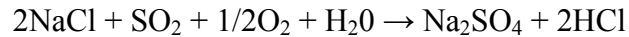
Chlorine occurs almost entirely as the alkali chlorides NaCl and KCl in the lower part of the furnace, because the vapour pressures of these compounds are higher than that of other sodium and potassium compounds. The chlorine compounds are therefore enriched in the gas phase.

The distribution of chlorine between smelt and furnace gas is strongly dependent on the temperature. At high temperatures ( $>1100\text{ }^\circ\text{C}$ ) most of the chlorine is vaporized.

The vaporized chlorides are condensed as the flue gases cool, and dust is formed. Chloride, especially in combination with potassium, lowers the melting temperature of dust significantly and makes the dust stickier and more fouling [Hupa et al., 1990; Tran, 1986].

## **C2.2. Hydrochloric Acid, HCl**

If sulphur dioxide exists in the flue gas, the chloride dust from condensation of NaCl is transformed in the upper furnace into sulphate:



During this reaction gaseous hydrogen chloride is formed. This hydrogen chloride passes the electrostatic precipitator and exits the process as a stack emission, which makes it possible to remove the chlorine from the recovery cycle.

At low furnace temperatures (<850 °C) most of the chlorine is transformed into hydrochloric acid and only a small amount is released in gaseous form. At high temperatures (>1100 °C), the amount of alkali chloride vaporized is much larger, but the S/Na<sub>2</sub> ratio in the combustion gases is low. Thereby no free sulphur dioxide is left in the flue gas to sulphate the alkali chloride. Instead, it is condensed into alkali chloride dust. Only at intermediate temperatures notable amount of hydrogen chloride is released.

## **C2.3. Potassium**

Potassium behaves a lot like sodium, but potassium compounds are more volatile, and are therefore enriched in the dust. The main potassium compounds in the lower furnace are K, KOH and KCl.

Potassium, especially in combination with chlorine, tends to lower the melting temperature of the dust and thereby increases the fouling. [Adams et al., 1997]

## APPENDIX D Modelling Fluid Flow in a Porous Medium

[Tse et al., 1996]

### Coefficients of Flow Resistance in the Flow Direction and the Transverse Direction

The additional momentum sink term,  $F_i$ , for a porous medium to the standard fluid flow equations is:

$$F_i = \alpha_1^i U_i + \alpha_2^i |\mathbf{V}| \cdot U_i = -\frac{\Delta p}{\Delta x} \quad i = 1, 2, 3 \quad (1)$$

where

$\alpha_1^i$  &  $\alpha_2^i$  = permeability coefficients  
 $U_i$  = velocity of respectively component, m/s  
 $\mathbf{V}$  = velocity vector, m/s

Grimison's correlation [1937] for the pressure drop past tube banks:

$$\Delta p = 2Nf'\rho U_{\max}^2 \quad (2)$$

where

$f'$  = empirical friction factor, -  
 $U_{\max}$  = velocity at minimum flow area, m/s  
 $\rho$  = density at free-stream conditions, kg/m<sup>3</sup>  
 $N$  = number of transverse rows

The empirical friction factor,  $f'$ , for in-line arrangements is given by Jakob [1938] as

$$f' = \left\{ 0.044 + \frac{0.08 S_L / D}{[(S_T - D) / D]^{[0.43 + 1.13 D / S_L]}} \right\} \text{Re}_{D, \max}^{-0.15} \quad (3)$$

where

$\text{Re}_{D, \max} = \rho U_{\max} D / \mu$   
 $D$  = tube diameter, m  
 $S_L$  = longitudinal tube separation, m  
 $S_T$  = transverse tube separation, m

Grimison's correlation is expected to be accurate to within 20% for  $5000 < \text{Re}_{D, \max} < 40\,000$ .

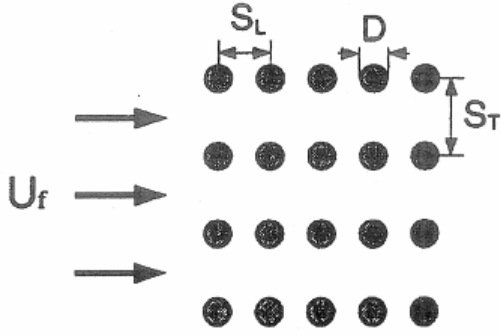


**Figure 56:** Flow past a tube bank [Tse et al., 1996].

In terms of the free stream velocity component,  $U_f$ , the maximum velocity is

$$U_{\max} = \frac{S_T}{S_T - D} \cdot U_f \quad (4)$$

Then Eq.(2) for pressure drop can be written as

$$\Delta p = 2Nf\dot{\rho} \left( \frac{S_T}{S_T - D} \right)^2 \cdot U_f^2 \quad (5)$$

The pressure gradient  $\Delta p/\Delta x$  is obtained from Eq.(5):

$$\frac{\Delta p}{\Delta x} \approx \frac{\Delta p}{N \cdot S_L} = \frac{2f\dot{\rho}}{S_L} \cdot \left( \frac{S_T}{S_T - D} \right)^2 \cdot U_f^2 \quad (6)$$

Since the flow resistance term  $F_i = -\frac{\Delta p}{\Delta x}$ , a comparison between Eq.(1) and (6) gives:

$$\alpha_1^i = 0 \quad (7)$$

$$\alpha_2^i = -\frac{2f\dot{\rho}}{S_L} \cdot \left( \frac{S_T}{S_T - D} \right)^2 \quad (8)$$

where  $i = 1, 2$  denotes the two cross-flow directions past the tube banks. The definitions for  $S_L$  and  $S_T$  have to be interchanged depending on which direction is being considered.

In the Fluent manual, the flow resistance term  $F_i$  is expressed as:

$$F_i = -\left( \frac{\mu}{\alpha} U_i + C_2 \frac{1}{2} \rho |V| U_i \right) \quad (9)$$

For porous calculations in Fluent, the viscous resistance term,  $1/\alpha$ , and the inertial resistance term,  $C_2$ , has to be evaluated. When comparing Eq.(1), (7), (8) and (9) the following may be stated:

$$1/\alpha = 0 \quad (10)$$

$$C_2 = \frac{4f'}{S_L} \cdot \left( \frac{S_T}{S_T - D} \right)^2 \quad [\text{m}^{-1}] \quad (11)$$

### **Coefficients of Flow Resistance in the Axial Direction**

In the axial direction, the permeability coefficients are given as follows:

$$\alpha_1^3 = 0 \quad (12)$$

$$\alpha_2^3 = -0.092 \cdot \rho \text{Re}_{L_H}^{-0.2} / L_H \quad (13)$$

where

$$\text{Re}_{L_H} = \rho |U_3| L_H / \mu \quad (14)$$

$$L_H = \frac{4}{\pi} \cdot \frac{S_T \cdot S_L - \pi D^2 / 4}{D}, \text{ which is the hydraulic diameter, m.} \quad (15)$$

Eq. (13) was obtained for the following range of  $\text{Re}_{L_H}$ :  $3000 < \text{Re}_{L_H} < 10^6$ .

A comparison of Eq.(1), (9), (12) and (13) gives:

$$1/\alpha = 0 \quad (16)$$

$$C_2 = 0.184 \cdot \text{Re}_{L_H}^{-0.2} / L_H \quad [\text{m}^{-1}] \quad (17)$$

## Calculation Examples

### The Coefficient of Flow Resistance in the Flow Direction for the Secondary Superheater

$$D = 0.0501 \text{ m}$$

$$S_T = 0.312 \text{ m}$$

$$S_L = 0.053 \text{ m}$$

$$U_f = 5.8 \text{ m/s}$$

$$\rho = 0.3 \text{ kg/m}^3$$

$$\mu = 43.32 \cdot 10^{-6} \text{ kg/ms} \quad (\text{air at } 800 \text{ }^\circ\text{C})$$

$$U_{\max} = \frac{S_T}{S_T - D} \cdot U_f = \frac{0.312}{0.312 - 0.0501} \cdot 5.8 = 6.9095 \text{ m/s}$$

$$\text{Re}_{D,\max} = \frac{\rho U_{\max} D}{\mu} = \frac{0.3 \cdot 6.9095 \cdot 0.0501}{43.32 \cdot 10^{-6}} = 2397.27$$

$$\begin{aligned} f' &= \left\{ 0.044 + \frac{0.08 S_L / D}{[(S_T - D) / D]^{[0.43 + 1.13 D / S_L]}} \right\} \text{Re}_{D,\max}^{-0.15} = \\ &= \left\{ 0.044 + \frac{0.08 \cdot 0.053 / 0.0501}{[(0.312 - 0.0501) / 0.0501]^{[0.43 + \frac{1.13 \cdot 0.0501}{0.053}]}} \right\} \cdot 2397.27^{-0.15} = 0.015903 \end{aligned}$$

$$C_2 = \frac{4f'}{S_L} \cdot \left( \frac{S_T}{S_T - D} \right)^2 = \frac{4 \cdot 0.015903}{0.053} \cdot \left( \frac{0.312}{0.312 - 0.0501} \right)^2 = 1.70335 \text{ m}^{-1}$$

### The Coefficient of Flow Resistance in the Axial Direction for the Secondary Superheater

$$L_H = \frac{4}{\pi} \cdot \frac{S_T \cdot S_L - \pi D^2 / 4}{D} = \frac{4}{\pi} \cdot \frac{0.053 \cdot 0.312 - \pi \cdot 0.0501^2 / 4}{0.0501} = 0.370145 \text{ m}$$

$$U_3 = 0.864 \text{ m/s}$$

$$\rho = 0.3 \text{ kg/m}^3$$

$$\mu = 40.87 \cdot 10^{-6} \text{ kg/ms} \quad (\text{air at } 700 \text{ }^\circ\text{C})$$

$$\text{Re}_{L_H} = \rho |U_3| L_H / \mu = \frac{0.3 \cdot 0.864 \cdot 0.370145}{40.87 \cdot 10^{-6}} = 2345.76$$

$$C_2 = 0.184 \cdot \text{Re}_{L_H}^{-0.2} / L_H = 0.184 \cdot 2345.76^{-0.2} / 0.370145 = 0.105290 \text{ m}^{-1}$$

# APPENDIX E Calculation of the Flow Resistance Coefficients

## Flow resistance coefficients, $C_2$ [ $m^{-1}$ ]

### Secondary SH

|                         | Flow direction | Transverse direction | Axial direction            |
|-------------------------|----------------|----------------------|----------------------------|
| uf, m/s                 | 5,8            | 0,156                | 0,864                      |
| density, $kg/m^3$       | 0,3            | 0,3                  | 0,3                        |
| viscosity, $kg/ms$      | 4,33E-05       | 4,09E-05             | 4,09E-05                   |
| St, m                   | 0,312          | 0,053                | 0,053                      |
| Sl, m                   | 0,053          | 0,312                | 0,312                      |
| d,tub, m                | 0,0501         | 0,0501               | 0,0501                     |
| umax, m/s               | 6,909507446    | 2,8510345            | hydraulic d, m 0,370145292 |
| Re,max, -               | 2,40E+03       | 1,05E+03             | Re,hd, - 2345,761848       |
| friction factor, emp, - | 1,59E-02       | 1,02E+00             | C2, $m^{-1}$ 0,105290      |
| C2, $m^{-1}$            | 1,70335        | 4358,46              |                            |

### Tertiary SH

|                         | Flow direction | Transverse direction | Axial direction            |
|-------------------------|----------------|----------------------|----------------------------|
| uf, m/s                 | 4,9            | 0,00471              | 0,221                      |
| density, $kg/m^3$       | 0,3            | 0,3                  | 0,3                        |
| viscosity, $kg/ms$      | 3,83E-05       | 3,83E-05             | 3,83E-05                   |
| St, m                   | 0,312          | 0,053                | 0,053                      |
| Sl, m                   | 0,053          | 0,312                | 0,312                      |
| d,tub, m                | 0,0501         | 0,0501               | 0,0501                     |
| umax, m/s               | 5,837342497    | 0,0860793            | hydraulic d, m 0,370145292 |
| Re,max, -               | 2,29E+03       | 3,38E+01             | Re,hd, - 640,7475936       |
| friction factor, emp, - | 1,60E-02       | 1,70E+00             | C2, $m^{-1}$ 0,136492      |
| C2, $m^{-1}$            | 1,71501        | 7295,75              |                            |

### Primary SH 2

|                         | Flow direction | Transverse direction | Axial direction            |
|-------------------------|----------------|----------------------|----------------------------|
| uf, m/s                 | 5,1            | 0,106                | 1,32                       |
| density, $kg/m^3$       | 0,3            | 0,3                  | 0,3                        |
| viscosity, $kg/ms$      | 3,55E-05       | 3,55E-05             | 3,55E-05                   |
| St, m                   | 0,312          | 0,10032              | 0,10032                    |
| Sl, m                   | 0,10032        | 0,312                | 0,312                      |
| d,tub, m                | 0,0501         | 0,0501               | 0,0501                     |
| umax, m/s               | 6,075601375    | 0,2117467            | hydraulic d, m 0,745352975 |
| Re,max, -               | 2,57E+03       | 8,96E+01             | Re,hd, - 8314,359943       |
| friction factor, emp, - | 2,31E-02       | 2,76E-01             | C2, $m^{-1}$ 0,0405966     |
| C2, $m^{-1}$            | 1,30567        | 14,1131              |                            |

### Primary SH 1

|                         | Flow direction | Transverse direction | Axial direction            |
|-------------------------|----------------|----------------------|----------------------------|
| uf, m/s                 | 4,9            | 0,417                | 2,42                       |
| density, $kg/m^3$       | 0,3            | 0,3                  | 0,3                        |
| viscosity, $kg/ms$      | 3,40E-05       | 3,40E-05             | 3,40E-05                   |
| St, m                   | 0,312          | 0,10032              | 0,10032                    |
| Sl, m                   | 0,10032        | 0,312                | 0,312                      |
| d,tub, m                | 0,0501         | 0,0501               | 0,0501                     |
| umax, m/s               | 5,837342497    | 0,8330036            | hydraulic d, m 0,745352975 |
| Re,max, -               | 2,58E+03       | 3,68E+02             | Re, hd, - 15915,47822      |
| friction factor, emp, - | 2,31E-02       | 2,23E-01             | C2, $m^{-1}$ 0,0356527     |
| C2, $m^{-1}$            | 1,30505        | 11,4179              |                            |

## APPENDIX F Example of the effect of a recirculation flow in the superheater

### Electricity production in steam turbine [Lundborg, 2005]

|   |                  |               |                  |               |
|---|------------------|---------------|------------------|---------------|
| Dry solids input, t DS/ 24 h                    | 3300             |               |                  |               |
| Steam flow, t/h                                 | 539,9            |               |                  |               |
|   | LT-steam         |               | MT-steam         |               |
|   | <b>Base case</b> | <b>Case A</b> | <b>Base case</b> | <b>Case A</b> |
| <b>Steam to turbine</b>                         |                  |               |                  |               |
| Temperature, °C                                 | 515              | 470           | 515              | 470           |
| Pressure, bar                                   | 113              | 84            | 113              | 84            |
| Enthalpy, kJ/kg                                 | 3397             | 3319          | 3397             | 3319          |
| Isentropic efficiency, %                        | 89               | 89            | 89               | 89            |
| <b>Steam from turbine</b>                       |                  |               |                  |               |
| Temperature, °C                                 | 147,9            | 147,9         | 224              | 224,5         |
| Pressure, bar                                   | 4,5              | 4,5           | 12               | 12            |
| Enthalpy, kJ/kg                                 | 2711             | 2711          | 2874             | 2876          |
| Electricity production, kWh/tonnes steam        | 190,7            | 169           | 145,3            | 123,3         |
| Electricity consumption feed water pump, kW     | 2619,7           | 2111          |                  |               |
| Pump efficiency, %                              | 82               | 82            |                  |               |
| Total steam generation, t/h                     | 539,9            | 555,5         |                  |               |
| LT-steam, %                                     | 45               |               |                  |               |
| Amount of LT- and MT-steam, t/h                 | 243              |               | 296,9            |               |
| Electricity production, kW                      | 46339            | 42235         | 43154            | 37657         |
| <b>Total electricity production, kW</b>         | <b>89492</b>     | <b>79892</b>  |                  |               |
| <b>Difference compared to the base case, kW</b> |                  | <b>-9264</b>  |                  |               |
| (incl. electricity consumption feed water pump) |                  |               |                  |               |

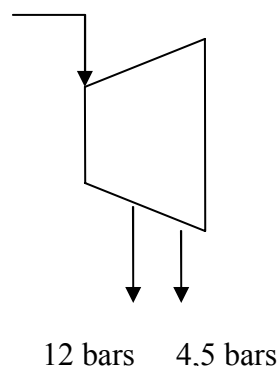


**Figure 57:** A steam turbine.

## Calculation of the value of the electricity production [Lundborg, 2005]

### Data

|   |      |
|---|------|
| Hours in operation/year, h/year                       | 7200 |
| Bio fuel part, %                                      | 100  |
| Electricity price, SEK/MWh                            | 360  |
| Renewable electricity certificates, SEK/MWh           | 250  |
| Electricity production of total heat, %               | 16   |
| Bark price, SEK/MWh                                   | 140  |
| Oil price, incl. taxes, SEK/tonne                     | 3195 |
| CO <sub>2</sub> allowances, SEK/tonne CO <sub>2</sub> | 220  |
| CO <sub>2</sub> tax, SEK/MWh fuel                     | 51   |
| NOx tax, SEK/kg                                       | 20   |
| Efficiency oil boiler, %                              | 90   |
| Efficiency bark boiler, %                             | 85   |
| Mech. & electr. efficiency turbine, %                 | 95   |

### Net value produced electricity

|                     |       |
|---------------------|-------|
| Oil based, SEK/MWh  | 220,3 |
| Bark based, SEK/MWh | 436,6 |

### Net value per year

|                           |        |
|---------------------------|--------|
| 470 °C compared to 515 °C |        |
| Oil based, MSEK/year      | -14,69 |
| Bark based, MSEK/year     | -29,12 |

